Title

FINAL REPORT

NASA GRANT NO. NGR 36-004-065

This report summarizes some of the work performed under NASA GRANT No. NGR 36-004-065 to the University of Cincinnati during the period from August 1, 1973 July 31, 1974. The report was prepared by Professor L. H. Sobel, the Project Manager, and by Mr. B. L. Agarwal, a Ph. D. candidate. Valuable contributions to this research effort were also made by Dr. J. Williams and Mrs. K. Hennessy of NASA-LRC, and by Dr. T. Weller, NRC Fellow at NASA-LRC.

A number of investigations pertaining to the buckling of cylindrical panels and complete cylindrical shells were performed. Some of the results obtained to date are presented in the following sections:

A. OPTIMIZATION OF COMPOSITE STIFFENED CYLINDERS

B. EFFECTS OF BOUNDARY CONDITIONS ON THE BUCKLING OF AXIALLY COMPRESSED CYLINDRICAL SHELLS

C. LOAD INTRODUCTION TECHNIQUES FOR BORON INFILTRATED ALUMINUM PANELS

(NASA-CR-139215) [STRESS TESTS ON CYLINDERS AND ALUMINUM PANELS] Final Report, 1 Aug. 1973 - 31 Jul. 1974 (Cincinnati Univ.) ~~125~~ 126 p HC $9.25
CSCL 20K G3/32
N74-30336
Unclas
54723

SECTION A

OPTIMIZATION OF COMPOSITE STIFFENED CYLINDERS*

* an expanded version of this section will be submitted for presentation at the AIAA/ASME/SAE 16th structures, structural Dynamics, and Materials Conference to be held in Denver, Colo. on May 27-29, 1975.

OPTIMIZATION OF COMPOSITE STIFFENED CYLINDERS

1. INTRODUCTION:- An optimization study of composite stiffened cylinders is discussed in this section. The mathematical model for the buckling analysis has been coupled successfully with the optimization program AESOP (Ref. 1). The buckling analysis is based on the use of so called "smeared theory" as used by Block, Card, and Mikulas (Ref. 2) for the buckling of stiffened orthotropic cylindrical shells. The equations used by Block, Card and Mikulas are modified to accomodate the laminated construction of the shell walls.

2. DESIGN VARIABLES:- The loading, radius and length of the cylinder are assumed to be known parameters. An optimum solution then should give the value of cross-sectional dimensions and laminate orientations. These will be design variables.

Figure 1 shows the optimized cylinder. It is assumed that stiffner spacing ℓ_s and ring spacing ℓ_r are unknown design variables. The skin of cylinder is allowed to have three different laminate orientations α_1, α_2, and α_3 which are assumed to be completely arbitrary. It should be noted that skin is assumed orthotropic and each layer balanced. Hence, so far, there are a total of 8 design variables as shown in figure 1. Dimensions of the stringers and rings are discussed next.

Figures 2(a) and (b) show a sketch of the rings and stringers, respectively. The rings and stiffners are assumed to behave as one-dimensional members. At this point the results previously obtained for the stiffened flat-plate (Ref. 3) are used to reduce the number of design variables.

Since the stringers and rings have similar characteristics, it will suffice to discuss only one of them. The stringers are composed of $\pm 45^\circ$ laminates and 0° laminates as is shown in Figure 2(b). It is assumed that b_s and h_s are unknown design variables which decides the size of the stiffner. b_{1s} and b_{3s} are assumed to be $.4b_s$ and $.8b_s$ respectively. These values are based on previous results obtained for flat panels and this leads to 5 design variables for the stringers and, similarly, 5 for the rings. Hence, a total of 18 design variables are chosen as a starting point for the optimization work.

3. BUCKLING MODES:- Five different types of buckling modes are considered. These modes are as follows:

(a) Gross buckling

(b) Panel buckling (buckling between rings)

(c) Skin buckling (buckling of the skin between contiguous rings and stringers)

(d) Local buckling of stringers

(e) Local buckling of rings

The buckling loads are determined from the analysis given in the next section.

4. THEORITICAL ANALYSIS

The notations and sign convention used in Ref. 2 is employed herein.

4.1 CONSTITUTIVE EQUATIONS

For a laminated shell the stress strain relations for p^{th} layer are given by

$$\begin{Bmatrix} \sigma_x \\ \sigma_y \\ \tau_{xy} \end{Bmatrix} = \begin{bmatrix} Q_{11} & Q_{12} & Q_{16} \\ Q_{12} & Q_{22} & Q_{26} \\ Q_{16} & Q_{26} & Q_{66} \end{bmatrix}_p \begin{Bmatrix} \varepsilon_x \\ \varepsilon_y \\ \gamma_{xy} \end{Bmatrix}_p$$

then, for a symmetric laminate layup, it can be shown for a Donnell-type analysis that (see ref. 4)

$$\begin{Bmatrix} N_x \\ N_y \\ N_{xy} \end{Bmatrix} = \begin{bmatrix} A_{11} & A_{12} & 0 \\ A_{12} & A_{22} & 0 \\ 0 & 0 & A_{66} \end{bmatrix} \begin{Bmatrix} u_{,x} \\ v_{,y} + w/R \\ u_{,y} + v_{,x} \end{Bmatrix}$$

or

$$\{N\} = [A]\ \{\varepsilon\}$$

and

$$\begin{Bmatrix} M_x \\ M_y \\ M_{xy} \end{Bmatrix} = - \begin{bmatrix} D_{11} & D_{12} & D_{16} \\ D_{12} & D_{22} & D_{26} \\ D_{16} & D_{26} & D_{66} \end{bmatrix} \begin{Bmatrix} w_{,xx} \\ w_{,yy} \\ 2w_{,xy} \end{Bmatrix}$$

or

$$\{M\} = -\ [D]\ \{W\}$$

In these equations v, v, w and N_x, N_y, N_{xy}, M_x, M_y, M_{xy} are, respectively, incremental displacements and stress resultants that take place during buckling. There positive sign conventions are shown in Fig. 4. A comma denotes partial derivative with respect to the indicated variable, and

$$A_{ij} = \sum_{p=1}^{P} (Q_{ij})_p \, (d_p - d_{p-1})$$

$$D_{ij} = \sum_{p=1}^{P} (Q_{ij})_p \, (d_p^3 - d_{p-1}^3)$$

$i,j = 1,2$ and 6, d_p is the distance of the center of p^{th} layer from the reference axis, and P is the total number of layers.

In general D_{16} and D_{26} terms are not zero, but in the present work they will be assumed to be zero.

4.2 BUCKLING ANALYSIS

• Gross, Panel and Skin Buckling

With the above more general constitutive relationships, the buckling equation of Ref. 2 have been modified to account for the laminated wall construction. This yields:

$$\bar{N}_x = \frac{K_{33} + \left(\dfrac{K_{12}\,K_{23} - K_{13}\,K_{22}}{K_{11}\,K_{22} - K_{12}^2}\right) K_{13} + \left(\dfrac{K_{12}\,K_{13} - K_{11}\,K_{23}}{K_{11}\,K_{22} - K_{12}^2}\right) K_{23}}{\left(\dfrac{\pi m}{L}\right)^2 + \dfrac{N_y}{\bar{N}_x}\left(\dfrac{n}{R}\right)^2} \qquad (1)$$

In this equation, $\bar{N}_x$ and $\bar{N}_y$ are prebuckling stress resultants (from now on, $\bar{N}_y$ will be taken equal to zero), m is the number of axial half waves, n is the number of circumferential full waves, and

$$K_{11} = \left[A_{11} + \left(\frac{EA}{\ell}\right)_s\right]\left(\frac{m\pi}{L}\right)^2 + A_{66}\left(\frac{n}{R}\right)^2$$

$$K_{12} = \left[A_{12} + A_{66}\right]\left(\frac{m\pi}{L}\right)\left(\frac{n}{R}\right)$$

$$K_{13} = A_{12}\left(\frac{m\pi}{LR}\right) + \left(\frac{EA\bar{Z}}{\ell}\right)_s\left(\frac{m\pi}{L}\right)^3$$

$$K_{22} = A_{66}\left(\frac{m\pi}{L}\right)^2 + \left[A_{22} + \left(\frac{EA}{\ell}\right)_r\right]\left(\frac{n}{R}\right)^2$$

$$K_{23} = \left[A_{22} + \frac{EA}{\ell}{}_r\right]\frac{n}{R^2} + \left(\frac{EA\bar{Z}}{\ell}\right)_r\left(\frac{n}{R}\right)^3$$

$$K_{33} = \left[D_{11} + \left(\frac{EI_o}{\ell}\right)_s\right]\left(\frac{m\pi}{L}\right)^4 + \left[2(D_{12} + 2D_{66}) + \left(\frac{GJ}{\ell}\right)_s + \left(\frac{GJ}{\ell}\right)_r\right]\left(\frac{m\pi}{L}\right)^2\left(\frac{n}{R}\right)^2 + \left[D_{22} + \left(\frac{EI_o}{\ell}\right)_r\right]\left(\frac{n}{R}\right)^4 + \left[A_{22} + \left(\frac{EA}{\ell}\right)_r\right]\frac{1}{R^2} + 2\left(\frac{EAZ}{\ell}\right)_r\frac{n^2}{R^3}$$

In these expressions, EA is the extensional stiffness of the stiffners, GJ is its torsional stiffness, and EI_o is the bending stiffness of the stiffner about the skin reference surface. Subscript s and r, respectively represent stiffner and ring. For the gross buckling mode, the above equation is used directly, but for panel and skin buckling modes it is modified slightly. For panel buckling, the length of the cylinder is assumed to be equal to ring spacing and all the ring stiffness properties are set equal to zero. And for skin buckling, all the terms due to stiffner stiffness and ring stiffnesses are set equal to zero and a buckling load corresponding to -

$$L = \ell r$$
$$n = \text{Integer}\left(\frac{\pi R}{\ell_s}\right)\bar{n} \quad , \quad \bar{n} = 1, 2, 3 \cdots$$

gives the skin buckling load.

• <u>Calculation of stringer and ring stiffness properties</u>:

Equation 1 requires knowledge of the stiffness properties of the rings and stringers. These will now be determined. Since the stringer and ring are similar geometrically, it will suffice to discuss the stringers only. Figure 5 shows three members of the stiffner, each having a width b_i. The width of each element is given by

$$b_1 = .4\, b_s$$
$$b_2 = \frac{(h_s - \bar{t}_s)}{\cos\beta}$$
$$b_3 = .8\, b_s$$

where

$$\bar{t}_s = \frac{t_{sk} + t_{1s} + t_{2s}}{2}$$

$$\tan \beta = \frac{.1\, b_s}{h_s}$$

If $[A]_i$ is the extensional stiffness matrix for i^{th} member then Young's Modulus E_{xis} for i^{th} member in x direction is given by (see ref. 4)

$$E_{xis} = A_{11} - \left(\frac{A_{12}^2}{A_{22}}\right)_i \frac{1}{h_i}$$

where h_i is the thickness of the i^{th} member given by

$$h_1 = t_{1s} + t_{2s}$$

$$h_2 = t_{2s}$$

$$h_3 = t_{2s} + t_{3s}$$

Let EA_{is} denote the extensional stiffness of each stiffner. Then the total extensional stiffness of the stiffner, EA_s is

$$EA_s = 2\, EA_{1s} + 2\, EA_{2s} + EA_{3s}$$

and

$$EA_{is} = E_{xis}\, b_i\, h_i \quad , \quad i = 1, 2, 3$$

The distance of the stiffner neutral axis from the skin reference axis, $\bar{z}_s$, is given by

$$\bar{z}_s = \frac{2\ EA_{1s}\ \bar{t}_s + EA_{2s}\ (h_s + \bar{t}_s) + EA_{3s}\ h_s}{EA_s}$$

The bending stiffness $(EI_o)_s$ about the skin reference axis is given by

$$\left(EI_o\right)_s = \frac{E\ A_{1s}\ h_1^2}{6} + \frac{EX_2 t_{2s} b_2^3 \cos^2\beta}{6} + \frac{E\ A_{3s}\ h_3^2}{12}$$

$$+ 2\ E\ A_{1s}\ \bar{t}_s^2 + 2\ E\ A_{2s}\ \frac{(h_s + \bar{t}_s)^2}{2}$$

$$+ E\ A_{3s}\ h_s^2$$

The torsional stiffness $(GJ)_s$ of the stiffner is computed as follows

$$\frac{1}{(GJ)_s} = \frac{1}{4\ (.9 b_i h_s)^2} \left[\frac{2\ b_2}{(A_{66})_2} + \frac{b_3}{(A_{66})_3} + \frac{b_s}{(A_{66})_{sk}}\right]$$

The contribution of the inplane shear stiffness due to stiffner $(A_{66})_s$ is given by

$$(A_{66})_s = (A_{66})_2 \left(\frac{.8\ b_s \cos\beta + h_s \sin\beta}{.8\ b_s \cos\beta + h_s}\right) \frac{1.8\ b_s}{\ell_s}$$

With the help of the above stiffness properties the gross, panel and skin buckling loads can be computed.

In order to determine the local buckling of stringer and ring it will again be sufficient to discuss only one of them.

• Local Buckling

For the local buckling modes of the stiffners, the buckling of members 2, 3 and the skin between the webs is considered. All these members are assumed to be orthotropic plate members simply supported on all four edges. Hence the buckling load for i^{th} member is given by (Ref. 5.)

$$\bar{P}_{xi} = \frac{2\pi^2}{b_i} \left[\sqrt{D_{11}\, D_{22}} + D_{12} + 2\, D_{66}\right]_i$$

4.3 CONSTRAINT CONDITIONS

• Buckling Constraints

For an optimum design to be a valid design, the applied load carried by each member cannot exceed the buckling load of the corresponding member. These buckling loads are now computed from a membrane prebuckling deformations, the relation between loads and strains can be written as

$$\begin{Bmatrix} N_{xp} \\ N_{yp} \end{Bmatrix} = \begin{bmatrix} A_{11} + \frac{EA}{\ell}_s & A_{12} \\ A_{12} & A_{22} + \frac{EA}{\ell}_r \end{bmatrix} \begin{Bmatrix} \varepsilon_{xp} \\ \varepsilon_{yp} \end{Bmatrix}$$

or

$$\{N_p\} = [\bar{A}]\{\varepsilon_p\}$$

Hence

$$\{\varepsilon_p\} = [\bar{A}]^{-1}\{N_p\}$$

The prebuckling strains can thus be computed from the total prebuckling stress resultants N_{xp} and N_{yp}. Next the loads carried by the skin and the individual members of the stiffners will be computed.

•• Load carried by the skin

$$\begin{Bmatrix} N_x \\ N_y \end{Bmatrix}_{sk} = \begin{bmatrix} A_{11} & A_{12} \\ A_{12} & A_{22} \end{bmatrix}_{sk} \begin{Bmatrix} \varepsilon_{xp} \\ \varepsilon_{yp} \end{Bmatrix}$$

•• Load carried by stringer members

$$P_{xsi} = EA_{is}\,\varepsilon_{xp}$$

•• Load carried by ring members

$$P_{xri} = EA_{ir}\,\varepsilon_{yp}$$

• Material Failure Constraints

The skin and stiffner laminates must be checked for possible material failure. For the case of laminated composite stiffened cylindrical shells it will be necessary to check the strain in each laminate for failure. This is the most conservative failure criterian and is used for the present problem in view of the lack of any other presently satisfactory failure criteria.

If the laminate fibers are oriented at an angle θ from the axial direction, then the strains in that laminate are given by (see. Ref. 4)

$$\begin{Bmatrix} \varepsilon_1 \\ \varepsilon_2 \\ \gamma_{12} \end{Bmatrix} = \begin{bmatrix} \cos\theta^2 & \sin^2\theta & 2\sin\theta\cos\theta \\ \sin\theta^2 & \cos^2\theta & -2\sin\theta\cos\theta \\ -\sin\theta\cos\theta & \sin\theta\cos\theta & \cos^2\theta - \sin^2\theta \end{bmatrix} \begin{Bmatrix} \varepsilon_{xp} \\ \varepsilon_{yp} \\ \gamma_{xyp} \end{Bmatrix}$$

where ε_1 is strain along the fiber, ε_2 strain perpendicular to the fiber and γ_{12} is the shear strain. The strains given by above equation are constrained to satisfy the yield strains of the material in each laminate.

5. NUMERICAL RESULTS

5.1 COMPUTER PROGRAM

A priliminary listing of the computer program developed for the optimization studies is given in appendix A. Detailed documentation of the use of this program and its capabilities will be given at the completion of this continuing effort.

5.2 CHECK CASES

In the use of smeared theory it is required to calculate the extensional, torsional and bending stiffness properties of the stiffners. In order to assess the effects of modifying the equations of Ref. 2 and of the assumptions made in calculation of the stiffness properties, the following three check cases were used:

1. Unstiffened cylinder using BUCLAP 2 (Ref. 6)

2. Stiffened cylinder using BUCLAP 2

3. Stiffened cylinder using BUCLASP 2 (Ref. 7)

These cases are briefly discussed next.

The first two check cases are used primarily to check the effect of modifying the equations of Ref. 2. BUCLAP 2 can be used for computing buckling loads of a sitffened cylindrical shell by adjusting the stiffness matrices to account for the effect of eccentricity and stiffners. These modified stiffness matrices, which were computed in a related panel buckling study, are given in appendix B. Buckling loads for both stiffened and unstiffened cylinder were found to be in good agreement.

The third case is used to check the effect of the use of smeared stiffners instead of discrete sitffners, and also to check the assumptions employed in the calculation of the stiffness properties of the stiffners.

It was disappointing to find that discrete theory using BUCLASP 2 gave a buckling load 30% lower than that predicted by smeared theory. The reason for this difference is probably in the computation of the torsional stiffness of the stiffner assumed for smeared theory. This contention is supported by the fact that, when the cylinder was forced to buckle in axisymmetric mode the buckling loads given by smeared and discrete theory were almost the same. An investigation is presently under way to resolve this problem. The optimization results for stiffened cylinders will then follow. However optimization studies for unstiffened composite cylinder have been successful. The results of these studies are given next.

5.3 RESULTS FOR UNSTIFFENED CYLINDERS

Some preliminary results for unstiffened composite cylinder are presented in Figs. 6 and 7.

Figure 6 shows the weight strength plot for unstiffened cylindrical shells under uniform axial compression. There is clearly a weight saving of about 40% using Graphite/Epoxy over aluminum. Furthermore, a similar or even better weight savings can be expected for stiffened cylinder, because Graphite/Epoxy stiffners can carry the load more effectively than aluminum stiffners.

Figure 7 shows results for unstiffened cylinders with the material properties used by Dow and Rosen (Ref. 8). They showed an "isotropic" arrangement of fibers was most optimum. But the present results show that a more optimum fiber orientation can be obtained using a general fiber orientations. Dow and Rosen also showed that isotropic configuration was better than ±15° configuration, but this was not found to be so in the present computations. Both ±15° and isotropic configuration gave the same value of weight parameter as indicated in Fig. 7.

REFERENCES

1. Hague, D. S., and Glatt, C. R., "A Guide to the Automated Engineering and Scientific Optimization Program, AESOP, NASA CR-73200, 1968.
2. Block, D. L., Card, M. F., and Mikulas, M. M. Jr., "Buckling of Eccentrically Stiffened Orthotropic Cylinders", NASA TN D-2960, 1965.
3. Agarwal, B. L., and Sobel, L. H., "Optimization of A Corrugated Stiffened Composite Panel Under Uniaxial Compression", NASA CR-132314, 1973.
4. Ashton, J. E., Halpin, J. C., and Petit, P. H., "Primer on Composite Materials: Analysis", Technomic Publishing Co., 1969.
5. Timoshenko, S. P., Gere, J. M., "Theory of Elastic Stability", McGraw-Hill Book Co.
6. Viswanathan, A. V., Tamekuni, M., and Baker, L. L., "Elastic Stability of Laminated, Flat and Curved, Long, Rectangular Plates Subjected to Combined Inplane Loads", NASA CR-2330, 1973.
7. Viswanathan, A. V., and Tamekuni, M., "Elastic Buckling Analysis For Composite Stiffened Panels and other Structures Subjected to Biaxial Inplane Loads", NASA CR-2216, 1973.
8. Dow, N. F., and Rosen, B. W., "Structural Efficiency of Orthotropic Cylindrical Shells Subjected to Axial Compression", AIAA Journal, Vol. 4, NO. 3, 1966.

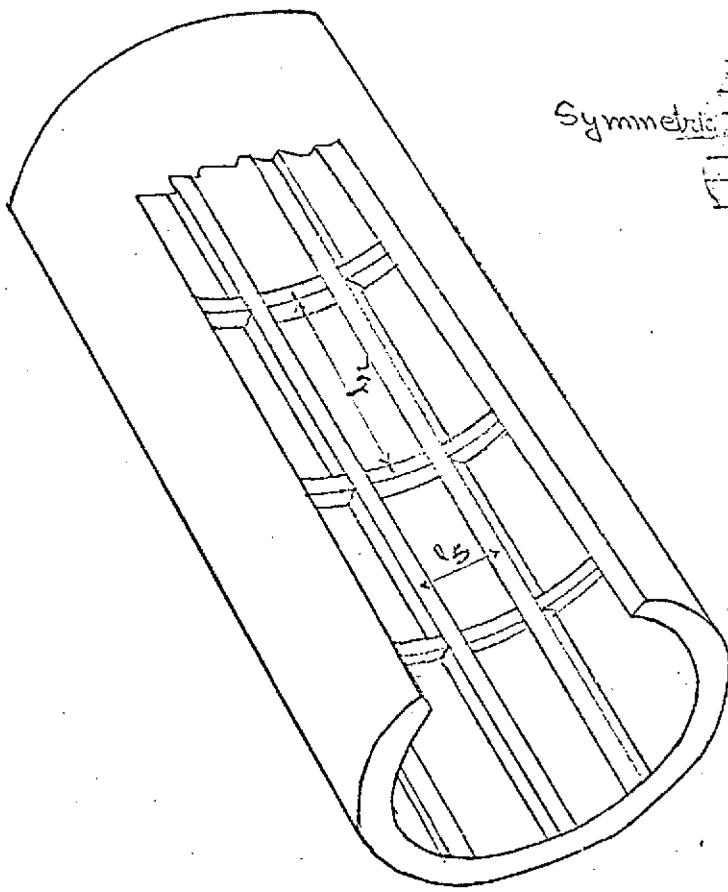

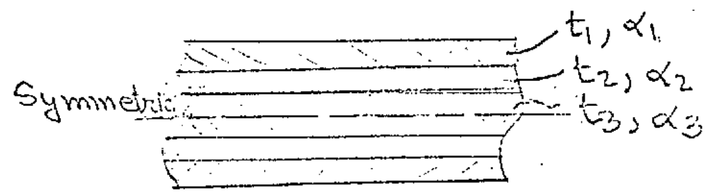

Skin Section

α_i – ply orientations

t_i – ply thicknesses

Subscripts :-

s- Stiffner

r- Rings

Design Variables $l_s, l_r, t_1, t_2, t_3, \alpha_1, \alpha_2, \alpha_3$

Total = 8

Fig 1.

$\frac{b_{1r}}{b_r} = .4$

$\frac{b_{3r}}{b_r} = .8$

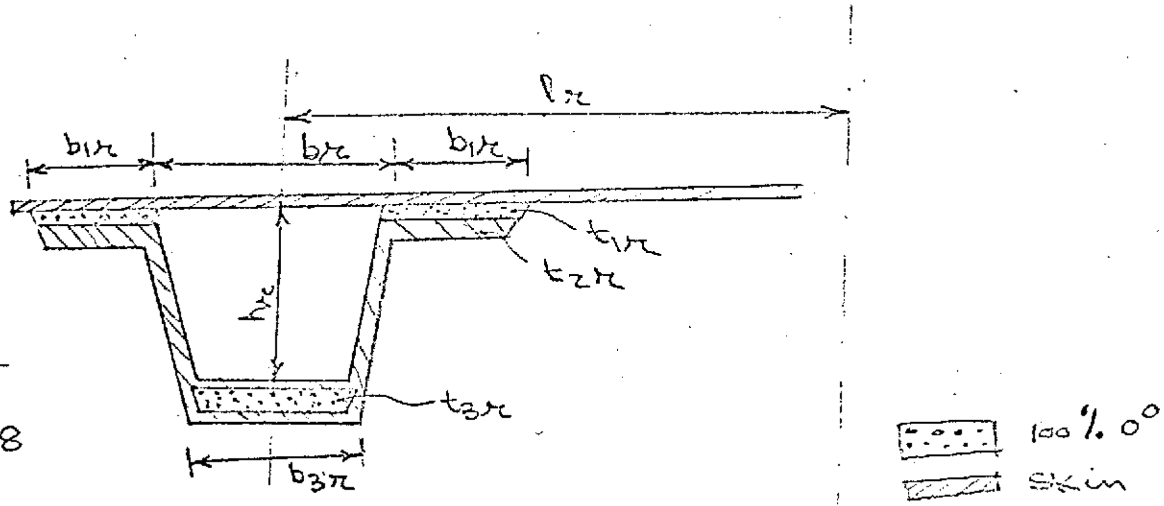

(a) Rings

$\frac{b_{1s}}{b_s} = .4$

$\frac{b_{3s}}{b_s} = .8$

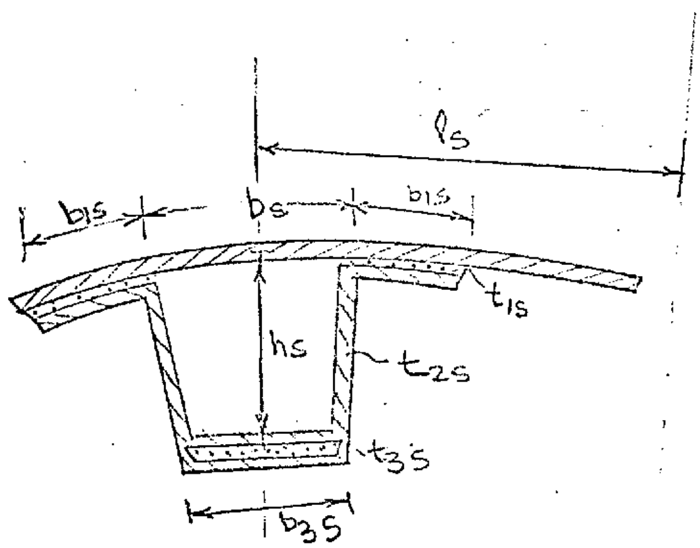

(b) Stiffners

Design Variables $b_r, h_r, t_{1r}, t_{2r}, t_{3r}$ & $b_s, h_s, t_{1s}, t_{2s}, t_{3s}$ } Total = 10

FIG. 2

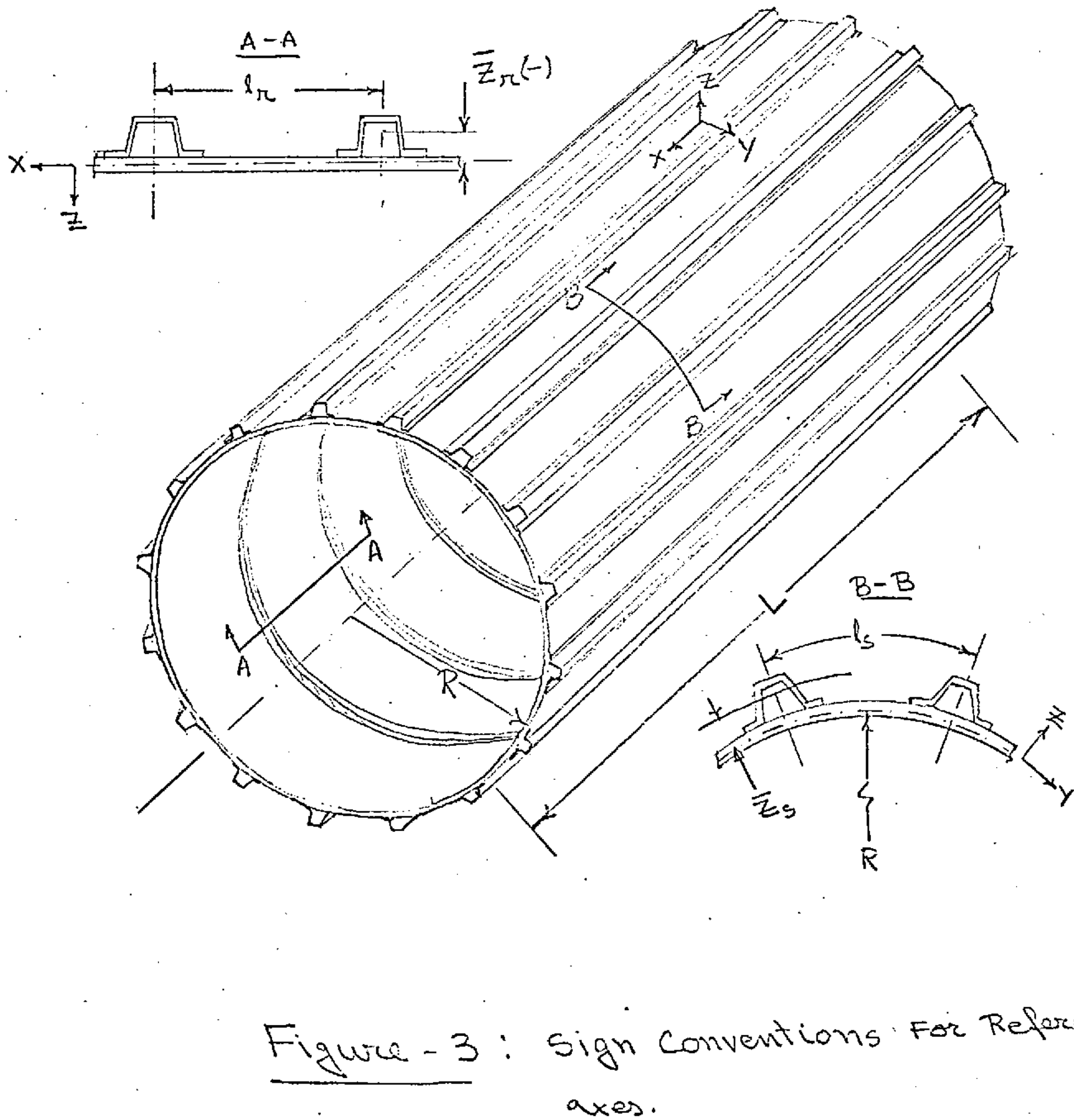

Figure - 3 : Sign Conventions For Reference axes.

July 31, 1974

To: NASA scientific and technical information facility.

From: B.L. Agarwal
Department Of Aerospace Engg.
University Of Cincinnati
Cincinnati, OHIO 45221

Subject: Final Report for NASA Grant No. NGR 36-004-065

Enclosed are the copies of final report for NASA Grant No. NGR 36-004-065 to the University of Cincinnati. This report summerizes the work performed during the period from august 1,1973 to july 31,1974.

Banarsi L. Agarwal

Banarsi L. Agarwal

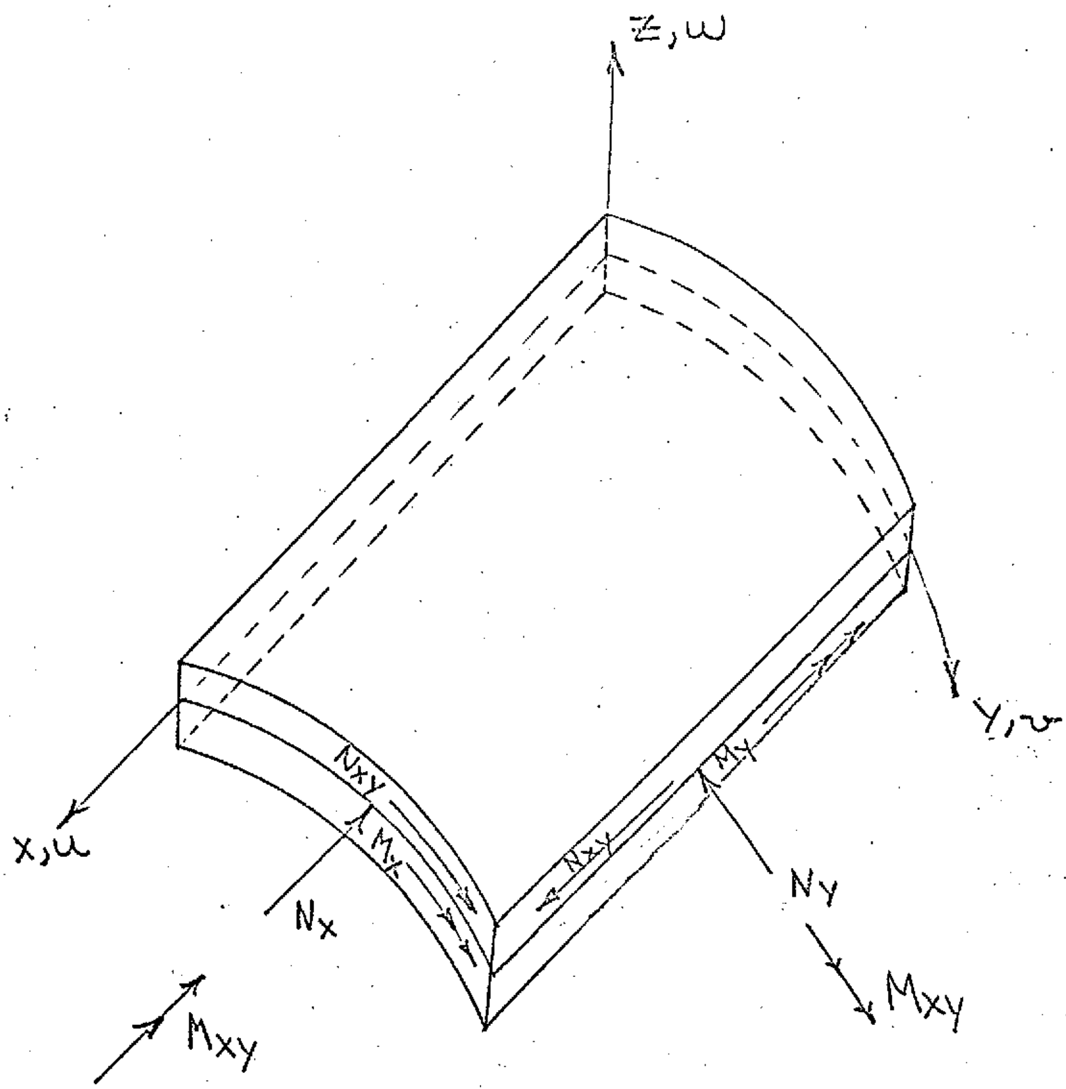

Fig 4. sign convention for stress resultants

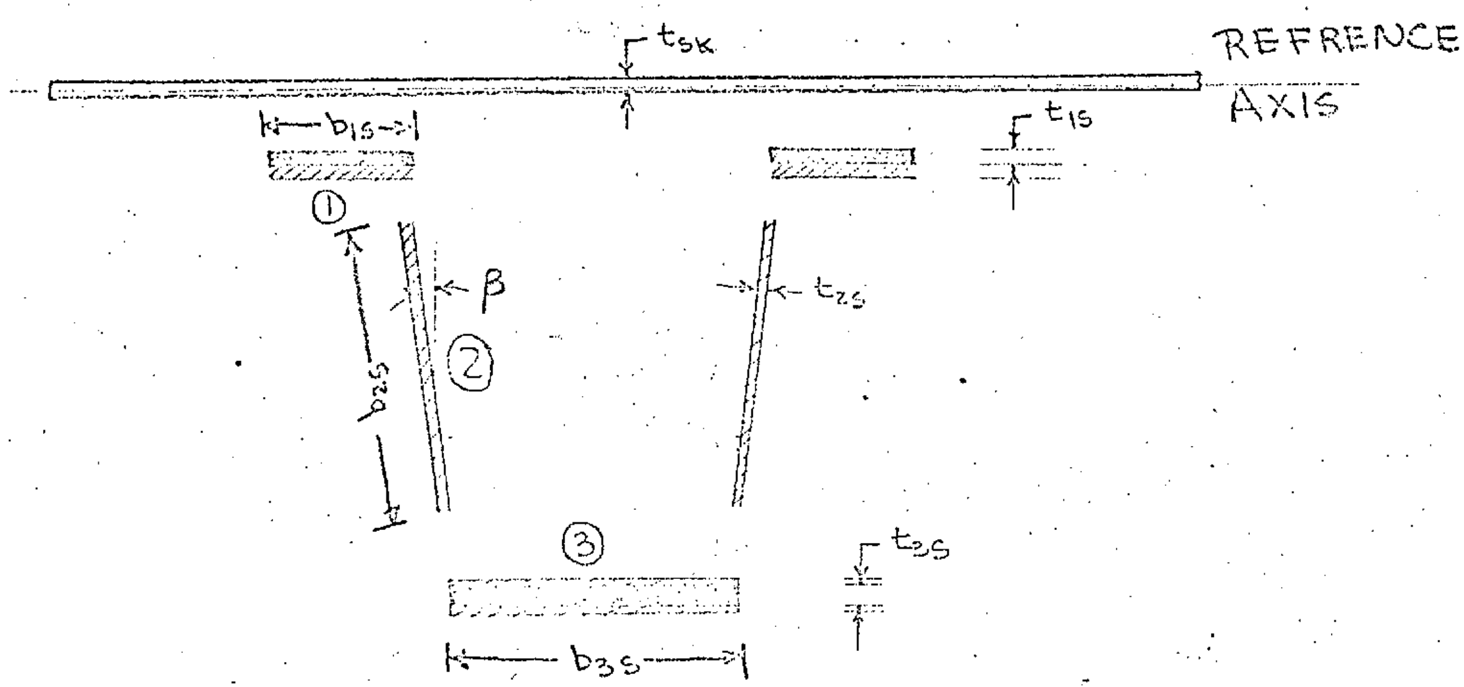

Figure - 5 . Elemental details of the stiffner.

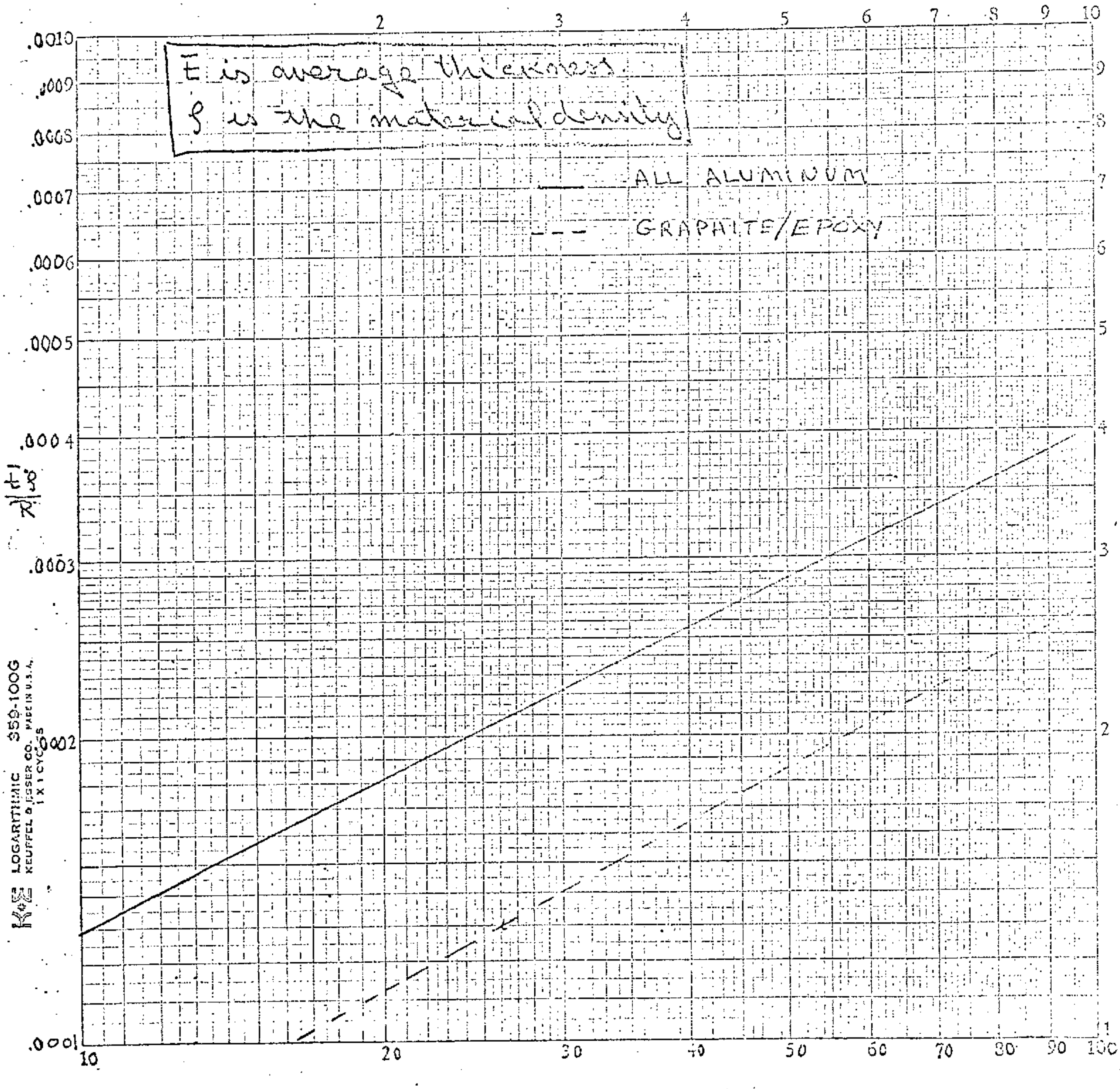

Figure 6 UNSTIFFENED CYLINDRICAL SHELL.

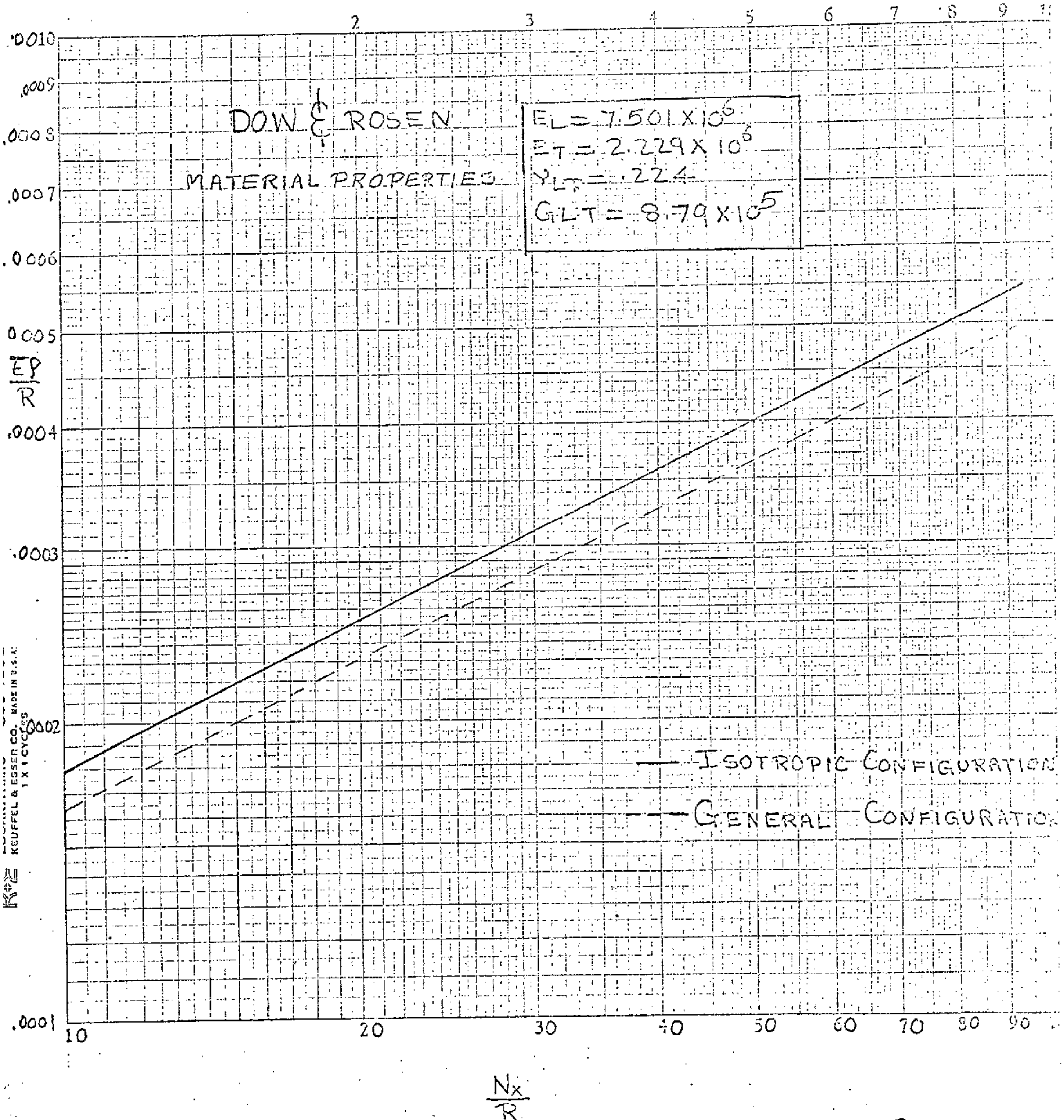

Figure 7. weight strength plot for unstiffened cylinder

APPENDIX A

LISTING OF COMPUTER PROGRAM

```
      SUB   UTINE CYLOPT
      REAL ALPHA(20)
      REAL FUNCTN(100)
      EQUIVALENCE(ADATA(742),ALPHA)
      EQUIVALENCE(ADATA(2736),JJJ)
      EQUIVALENCE(ADATA(2948),MAXJJJ)
      EQUIVALENCE(ADATA(2552),FUNCTN)
      COMMON /AESOPD/ ADATA(5000)
      COMMON/SUB/ FTOL(25),PSIWT(25),SIBAR(25),TOLFAC(25),TTOL(25),
     1 WTDOWN(25),WTUP(25),NPSI(25)
      COMMON /AREA/ TS,ASS,ASR
      DIMENSION QR(4),D(5,4),A(4),EAS(3),EAR(3),PXS(3),PXR(3),BUCKL(9),N
     1 CR(3),MCR(3),NCOUNT(3),EPSL1(5),EPSL2(5)
      COMMON /DATA/ BUCKL,EAS,EAR,B2S,B2R
      COMMON /Q/ QL(4,5)
      COMMON /MAT/ EX,EY,ENUXY,GXY,RO
      COMMON/SAVE1/EAD,GJD,EISD,ECECK1,EAL,GJR,EIRL,ECECK2,ISTOP1,ISTOP2
      COMMON /RATIO/ ANYR
      DIMENSION DISS(4),GAMA12(5),ALOAD(9)
      NAME LIST/CYLDATA/ ISTOP1,ISTOP2,CARGE1,CARGE2,ANX,ANYR,EL,R,
     1 EX,EY,GXY,ENUXY,RO
      COMMON/LIST/ CARGE1,CARGE2
      PI=3.14159265
    2 FORMAT(8E15.6)
      IF(JJJ.NE.1) GO TO 1111
      READ(5,CYLDATA)
 1111 CONTINUE
      ANY=ANYR*ANX
      ENUYX=EY*ENUXY/EX
      ENT=1.-ENUXY*ENUYX
      QR(1)=EX/ENT
      QR(2)=EY/ENT
      QR(3)=ENUYX*EX/ENT
      QR(4)=GXY
      CALL QLAMNA(QR,0.,QL,4)
      CALL QLAMNA(QR,45.,QL,5)
      CALL ASEMBL(D,QR,A,EAS,EAR,B2S,B2R,CARGE1,CARGE2)
C           CALCULATION OF STRAIN
      A(1)=A(1)+EAD
      A(2)=A(2)+EAL
      DELTA=A(1)*A(2)-A(3)**2
      AA1=A(2)/DELTA
```

```
      AA2=A(1)/DELTA
      AA3=-A(3)/DELTA
      AA4=1./A(4)
      EPSLX=AA1*ANX+AA3*ANY
      EPSLY=AA3*ANX+AA2*ANY
C     ******* CALCULATION OF STRAIN IN EACH LAYER
      DO 2000 I=1,3
      CALL STRAIN(ALPHA(I),EPSLX,EPSLY,EPSL1(I),EPSL2(I),GAMA12(I))
 2000 CONTINUE
      EPSL1(4)=EPSLX
      EPSL2(4)=EPSLY
      GAMA12(4)=0.
      CALL STRAIN(45.,EPSLX,EPSLY,EPSL1(5),EPSL2(5),GAMA12(5))
C       TO FIND LOAD CARRIED BY EACH MEMBER***************
      DO 10 I=1,3
      PXS(I)=EPSLX*EAS(I)
   10 PXR(I)=EPSLY*EAR(I)
      A(1)=A(1)-EAD
      A(2)=A(2)-EAL
      PXSK=A(1)*EPSLX+A(3)*EPSLY
      PYSK=A(3)*EPSLX+A(2)*EPSLY
      IF(JJJ.EQ.MAXJJJ) PRINT 2,EAD,GJD,EISD,ECECK1,EAL,GJR,EIRL,ECECK2
C       ******   TO FIND BUCKLING LOADS*************
      DO 1000 I=1,4
 1000 DISS(I)=D(1,I)
      CALL ITRATE(1,30,0,2,NCOUNT(1),BUCKL(1),NCR(1),MCR(1),A,
     1 DISS,EL,R)
      PII=2.*PI*PI
      IF( ISTOP2.EQ.1) BUCKL(2)=BUCKL(1)
      IF(ISTOP2.EQ.1) GO TO 8000
      EAL=0.
      GJR=0.
      ECECK2=0.
      EIRL=0.
      CALL ITRATE(1,5,0,2,NCOUNT(2),BUCKL(2),NCR(2),MCR(2),A,DISS,
     1  ALPHA(8),R)
 8000 CONTINUE
      IF( ISTOP1.EQ.1) BUCKL(3)=BUCKL(2)
      IF(ISTOP1.EQ.1) GO TO 7000
      EAD=0.
      GJD=0.
      ECECK1=0.
      EISD=0.
```

```
      NNNN=INT(PI*R/ALPHA(7))
      BUC   (3)=10.E20
      IF(NNNN.EQ.0.OR.NNNN.EQ.1) GO TO 8888
      DO 100 J=1,10
      NNX=NNNN*J
      DO 100 I=1,30
      CALL BUCKLG(I,NNX ,A,DISS,ANXX,ALPHA(8),R)
      IF(ANXX.LT.BUCKL(3)) MCR(3)=I
      IF(ANXX.LT.BUCKL(3)) NCR(3)=J
      IF(ANXX.LT.BUCKL(3)) BUCKL(3)=ANXX
  100 CONTINUE
 8888 IF(NNNN.EQ.0.OR.NNNN.EQ.1)CALL  ITRATE(1,30,0,2,NCOUNT(3),BUCKL(3),
     1 NCR(3),MCR(3),A,DISS,ALPHA(8),R)
 7000 CONTINUE
      IF(ISTOP1.EQ.1)GO TO 5000
      BUCKL(4)=PII*(SQRT(D(1,1)*D(1,2))+D(1,3)+D(1,4)*2.)/ALPHA(12)
      BUCKL(5)=PII*(SQRT(D(2,1)*D(2,2))+D(2,3)+2.*D(2,4))/B2S
      BUCKL(6)=PII*(SQRT(D(3,1)*D(3,2))+D(3,3)+2.*D(3,4))/(.8*ALPHA(12))
 5000 CONTINUE
      IF(ISTOP2.EQ.1) GO TO 5001
      BUCKL(7)=PII*(SQRT(D(1,1)*D(1,2))+D(1,3)+2.*D(1,4))/ALPHA(17)
      BUCKL(8)=PII*(SQRT(D(4,1)*D(4,2))+D(4,3)+2.*D(4,4))/B2R
      BUCKL(9)=PII*(SQRT(D(5,1)*D(5,2))+D(5,3)+2.*D(5,4))/(.8*ALPHA(17))
 5001 CONTINUE
      ALOAD(1)=ANX
      ALOAD(2)=ANX
      ALOAD(3)=PXSK
      ALOAD(4)=PXSK
      ALOAD(5)=PXS(2)
      ALOAD(6)=PXS(3)
      ALOAD(7)=PYSK
      ALOAD(8)=PXR(2)
      ALOAD(9)=PXR(3)
C  MATERIAL PROPERTIES USED ARE FOR THORNELL 300    NARMCO 5208
C
C E11 2.12E7,  E22 2.39E6 ,   G12 6.5E5,    NUE12 .31
C
      DO 3300 I=1,9
      FUNCTN(I)=SIBAR(I)
      IF(ALOAD(I).LT.0.)GO TO 3300
      IF(ALOAD(I).GT.BUCKL(I))FUNCTN(I)=(ALOAD(I)-BUCKL(I))/ALOAD(I)
 3300 CONTINUE
      DO 3400 I=10,14
```

```
      FUNCTN(I)=SIBAR(I)
      FUNCTN(I+5)=SIBAR(I+5)
      FUNCTN(I+10)=SIBAR(I+10)
      IF(EPSL1(I-9).LT.0.)GO TO 3420
      IF(ABS(EPSL1(I-9)).GT..012) FUNCTN(I)=(EPSL1(I-9)-.012)/EPSL1(I-9)
      IF(ABS(EPSL2(I-9)).GT..02)FUNCTN(I+5)=(EPSL2(I-9)-.02)/EPSL2(I-9)
      IF(ABS(GAMA12(I-9)).GT..015)FUNCTN(I+10)=(GAMA12(I-9)-.015)/GAMA12
     1(I-9)
      GO TO 3400
 3420 IF(ABS(EPSL1(I-9)).GT. .01)FUNCTN(I)=(EPSL1(I-9)-.01)/EPSL1(I-9)
      IF(ABS(EPSL2(I-9)).GT..0045)FUNCTN(I+5)=(EPSL2(I-9)-.0045)/EPSL2(I
     1-9)
      IF(ABS(GAMA12(I-9)).GT..015)FUNCTN(I+10)=(GAMA12(I-9)-.015)/GAMA12
     1(I-9)
 3400 CONTINUE
      FUNCTN(25)=2.*PI*R*EL*(TS+ASS/ALPHA(7)+ASR/ALPHA(8))
      IF(JJJ.NE.MAXJJJ) GO TO 1113
    8 FORMAT(//*********** SOME RESULTS *******///)
      PRINT 8
    3 FORMAT(*    NX               NY/NX              EL                R*)
      PRINT 3
      PRINT 2,ANX,ANYR,EL,R
    4 FORMAT(/*     EX                EY               GXY           ENUXY*)
      PRINT 4
      PRINT 2, EX,EY,GXY,ENUXY
    5 FORMAT(//*     ALPHA1            ALPHA2             ALPHA3             T1
     1              T2                T3                ELS            ELR*)
      PRINT 5
      PRINT 2, (ALPHA(I),I=1,8)
    6 FORMAT(/*     T1S               T2S               T3S             BS
     1         HS*)
      PRINT 6
      PRINT 2,(ALPHA(I),I=9,13)
    7 FORMAT(/*     T1R               T2R               T3R             BR
     1         HR*)
      PRINT 7
      PRINT 2,(ALPHA(I),I=14,18)
 2001 FORMAT(//*  STRAININ THE FIBER DIRECTION *)
      PRINT 2001
 2003 FORMAT(*     ALPHA             EPSL1             EPSL2        GAMA12 *)
      PRINT 2003
 2002 FORMAT(F7.3, 4X,3E15.6/)
      ZE=0
```

```
      ZEE=45.
      PRI   2002,((ALPHA(I),EPSL1(I),EPSL2(I),GAMA1  I)),I=1,3)
      PRI.., 2002,ZE,EPSL1(4),EPSL2(4),GAMA12(4)
      PRINT 2002,ZEE,EPSL1(5),EPSL2(5),GAMA12(5)
 1123 FORMAT(* STIFFNER PROPERTIES*//*EAD=*,E14.7,*GJD=*,E14.7,*EISD=*
     1 ,E14.7,*ECECK1=*,E14.7)
      PRINT 1123,EAD,GJD,EISD,ECECK1
    9 FORMAT(/*  AXIAL STRAIN   TRANSVERSE STRAIN*)
      PRINT 9
      PRINT 2,EPSLX,EPSLY
   20 FORMAT(***LOAD CARRIED BY EACH MEMBER*)
      PRINT 20
   11 FORMAT(*  PXS,PXR,PXSK,PYSK*)
      PRINT 11
      PRINT 2,(PXS(I),I=1,3)
      PRINT 2,(PXR(I),I=1,3)
      PRINT 2,PXSK,PYSK
   12 FORMAT(//***** BUCKLING LOADS*)
      PRINT 12
   13 FORMAT(/*GROSS BUCKLING  PANEL BUCKLING   SKIN BUCKLING*)
      PRINT 13
      PRINT 2, (BUCKL(I),I=1,3)
   14 FORMAT(/*LOCAL BUCKLING STIFFNER*)
      PRINT 14
      PRINT 2,(BUCKL(I),I=4,6)
   15 FORMAT(/* LOCAL  BUCKLING RING*)
      PRINT 15
      PRINT 2,(BUCKL(I),I=7,9)
   16 FORMAT(/*** MCR(I),NCR(I),NCOUNT(I)*)
      PRINT 16
   21 FORMAT(3I8)
      PRINT 21, ((MCR(I),NCR(I),NCOUNT(I)),I=1,3)
      CALL OUTPUT(FUNCTN,ALPHA,ISTOP1,ISTOP2,EL,R,RO,ANX)
 1113 CONTINUE
      RETURN
      END
```

```
      SUBROUTINE ASEMBL(D,QR,A,EAS,EAR,B2S,B2R,CARG   ,CARGE2)
      COMMON /AREA/ TS,ASS,ASR
      DIMENSION QR(4),THICK(6),KP(6),DS(4),D(5,4),DSS(2,4),EAS(3),EAR(3)
     1 ,A(4)
      COMMON /Q/ QL(4,5)
      COMMON/SAVE1/EAD,GJD,EISD,ECECK1,EAL,GJR,EIRL,ECECK2,ISTOP1,ISTOP2
      COMMON /AESOPD/ ADATA(5000)
      REAL ALPHA(20)
      EQUIVALENCE(ADATA(742),ALPHA)
      DO 1 I=1,3
      CALL QLAMNA(QR,ALPHA(I),QL,I)
      THICK(I)=ALPHA(I+3)
      THICK(7-I)=ALPHA(I+3)
      KP(I)=I
      KP(I+3)=4-I
    1 CONTINUE
      DIST=ALPHA(4)+ALPHA(5)+ALPHA(6)
      CALL STIFF(A,KP,DS,THICK,DIST,6)
      DO 2 I=1,4
    2 D(1,I)=DS(I)
      TS=2.*DIST
      GXYSK=A(4)/TS
      IF(ISTOP1.EQ.1)GO TO 5000
      CALL STIFPR(ALPHA(9),ALPHA(10),ALPHA(11),ALPHA(12),ALPHA(13),TS,
     1 EAD,GJD,ECECK1,EISD,DSS,ALPHA(7),EAS,B2S,CARGE1,ASS,GXYSK,GXYBST)
      DO 3 I=1,4
      D(2,I)=DSS(1,I)
    3 D(3,I)=DSS(2,I)
      A(4)=A(4)+1.8*ALPHA(12)*GXYBST/ALPHA(7)
 5000 CONTINUE
      IF(ISTOP2.EQ.1) GO TO 5001
      CALL STIFPR(ALPHA(14),ALPHA(15),ALPHA(16),ALPHA(17),ALPHA(18),
     1 TS,EAL,GJR,ECECK2,EIRL,DSS,ALPHA(8),EAR,B2R,CARGE2,ASR,GXYSK,GXY
     2 BRN)
      DO 4 I=1,4
      D(4,I)=DSS(1,I)
    4 D(5,I)=DSS(2,I)
      A(4)=A(4)+1.8*ALPHA(17)*GXYBRN/ALPHA(8)
 5001 CONTINUE
      RETURN
      END
```

```
      BLOCK DATA
      DIMENSION BUCKL(9),EAS(3),EAR(3)
      COMMON /DATA/ BUCKL,EAS,EAR,B2S,B2R
      COMMON/SAVE1/EAD,GJD,EISD,ECECK1,EAL,GJR,EIRL,ECECK2,ISTOP1,ISTOP2
      COMMON /AREA/ TS,ASS,ASR
      COMMON /MAT/ EX,EY,ENUXY,GXY,RO
      COMMON/LIST/ CARGE1,CARGE2
      DATA ISTOP1,ISTOP2/2*0/,CARGE1,CARGE2/2*1./,EX/10.E6/,EY/10.E6/,
     1 GXY/3.75E6/,ENUXY/.33333333/,RO/.1/
      DATA TS,ASS,ASR/3*0./
      DATA BUCKL /9*1.E30/,EAS/3*0./,EAR/3*0./,B2S,B2R,EAD,GJD,EISD,ECEC
     1 K1,EAL,GJR,EIRL,ECECK2 /10*0./
      END
```

```
      SUBROUTINE BUCKLG(M,N,A,D,ANX,EL,R)
      COMMON/SAVE1/EAD,GJD,EISD,ECECK1,EAL,GJR,EIRL,ECECK2,ISTOP1,ISTOP2
      COMMON /RATIO/ ANYR
      DIMENSION A(4),D(4)
      PI=3.1415927
      PIM=FLOAT(M)*PI/EL
      RN=FLOAT(N)/R
    5 A11=(A(1)+EAD)*PIM**2+A(4)*RN**2
      A12=(A(3)+A(4))*PIM*RN
      A13=A(3)*PIM/R+ECECK1*PIM**3
      A22=A(4)*PIM**2+(A(2)+EAL)*RN**2
      A23=(A(2)+EAL)*RN/R+ECECK2*RN**3
      A33=(D(1)+EISD)*PIM**4+(2.*(D(3)+2.*D(4))+GJD+GJR)*PIM**2*RN**2
     1+(D(2)+EIRL)*RN**4+(A(2)+EAL)/R**2+2.*ECECK2*RN**2/R
      APP=A11*A22-A12*A12
      APX=A33+(A12*A23-A13*A22)*A13/APP+(A12*A13-A11*A23)*A23/APP
      ANX=APX/(PIM**2+ANYR*RN**2)
      RETURN
      END
```

```
      SUBROUTINE ITRATE(MI,MF,NI,NDEL,NCOUNT,CMIN,NCR,MCR,A,D,EL,R)
      DIMENSION A(4),D(4)
    1 FORMAT(1H0,* WARNING  VALUE OF N WENT BEYOND 100 *//)
      NCOUNT=0
      NN=NI
      NDELTA=NDEL
      DO 100 I=MI,MF
      IF(I.NE.1) NN=NC1
      IF(I.NE.1) NDELTA=1
      INN=1
      NCHECK=0
   50 IF(NN.GT.100)PRINT 1
      IF(NN.GT.100) GO TO 100
      CALL BUCKLG(I,NN,A,D,FUNCTN,EL,R)
      NCOUNT=NCOUNT+1
      IF(INN.EQ.1)GO TO 30
      IF(FUNCTN.LT.CFUNTN) GO TO 30
   20 NCHECK=NCHECK+1
      NDELTA=-1
   30 NN=NN+NDELTA
      INN=2
      IF(NCHECK.EQ.2) NC1=NN+2
      IF(NCHECK.EQ.2)GO TO 10
      CFUNTN=FUNCTN
      GO TO 50
   10 IF(I.NE.MI) GO TO 200
      MCR=MI
      NCR=NC1
      IF(I.EQ.MI) GO TO 70
  200 IF(CMIN.LT.CFUNTN) CFUNTN=CMIN
   40 IF(CFUNTN.LT.CMIN) MCR=I
      IF(CFUNTN.LT.CMIN) NCR=NC1
   70 CMIN=CFUNTN
  100 CONTINUE
      RETURN
      END
```

```
      SUBROUTINE QLAMNA(A,THETA,B,K)
      DIMENSION A(4),B(4,5)
      THETE=THETA*3.14159265/180.
      S=SIN(THETE)
      C=COS(THETE)
      C4=C**4
      S4=S**4
      CS22=C*C*S*S
      CS3=C*S**3
      SC3=S*C**3
      A1=2.*(A(3)+2.*A(4))*CS22
      A2=A(1)-A(3)-2.*A(4)
      A3=A2+A(2)-A(3)
      A4=A(3)-A(2)+2.*A(4)
      B(1,K)=A(1)*C4+A1+A(2)*S4
      B(2,K)=A(1)*S4+A1+A(2)*C4
      B(3,K) = (A(1)+A(2)-4.*A(4))*CS22+A(3)*(C4+S4)
      B(4,K)=A3*CS22+A(4)*(C4+S4)
      RETURN
      END
```

```
      SUBROUTINE STIFF(A,KP,D,THICK,DIST,NL)
      COMMON /Q/ QL(4,5)
      DIMENSION A(4),KP(6),D(4),THICK(6)
      DO 50 I=1,4
      A(I)=0.0
      D(I)=0.0
   50 CONTINUE
      HK1=-DIST
      DO 100 I=1,NL
      KK=KP(I)
      HK2=HK1+THICK(I)
      HPA=HK2-HK1
      HPD=(HK2**3-HK1**3)/3.
      DO 20 K=1,4
      A(K)=A(K)+QL(K,KK)*HPA
   20 D(K)=D(K)+QL(K,KK)*HPD
      HK1=HK2
  100 CONTINUE
      RETURN
      END
```

```
      SUB  UTINE STIFFPR(T1,T2,T3,BB,H,TS,EAD,GJD,EC  1,EISD,DS,ELD,EA,B
     1AB,CHARGE,ASSS,GXYSK,GXYB)
      DIMENSION THICK(6),KP(6),A(4),D(4),EX(3),GXY(3),DS(2,4),EA(3),B(3)
      COMMON /Q/ QL(4,5)
      THICK(1)=T2
      KP(1)=5
      DIST=T2/2.
      CALL STIFF(A,KP,D,THICK,DIST,1)
      DO 1 I=1,4
    1 DS(1,I)=D(I)
      EX(2)=(A(1)*A(2)-A(3)**2)/(A(2)*T2)
      GXY(2)=A(4)/T2
      THICK(1)=T2/2.
      THICK(2)=T3
      THICK(3)=T2/2.
      DIST=(T3+T2)/2.
      KP(1)=5
      KP(2)=4
      KP(3)=5
      CALL STIFF(A,KP,D,THICK,DIST,3)
      DO 2 I=1,4
    2 DS(2,I)=D(I)
      EX(3)=(A(1)*A(2)-A(3)**2)/(A(2)*(T2+T3))
      GXY(3)=A(4)/(T2+T3)
      EZ=(QL(1,4)*QL(2,4)-QL(3,4)**2)/QL(2,4)
      EF=(QL(1,5)*QL(2,5)-QL(3,5)**2)/QL(2,5)
      EX(1)=(EZ*T1+EF*T2)/(T1+T2)
      GXY(1)=(QL(4,4)*T1+QL(4,5)*T2)/(T1+T2)
      BETA=ATAN(.1*BB/H)
      TAVG=(TS+T1+T2)/2.
      B(1)=.4*BB
      B(2)=(H-TAVG)/COS(BETA)
      B(3)=.8*BB
      ASSS=B(1)*(T1+T2)*2.+2.*B(2)*T2+B(3)*(T2+T3)
      BAB=B(2)
      EA(1)=EX(1)*B(1)*(T1+T2)
      EA(2)=EX(2)*B(2)*T2
      EA(3)=EX(3)*B(3)*(T2+T3)
      EAA=2.*EA(1)+EA(2)*2.+EA(3)
      ZBAR=(2.*EA(1)*TAVG+EA(2)*(H+TAVG)+EA(3)*H)/EAA
      ZBAR=ZBAR*CHARGE
      EIC=(EX(1)*B(1)*(T1+T2)**3)/6.+(EX(2)*T2*(B(2)*COS(BETA))**3
```

```
     1 )/(6.*COS(BETA))+(EX(3)*B(3)*(T1+T3)**3)/12.   +2.*EA(1)*TAVG**2
     2 +2  EA(2)*((H+TAVG)/2.)**2 + EA(3)*H**2
      GJ2=B(2)/(T2*GXY(2))
      GJ3=B(3)/((T2+T3)*GXY(3))
      GJ4=BB/(TS*GXYSK)
      GJ4=0.
      GJ=(4.*(.9*BB*H)**2)/(2.*GJ2+GJ3+GJ4)+(2.*B(1)*(T1+T2)**3/3.)*GXY
     1  (1)
      GXYB=GXY(2)*T2*(.3*BB+H*TAN(BETA))/(.8*BB+H/COS(BETA))
      EAD=EAA/ELD
      GJD=GJ/ELD
      EISD=EIC/ELD
      ECECK1=EAD*ZBAR
      RETURN
      END
```

```
      SUBROUTINE STRAIN (THETA,EPSLX,EPSLY,EPSL1,EPSL2,GAMA12)
      COMMON /AESOPD/ ADATA(5000)
      REAL ALPHA(20)
      EQUIVALENCE(ADATA(742),ALPHA)
      THETE=3.14159265*THETA/180.
      C=COS(THETE)
      S=SIN(THETE)
      CC=C*C
      SS=S*S
      CS=C*S
      EPSL1=CC*EPSLX+SS*EPSLY
      EPSL2=SS*EPSLX+CC*EPSLY
      GAMA12=2.*(-CS*EPSLX+CS*EPSLY)
      RETURN
      END
```

```
      SUB' UTINE OUTPUT(FUNCTN,ALPHA,ISTOP1,ISTOP2,'  R,RO,ANX)
C  THIS SUBROUTINE OUTPUTS THE OPTIMIZAION RESULTS
      DIMENSION FUNCTN(100),ALPHA(100)
    1 FORMAT(1H1)
    2 FORMAT(* OPTIMIZATION RESULTS FOR UNSTIFFENED CYLINDER*)
    3 FORMAT(* OPTIMIZATION RESULTS FOR STIFFEN CYLINDER WITH NO RING*)
    4 FORMAT(* OPTIMIZATION RESULTS FOR STIFFENED CYLINDER*)
    5 FORMAT(* BUCKLING CONSTRAINT VOILATIONS, GROSS, PANEL,SKIN BUCKL*)
    6 FORMAT(* LOCAL BUCKLING CONSTRAINT VOILATIONS OF STIFFNERS*)
    7 FORMAT(* LOCAL BUCKLING CONSTRAINT VOILATIONS OF RINGS*)
    8 FORMAT(1H0)
    9 FORMAT(//1X,5F22.6/)
   10 FORMAT(* CONSTRAIN VOILATIONS FOR STRAINS, EPSL1(I),EPSL2(I),GAMA1
     12(I)*)
   11 FORMAT(* TBAR/R=*,F8.5,5X,*NX/R=*,F8.3,5X,*TBARD/R=*,E15.8)
   12 FORMAT(* ALPHA1=*F5.1,3X,*ALPHA2=*,F5.1,3X,*ALPHA3=*,F5.1,3X,* T1=
     1*,F6.4,3X,*T2=*,F6.4,3X,*T3=*,F6.4)
   13 FORMAT(* T1S=*,F6.4,3X,*T2S=*,F6.4,3X,*T3S=*,F6.4,3X,*BS=*F5.2,3X,
     2*HS=*,F5.2,5X,*ELS=*,F6.2)
   14 FORMAT(* T1R=*,F6.4,3X,*T2R=*,F6.4,3X,*T3R=*,F6.4,3X,*BR=*,F5.2,3X
     2,*HR=*,F5.2,5X,*ELR=*,F6.2)
   15 FORMAT(* NX=*,F8.3,5X,*L=*,F8.3,5X,*R=*,F8.3)
      PRINT 1
      IF(ISTOP1.AND.ISTOP2.EQ.1)PRINT 2
      IF(ISTOP1.EQ.0)PRINT 4
      IF(ISTOP2.EQ.0)PRINT 3
      PRINT 8
      PRINT 15,ANX,EL,R
      PRINT 8
      PRINT 5
      PRINT 9,(FUNCTN(I),I=1,3)
      PRINT 8
      IF(ISTOP1.EQ.0)PRINT 6
      IF(ISTOP1.EQ.0) PRINT 9,(FUNCTN(I),I=4,6)
      IF(ISTOP1.EQ.0) PRINT 8
      IF(ISTOP2.EQ.0)PRINT 7
      IF(ISTOP2.EQ.0) PRINT 9,(FUNCTN(I),I=7,9)
      IF(ISTOP2.EQ.0) PRINT 8
      PRINT 10
      PRINT 9,(FUNCTN(I),I=10,14)
      PRINT 9,(FUNCTN(I),I=15,19)
      PRINT 9,(FUNCTN(I),I=20,24)
```

```
      TBAR=FUNCTN(25)/(2.*3.14159265*R*EL)
      ENXR=ANX/R
      TR=TBAR/R
      TRD=TR*RO
      PRINT 8
      PRINT 8
      PRINT 12,(ALPHA(I),I=1,6)
      PRINT 8
      IF(ISTOP1.EQ.0)PRINT 13,(ALPHA(I),I=9,13),ALPHA(7)
      IF(ISTOP1.EQ.0) PRINT 8
      IF(ISTOP2.EQ.0)PRINT 14,(ALPHA(I),I=14,18),ALPHA(8)
      IF(ISTOP2.EQ.0) PRINT 8
      PRINT 8
      PRINT 11,TR,ENXR,TRD
      PRINT 1
      RETURN
      END
```

APPENDIX B

MODIFIED STIFFNESS MATRICES

FOR USE OF BUCLAP 2

SECTION B

EFFECTS OF BOUNDARY CONDITIONS
ON THE BUCKLING OF AXIALLY
COMPRESSED CYLINDRICAL SHELLS*

* This section will form the basis for a paper to be submitted for publication in the AIAA Journal.

Modified stiffness matrices for BUCLAP 2 to include the effect of stiffners and eccentricity

BUCLASP 2 requires the input of [A], [B] and [D] matrices (see Ref. 6 for definitions) which, for the present problem, are given by

$$[A] = \begin{bmatrix} A_{11} + \frac{EA}{\ell}_s & A_{12} & 0 \\ A_{12} & A_{22} + \frac{EA}{\ell}_r & 0 \\ 0 & 0 & A_{66} \end{bmatrix}$$

$$[B] = \begin{bmatrix} -\frac{EA}{\ell}z_s & 0 & 0 \\ 0 & -\frac{EA}{\ell}z_r & 0 \\ 0 & 0 & 0 \end{bmatrix}$$

$$[D] = \begin{bmatrix} D_{11} + \frac{EI_o}{\ell}_s & D_{12} & 0 \\ D_{12} & D_{22} + \frac{EI_o}{\ell}_r & 0 \\ 0 & 0 & D_{66} + \frac{1}{4}\left\{\left(\frac{GJ}{\ell}\right)_s + \left(\frac{GJ}{\ell}\right)_r\right\} \end{bmatrix}$$

1. INTRODUCTION

1.1 PRELIMINARY CONSIDERATIONS

The literature is replete with inverstigations devoted to the buckling of unstiffened, isotropic, complete cylindrical shells under axial compression. In contrast, relatively little attention has been focused on the corresponding buckling problem for cylindrical panels. However, unstiffened, isotropic cylindrical panels are frequently employed in a vast number of structures, such as, for example, in launch vehicles. Furthermore, knowledge of panel buckling loads is needed for consideration of the local panel buckling modes in the analysis and minimum-weight design of stringer stiffened cylindrical shells. Therefore, the present paper is devoted to a study of the buckling behavior of unstiffened, elastic, isotropic, cylindrical panels. The loading condition of uniform axial compression is chosen as this condition is often the critical one, especially in aerospace applications. Buckling loads are presented for panels with eight sets of boundary conditions along the straight edges of the panel. Four sets are considered for both simply supported ($w = M_y = 0$) and clamped ($w = w_{,y} = 0$) straight edges. The eight sets of boundary conditions are designated by SS1, .., SS4, CC1, .., CC4 and are defined below. The boundary conditions for the simply supported straight edges are

$$\begin{array}{lcl} \text{SS1} & : & w = M_y = N_{xy} = N_y = 0 \\ \text{SS2} & : & w = M_y = N_{xy} = v = 0 \\ \text{(classical) SS3} & : & w = M_y = u = N_y = 0 \\ \text{SS4} & : & w = M_y = u = v = 0 \end{array} \qquad (1)$$

The corresponding boundary conditions for the clamped straight edges are

$$
\begin{array}{llll}
CC1 & : & w = w_{,y} = N_{xy} = N_y = 0 & \\
CC2 & : & w = w_{,y} = N_{xy} = v = 0 & \quad (2) \\
CC3 & : & w = w_{,y} = u = N_y = 0 & \\
CC4 & : & w = w_{,y} = u = v = 0 &
\end{array}
$$

In these equations, u, v, w and N_y, N_{xy}, M_y are, respectively, incremental displacements and stress resultants that take place during buckling. Their positve directions are shown in Figs. 1 and 2 along with the other stress resultants considered herein. Different sets of boundary conditions along the curved edges of the panel will not be considered here since it seems reasonable to conjecture, as was done in Ref. 1, that the qualitative effects of these boundary conditions should not differ appreciably from those found for complete cylinders, which have been thoroughly documented in the literature. Therefore, only one set of boundary conditions for the curved edges is considered herein; namely "classical" simple support edge conditions defined by

$$w = M_x = N_x = v = 0 \qquad (3)$$

1.2 PREVIOUS INVESTIGATIONS

Analyses of the axial buckling behavior of cylindrical panels have been performed in a number of references. The references cited herein pertain to long and narrow panels analyzed by Donnell-type shell theory. In all cases, the effects of prebuckling deformations are omitted and the only non-zero prebuckling stress resultant is the axial one, N_{xo}, which is assumed to be constant. The effects of initial imperfections are not considered. A brief discussion of the results of some of the other investigations follows.

Marguerre (Ref. 2) presented solutions for panels with the following types of edge conditions: SS2, SS3, SS4, CC2, and CC3. The solutions are approximate except for the case of classical simple support conditions, SS3, for which the following closed form solution was obtained (also presented in Refs. 3-5):

$$N_{xo} = \begin{cases} (N_x)_{pl}\,(1 + \frac{K^2}{4}) = (N_x)_{pl} + \frac{1}{4}\,\frac{(N_x)^2_{cyl}}{(N_x)_{pl}}\,, & K < 2 \\[2ex] (N_x)_{cyl}\,, & K \geq 2 \end{cases} \tag{4}$$

In this equation, N_{xo} is the panel buckling load; $(N_x)_{pl}$ is the classical uniaxial compressive buckling load for a long flat plate with simple support conditions on the long unloaded edges, i.e.,

$$(N_x)_{pl} = \frac{\pi^2 E}{3(1-\nu^2)}\,(\frac{h^3}{b^2}) \tag{5}$$

where h and b are the plate thickness and width, respectively, E is Young's modulus, and ν is Poisson's ratio; $(N_x)_{cyl}$ is the classical axial compressive buckling load for a long complete cylinder, i.e.,

$$(N_x)_{cyl} = \frac{E}{[3(1-\nu^2)]^{1/2}}\,(\frac{h^2}{a}) \tag{6}$$

where a is the radius of the cylinder and h is its thickness; K is a panel curvature parameter defined by

$$K = \frac{(N_x)_{cyl}}{(N_x)_{pl}} = \frac{1}{\pi^2} [3(1-\nu^2)]^{1/2} \left(\frac{b^2}{ah}\right)$$
$$= \frac{1}{\pi^2} [3(1-\nu^2)]^{1/2} \left(\frac{a}{h}\right) \phi_o^2 \qquad (7)$$

where (see Fig. 1) a is the radius of the panel, h is the panel thickness, ϕ_o is the central angle of the panel, and $b = a\phi_o$ is the panel width. With regard to Eq. (4) it is noted that Sullins, Smith, and Spier (Ref. 6), employed this equation, referred to therein as the "Schapitz criterion", in conjunction with a "knockdown" factor (from Ref. 7) for $(N_x)_{cyl}$ and obtained a design curve which provided a rather close lower bound to experimental results for unstiffened isotropic cylindrical panels.

For all sets of boundary conditions, Marguerre's numerical results show that the panel buckling loads tend to monotonically approach a lower bound asymptote, which is the complete cylinder buckling load, as the curvature parameter K is increased. For the range of K values considered, namely $K \leq 9$, the complete cylinder buckling load was actually reached only for the classical simple support set of boundary conditions, SS3, for which $N_x = (N_x)_{cyl}$ for $K \geq 2$, as shown by Eq. (4).

Rehfield and Hallauer (Ref. 8) presented buckling loads appropriate to the eight sets of boundary conditions defined by Eqs. (1) and (2). Thus, in addition to the panels studied by Marguerre, Ref. 8, considered SS1, CC1 and CC4 panels. With the assumptions of a linear membrane prebuckling solution and sinusoidal axial buckling modes, the partial differential equation governing the buckling problem were reduced to a set of ordinary linear differential equations with constant coefficients and "exact" results were obtained in a straight forward manner through an iterative numerical solution of a transcendential eigenvalue equation. The solutions of Ref. 8 are based on the assumption that $N_{xo} \geq (N_x)_{cyl}$. This assumption was imposed to insure that the roots of a characteristic equation would always be real or purely imaginary, but never complex. As a consequence of this assumption, the results of Ref. 8 are somewhat incomplete for certain cases, as will be discussed in what follows.

The results presented by Rehfield and Hallauer are replotted* in Fig. 3 using a different ordinate, namely the non-dimensional load parameter

$$\rho = \frac{N_{xo}}{(N_x)_{cyl}} \tag{8}$$

Note that buckling loads for the cases SS2 and CC2 are not shown since, to the scale of Fig. 3, they are always close to the buckling loads for SS4 and CC4 panels, respectively. For SS2, SS4, CC2, CC3 panels, Marquerre's (Ref. 2) approximate results are in close agreement with the exact results obtained by Rehfield and Hallauer. For SS3 panels the results of Refs. 2 and 8 are identical.

* Ref. 8 plots $N_{xo}/(N_x)_{pl}$ against K and shows complete curves for the range of K from K = 0 to K = 5.

For SS3 panels, it is seen from Fig. 3 that the complete cylinder buckling load is achieved for a relatively small value of the curvature parameter, namely $K = 2$ (see also Eq. (4)), at which the slope of the ρ - K curve is horizontal. This is hardly surprising since the SS3 boundary conditions ($w = M_y = N_y = u = 0$) are precisely the conditions satisfied on axial nodal lines of the nonsymmetric buckle pattern of the complete cylinder. Thus, for $K \geq 2$, the panel is sufficiently wide to permit the formulation of one of the (infinite number of) buckle patterns that are possible for the complete cylinder at the classical cylinder load (Eq. (6)). It is also interesting to note that it can be shown that $K = 2$ corresponds to a panel width b equal to a full wave length appropriate to the axi-symmetric buckling mode of the complete cylinder at $(N_x)_{cyl}$ (see Ref. 3). For CC1 panels, $\rho = 1$ was reached within the small range of K values considered in Ref. 8. Hallauer (Ref. 5) give the following closed form solution for CC1 panels:

$$\rho = \frac{B_\infty}{K} + \frac{K}{4B_\infty} \quad , \qquad K \leq 2B_\infty \tag{9}$$

where

$$B_\infty = 1.7428 \tag{10}$$

is the uniaxial buckling coefficient for infinitely long flat plates with clamped unloaded long edges (Ref. 3). For $K > 2B_\infty$, Hallauer;

on the one hand states that $\rho = 1$, and, on the other hand, points out that in view of some low buckling loads obtained for SS1 panels (see Pope's results in Fig. 3), that there is a possibility that the CC1 panels have solutions $\rho < 1$ for $K > 2B_\infty$. However, Eq. (9) shows that the $\rho_{CC1} - K$ curve (see also Fig. 3) has a horizontal tangent at $K = 2B_\infty$ which strongly suggest that $\rho_{CC1} = 1$ for all $K > 2B_\infty$ (as will be demonstrated in the present paper). For all other cases (with the exception of SS1), the curves in Fig. 3 tend to suggest that $\rho \to 1$ asymptotically with increasing K. Now one would expect intuitively, perhaps, that the buckling load for a sufficiently wide panel ($\phi_o \leq 2\pi$), with appropriate support conditions along the straight edges, should not differ appreciably from the buckling load of the corresponding complete cylinder. The results of Ref. 8, since they are limited to rather narrow panels. ($K \leq 5$)* cannot predict in all cases the value of ϕ_o above which the panel and cylinder buckling loads coincide. The behavior of ρ with increasing and arbitrary K will be studied in the present work.

Figure 3 also shows the results obtained by Rehfield and Hallauer for SS1 panels. As may be seen from the figure, their SS1 results are restricted to the very narrow curvature range $K \leq 1.2$ for which $\rho \geq 1$, in accordance with their analysis assumption previously mentioned. The non-zero slope of the $\rho_{SS1} - K$ curve in the neighborhood

---

* For, say, $a/h = 600$, $K = 5$ corresponds to panel central angle ϕ_o 14°.

of $\rho = 1$ and $K = 1.2$ suggests that $\rho_{SS1} < 1$ for larger values of K. That this is the case is confirmed by the unconnected points shown in Fig. 3. These points are bifurcation buckling points that were taken from Pope's (Ref. 9) postbuckling curves for long and narrow SS1 panels. Rehfield and Hallauer used these points to extrapolate their SS1 results (see Ref. 8, Fig. 2) into the larger K region for which $\rho_{SS1} < 1$. Thus, Pope's limited number of SS1 results, show, perhaps somewhat surprisingly, that the panel buckling loads are less than the complete cylinder buckling loads, except for the relatively extremely narrow panels ($K \leq 1.2$). The smallest value of the non-dimensional load parameter obtained from Pope's SS1 results is $\rho \approx .6$ for $K \approx 2.8$. However, the trend of Pope's results with increasing K suggests that an even lower value of ρ will be realized for a larger value of K. The existence of such low panel buckling loads is somewhat analogous to the well known low buckling loads for simply supported complete cylinders with no circumferential constraint ($v \neq 0$, $N_{xy} = 0$, "weak in shear" boundary condition) on the curved edges. For that case, the cylinder buckling load is approximately one-half (Refs. 10-12) of the classical cylinder buckling load (for which $w = M_x = N_x = v = 0$). However, for the complete cylinder, the "weak in shear" boundary condition rarely occur in practice (Ref. 13), whereas, in contrast, the SS1 panel is of some practical interest since free "in-plane" movement of the straight edges can be simulated experimentally. Also of interest for the SS1 panels is whether the SS1 panel load ever reaches the full cylinder buckling load for sufficiently large K with $\phi_o \leq 2\pi$. This will also be investigated herein.

1.3 SCOPE OR PRESENT INVESTIGATION

In view of the above discussion, it seems desirable to perform a comphrensive analysis that covers the complete range of panel widths ($0 \leq \phi_o \leq 2\pi$). This is the aim of the present paper. Buckling loads and mode shapes will be presented for panels with the eight sets of boundary conditions defined in Eqs. (1) and (2). The panels will not necessarily be assumed to be long; buckling loads will be generated for different L/a values. The results will be based on both Donnell-type linear shell theory and a more complete shell theory. As was also employed in the previously cited references, a linear membrane analysis is used for the prebuckling solution and the effects of initial inferfections are not considered. The "exact" results presented herein were obtained from the BUCLASP 2 computer program (see Appendix A).

2. NUMERICAL RESULTS AND PARAMETRIC STUDIES

The present investigation is aimed at locating the critical angle, ϕ_{cr}, where ϕ_{cr} is the smallest value of ϕ for which the panel axial buckling load is identical with that of the complete cylinder. Studying of the influence of the different combinations of in-plane boundary conditions along the straight edges of the panel, namely SS1 to SS4 and CC1 to CC4 (Equations (1) & (2)) on the location of ϕ_{cr} and the panel critical axial loads. Parametric studies on the effect of panel geometry, (L/a) and (a/h) on the critical load and verification of the existance of a panel geometry parameter $K = (1/\pi^2)[3(1-\nu^2)]^{1/2}(b^2/ah) = (1/\pi^2)[3(1-\nu^2)]^{1/2}(a/h)\phi_o^2$, analog to the Batdorf shell curvature parameter $Z = \sqrt{1-\nu^2}\,(L^2/R_h)$, which has been defined in References 5 and 8.

A main shell geometry, the so called "MARSHALL unstiffened Cylinder", has been chosen for the present thorough investigations. The dimensions and properties of this shell are as follows:

$L = 94"$; $a = 60"$; $h = .1"$; $E = 10^7$ p.s.i. and $\nu = 1/3$ ($L/a = 1.567$; $a/h = 600$)

For the parametric studies L/a has been changed to .1 and 5.0 and a/h to 100 and 2000, thus allowing studies with short and long panels as well as thick and thin ones.

In Figures 4A and 4B, the ratio of panel buckling load over the complete cylinder buckling load, $\rho = N_{x_o}/(N_x)_{cyl}$ (obtained by BUCLASP for Donnell type analysis), versus the panel angle, ϕ, is shown for the "MARSHALL" type panel. Figure 4A shows the influence of the SS type boundary conditions and Figure 4B that of the CC type boundary conditions. It is seen from these figures that the most effective in-plane restraint is $\mathcal{N}=0$ along the straight edges of the panel resulting in higher and almost identical loads for the SS2 and SS4 as well as CC2 and CC4 boundary conditions. However, Figure 4B reveals that the CC curves are closer together than the SS curves in Figure 4A, which indicates that the in-plane boundary conditions are more influential for the SS type boundary conditions. Also, the prevention of out of plane edge rotation dominates and hence is more important than the condition $\mathcal{N}=0$.

It can also be observed in Figure 4B that for narrow panels, clamping of the straight edges results in higher critical loads than for simply supported edges.

It is observed in Figures 4B that in the case of CC boundary conditions, all of the curves approach $\rho=1$, the complete cylinder buckling load from above and the smallest value of ϕ_{cr} is observed for the CC1 boundary conditions with $\phi_{cr} \approx 10°$. It is seen from this figure, that ϕ_{cr} varies in the range, $10 \lesssim \phi_{cr} \lesssim 20$ for all of the sets of in-plane boundary conditions. In contrast, Figure 4A shows that in the case of SS boundary conditions only SS2 to SS4 approach the complete cylinder critical load from above whereas the SS1 boundary conditions are poorly behaved; cut the line $\rho=1$ at about $\phi \approx 6.5°$, decrease to a minimum of $\rho \approx .465$ for $\phi \approx 25.0$ and then increase to approach an asymptotic value of $\rho \approx .819$ rather than $\rho=1$. This behavior is qualitatively similar to that experienced for "lightly" stringer-stiffened shells (Reference 14) with weak in-shear in-plane boundary conditions. Conclusively, the poorly behaved set SS1 boundary conditions makes the CC1 set much more prefferable to the experimentalist, but of course he would have to guarantee the prevailing of the CC1 boundary conditions. This also calls for the analysis of the combined effect of out of plane rotational springs together with the different sets of in-plane boundary conditions on the panel critical load.

The critical loads were calculated with the aid of BUCLASP both for Donnell and Flugge type stability equations and the results are presented in Table 1 of Appendix B. It can be observed in this Table that the results obtained by Flugge type equations are close to the ones discussed above, with the following exceptions: the CC1 boundary conditions also reveal a tendency to approach the critical value from below, but with a value of ρ very close to $\rho = 1$, only the SS3 boundary conditions approach the value $\rho=1$ from above whereas SS2, SS4 and CC2 to CC4 approach a value of ρ slightly above $\rho=1$ and hence there is actually no existance of ϕ_{cr} for these sets of boundary conditions. It is also seen that for a panel with $\phi=360°$, Donnell type analysis predicts an axially multiwave buckling mode (excluding SS1) whereas Flugge type analysis predicts half a single wave mode.

In Tabels 2 to 5 of Appendix B, the calculated results for a/h = 100; a/h = 2000, L/a = .1 and L/a = 5.0 are presented respectively.

Plotting of the results for the "thick" panel (a/h) = 100 in a similar manner to Figures 4A and 4B show that the in-plane boundary conditions are less effective for this type of panels - almost no effect for the clamped boundary conditions and less influence of the SS3 boundary conditions when compared with the SS2 and SS4 boundary conditions. The SS1 boundary conditions behave similary to the "MARSHALL" type panels. The discussion on the correlation of the Donnell and Flugge buckling loads applies also for this type of panels, except for the very narrow panels with SS1 and CC1 boundary conditions. It is found that the Flugge type analysis results in an in-plane Euler buckling load not included in Donnell type analysis. Hence the Flugge critical loads are much lower than the Donnell ones and it can be shown that when this mode becomes critical for a "thick" panel, the second Flugge buckling load corresponds to the Donnell critical load for the same panel. In the CC1 case there are no "pure" Euler modes because clamping along the straight edges imposes the condition $v=-w,_{\phi}$.

The results for the thin panels, a/h = 2000 - Table 3 of Appendix B-reveal that these panels behave very similar to the "Marshall" type panels, abrupt curves obtained for this except for the SS1 boundary conditions where an abrupt change in the value of ρ is noticed for $\phi=360^{\circ}$. This value of $\rho=.977$ contradicts the value of $\rho=.805$ obtained by the Flugge type analysis.

It is also found that for this type of panels, the SS1, SS3, CC1 and CC4 boundary conditions all approach $\rho=1$ from below with a value of ρ very close to unity.

Plotting the results for the short panels, L/a = .1 (See Table 4 of Appendix B) results in conclusions similar to those obtained for the "MARSHALL" type panels, except for the SS1 boundary conditions where $\rho>1$ for $\phi=360°$ and ρ does not reach the minimum values obtained for the cases discussed above. Also, results obtained by Flugge type analysis are in better agreement with the Donnell type results for this panel configurations.

From Table 5 of Appendix B it is found that for long panels, L/a = 5.0 the behavior of the panels is also similar to that of the "MARSHALL" type panels. No correlation between Flugge and Donnell buckling loads has been obtained for the 5° panel and SS1 boundary conditions. Calculations show that the Flugge critical load corresponds to an in-plane Euler buckling load, which Donnell's analysis excludes. It is also found that the CC1 curve approaches $\rho=1$ from below.

It should also be noted in Tables 1 to 5 that the results obtained with aid of BUCLASP for SS3 and CC1 boundary conditions are in excellent agreement with those obtained by the close form solution, Equations (4) and (9).

As stated previously the present paper is aimed at verifying the existance of the panel geometry parameter K of Equation (7). In Figures 5, ρ has been plotted versus K for SS boundary conditions and in Figures 6 for the CC boundary conditions. All of these figures except 5A, for the SS1 boundary conditions, indeed verify the existance of K independent of (a/h) and the panel angle, ϕ. For each set of boundary conditions a single curve is obtained. Note that the results for SS4 and CC4 boundary conditions are not included as they coincide with those for SS2 and SS4 boundary conditions respectively.

A similar study has been performed on the length effect and is presented in Figures 7 and 8. These figures reveal that only for short panels, L/a = .1, such an effect exists.

The representation of Figure 5A has not verified the existance of the unique parameter K for the SS1 boundary conditions. Hence, instead of presenting the results for this type of boundary conditions as ρ vs. K like in Figure 5A, an attempt has been made to present the results in the form $\lambda = \frac{N_{xo}}{N_{pl}}$ vs. K on a log representation. This is shown in Figure 9 and it is observed that by this kind of representation K does also become a single parameter for the SS1 boundary conditions.

REFERENCES

1. Singer, J., Meer, A., and Baruch, M., "Buckling of Cylindrical Panels Under Lateral Pressure," The Aeronautical Journal of the Royal Aeronautical Society, V. 73, Feb. 1969, p. 169-172.

2. Marguerre, K., "Uber Den Einfluss Der Lagerungsverhaltnisse Auf Die Stabilitat Gedrockter Krummer Platten," Lilienthal Gesellshfaft Fur Luftfahrtforschung, Bericht 119, July 1939.

3. Timoshenko, S.P., and Gere, J.M., "Theory of Elastic Stability," Second Edition, McGraw-Hill, 1961.

4. Schapitz, E., "Festigkeitslehre Fur Den Leichtbau," 2 Aufl., VDI G_{MB}H, Dusseldorf, 1963, pp. 206-221.

5. Hallauer, W.L., Jr., "Influence of Edge Conditions on the Buckling of Axially Compressed Cylindrical Panels," M.S. Thesis, Massachusetts Institue of Technology, 1966.

6. Sullins, R.T., Smith, G.W., and Spier, E.E., "Manual for Structural Stability Analysis of Sandwich Plates and Shells," NASA CR-1457, Dec. 1969.

7. Seide, P., and Weingarten, V., "Buckling of Thin-Walled Circular Cylinders," NASA SP-8007, 1966.

8. Rehfield, L.W., and Hallauer, W.L., "Edge Restraint Effect on Buckling of Compressed Curved Panels," AIAA Journal, Vol. 6, No. 1, pp. 187-189, Jan., 1968.

9. Pope, G.G., "On the Axial Compression of Long, Slightly Curved Panels," British A.R.C., R.&M., No. 3392, 1963.

10. Hoff, N.J., "The Effect of Edge Conditions on the Buckling of Thin-Walled Circular Cylindrical Shells in Axial Compression," Proceedings of the Eleventh International Congressor Applied Mechanics, Munchen, 1964, Springer Verlag 1966, pp. 326-321.

11. Hoff, N.J., and Rehfield, L.W., "Buckling of Axially Compressed Circular Cylindrical Shells at Stresses Smaller than the Classical Critical Value," Trans. ASME; J. Appl. Mech., Vol. 32, Series E, No. 3, pp. 542-546, Sept. 1965.

12. Almroth, B.O., "Influence of Edge Conditions on the Stability of Axially Compressed Cylindrical Shells," AIAA Journal, Vol. 4, No. 1, pp. 134-140, Jan. 1966, also NASA CR-161, Feb. 1965.

13. Singer, J., "Buckling of Integrally Stiffened Cylindrical Shells, A Review of Experiment and Theory," Contributions to the Theory of Aircraft Structures, Delft University Press, pp. 325-358, 1972.

14. Weller, T., "Further Studies on the Effect of In-plane Boundary Conditions on the Buckling of Stiffened Cylindrical Shells", TAF Report No. 120, Technion Research and Development Foundation, Haifa, Israel, January 1971.

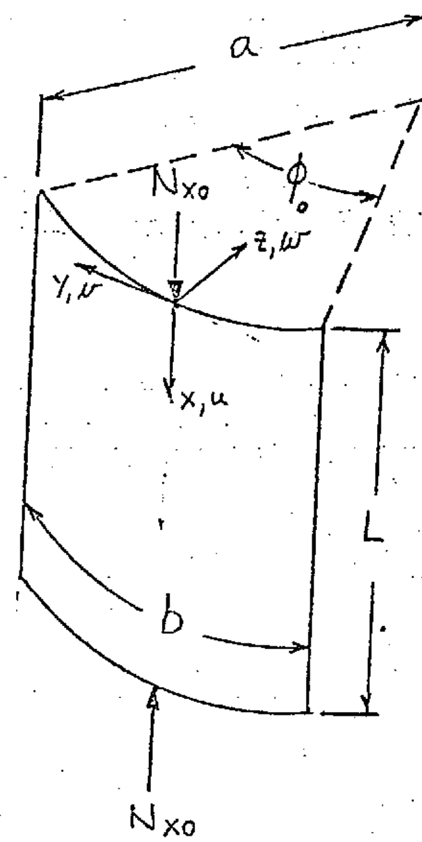

FIGURE 1 GEOMETRY, COORDINATE SYSTEM AND DISPLACEMENTS

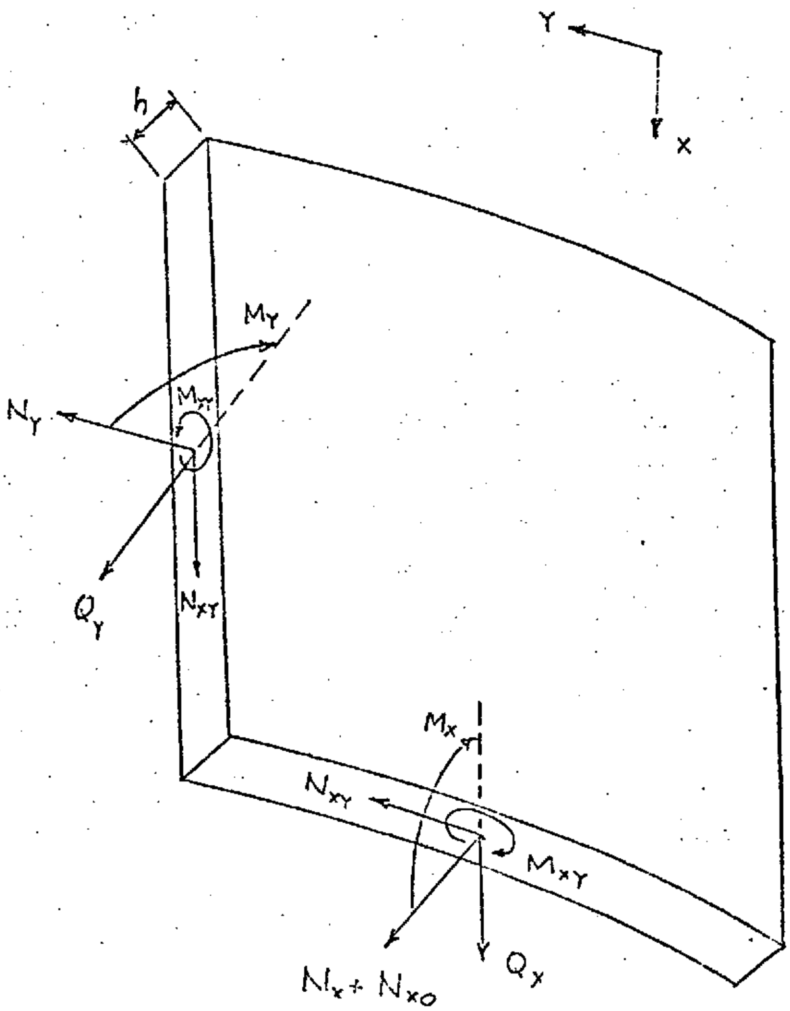

FIGURE 2 STRESS RESULTANTS

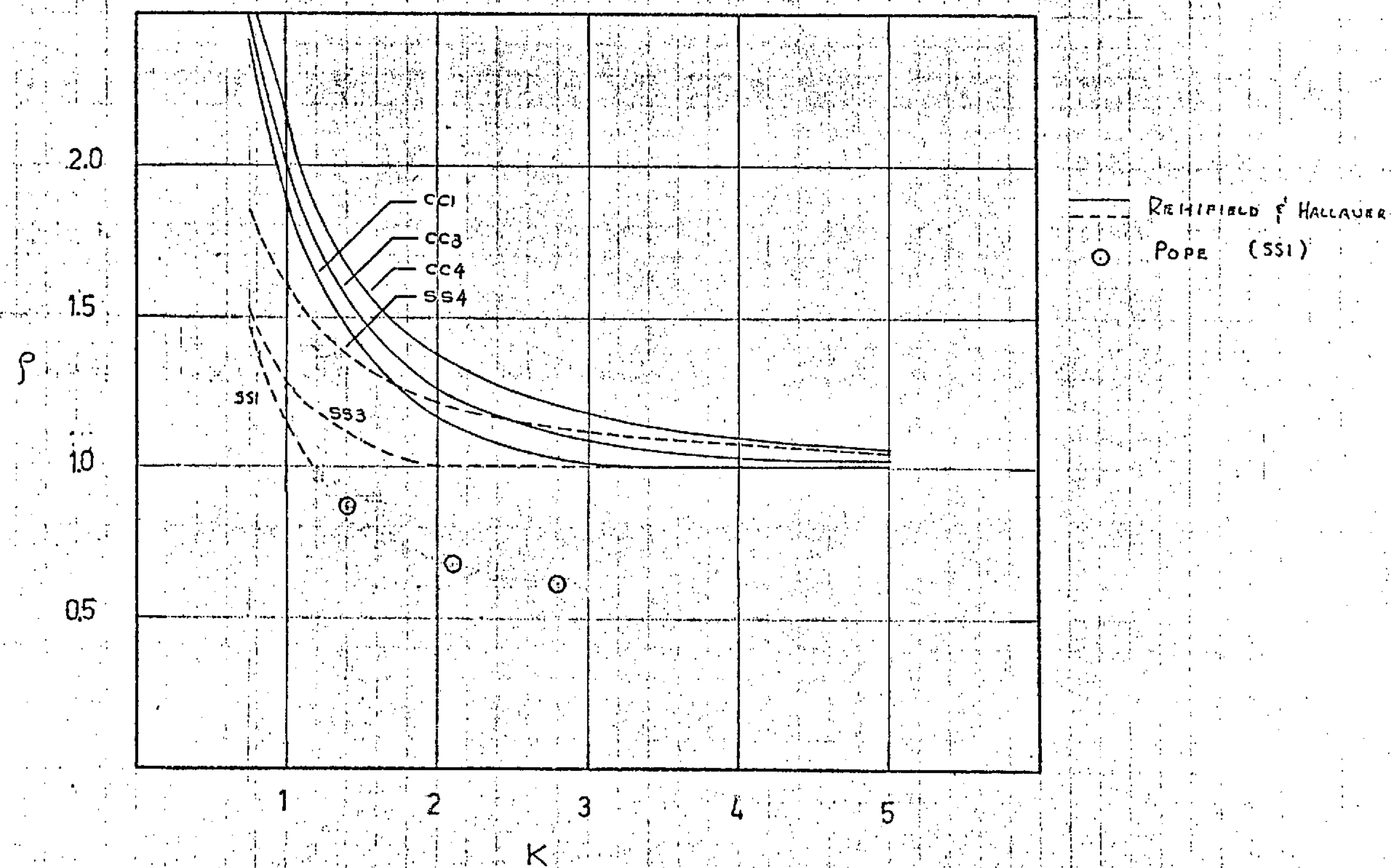

FIGURE 3 RESULTS OF OTHER INVESTIGATORS

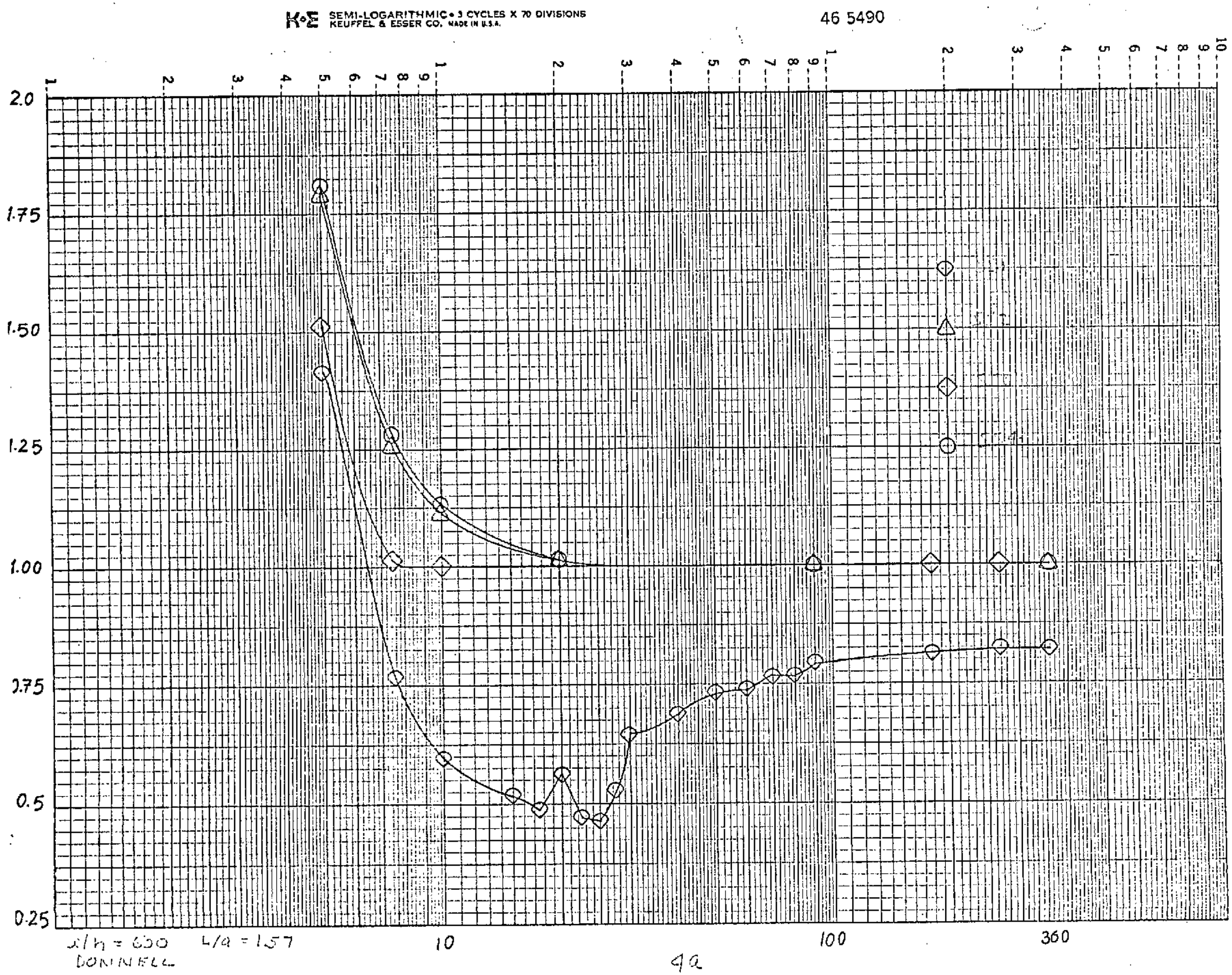

K&E SEMI-LOGARITHMIC • 3 CYCLES X 70 DIVISIONS
KEUFFEL & ESSER CO. MADE IN U.S.A.
46 5490
2.0
1.75
1.50
1.25
1.00
0.75
0.5
0.25
10
100
360
x/h = 650 L/a = 157
DONNELL
qa

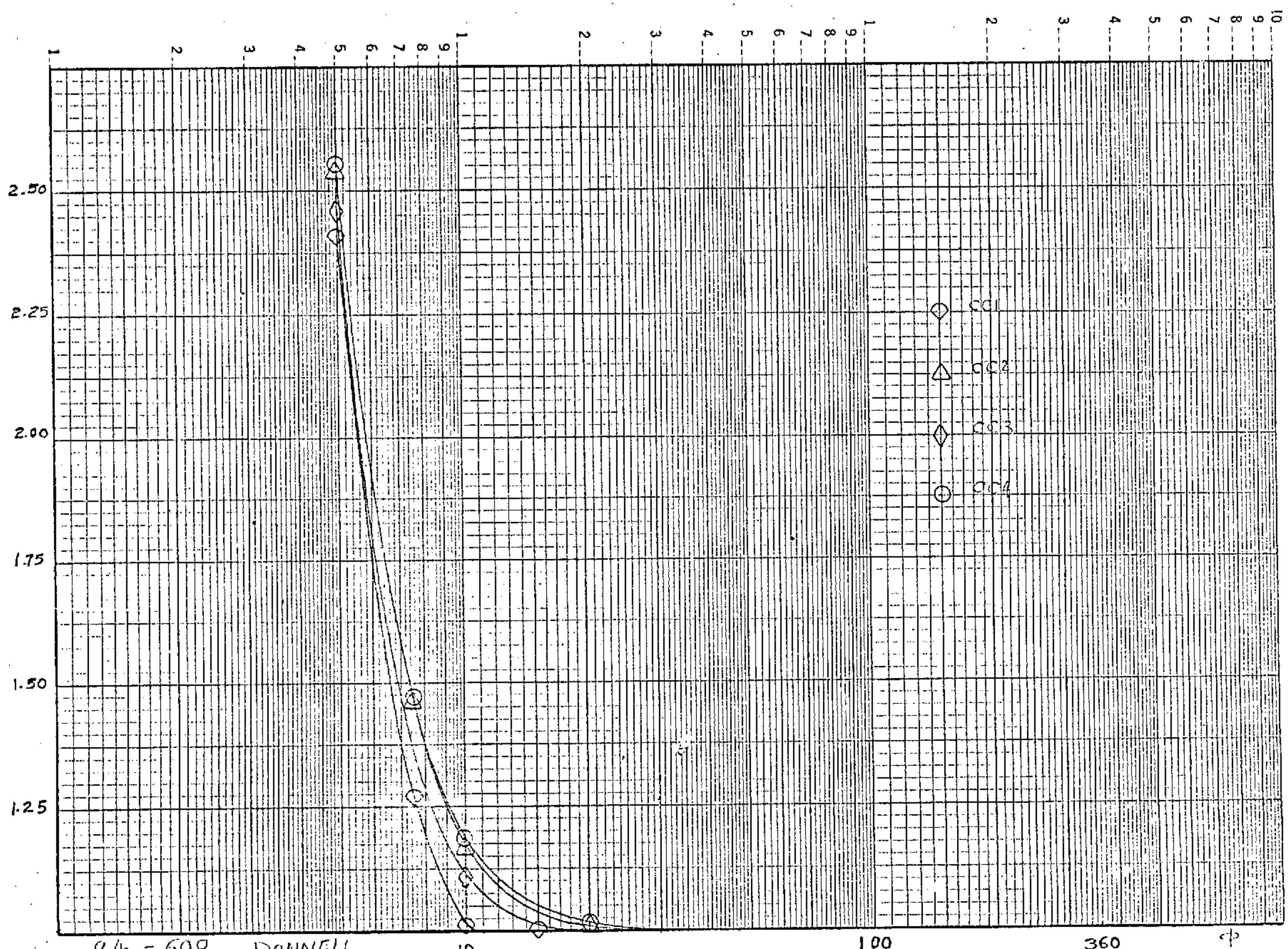

$a/h = 600$ DONNELL
$L/a = 1.57$

4 b

SSI, L/a = 1.57, DONNELL

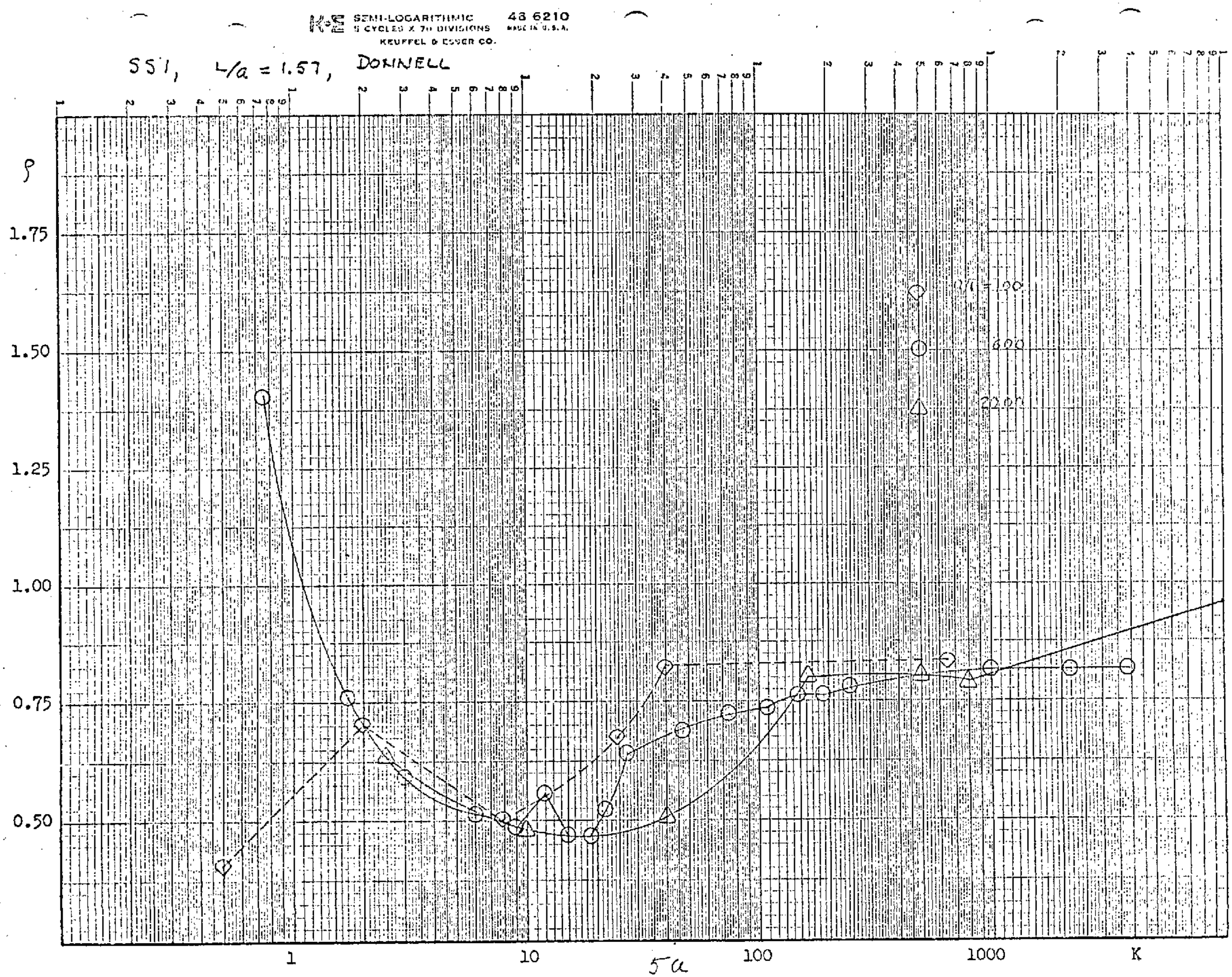

SS2, L/a = 1.57, DONNELL

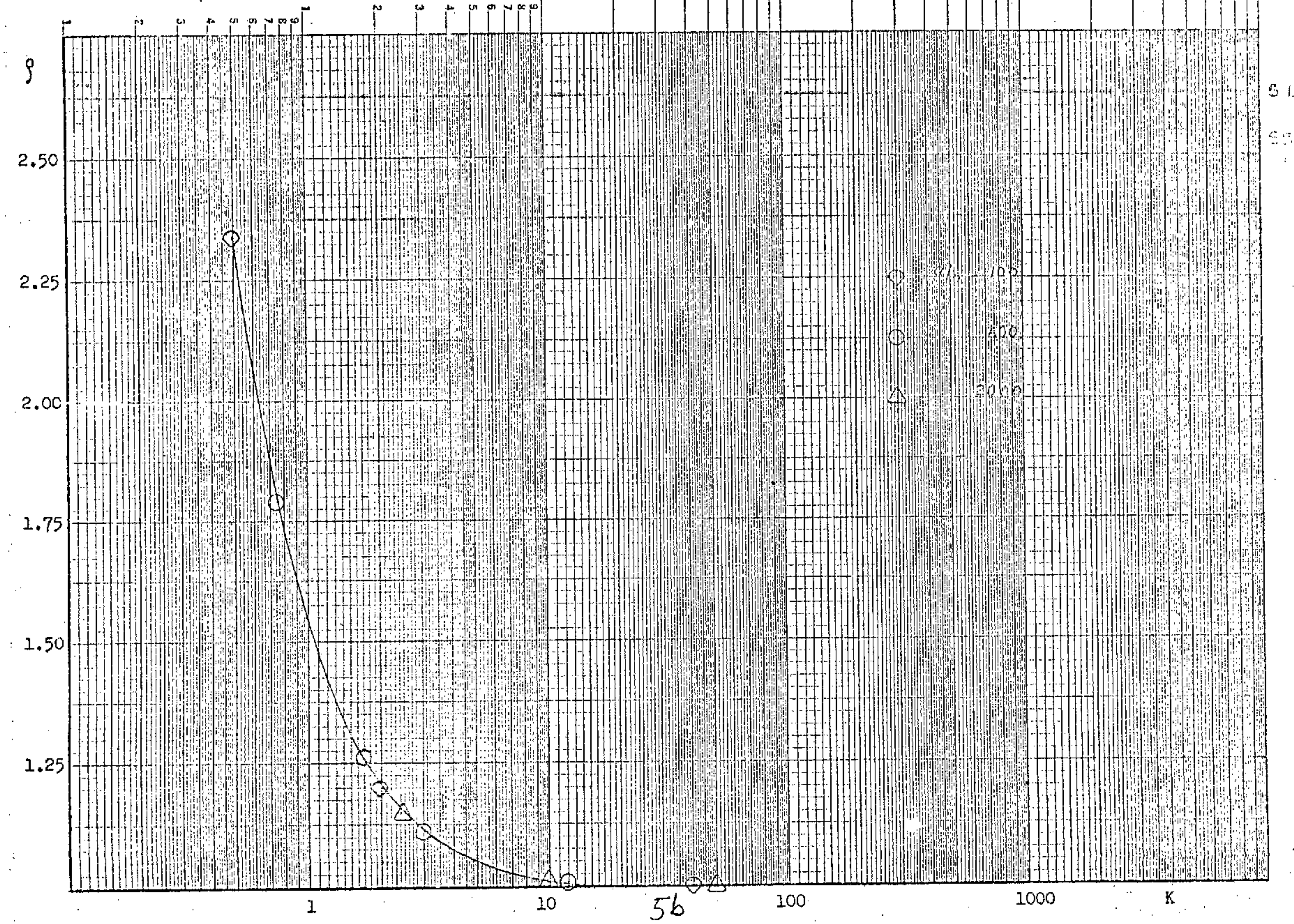

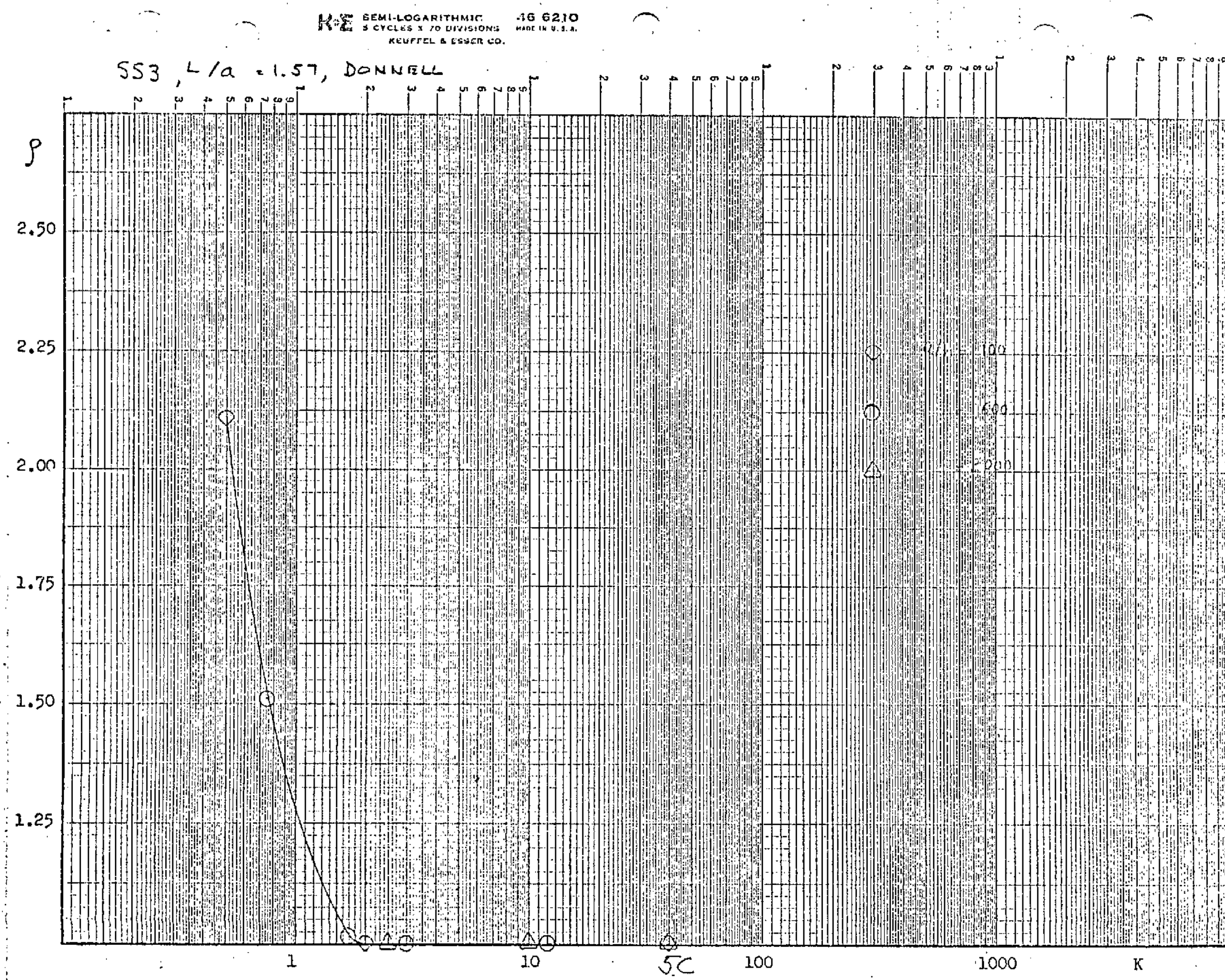
K+E SEMI-LOGARITHMIC 46 6210
5 CYCLES X 70 DIVISIONS MADE IN U.S.A.
KEUFFEL & ESSER CO.
SS3, L/a = 1.57, DONNELL
ρ
2.50
2.25
2.00
1.75
1.50
1.25
1
10
50
100
1000
K
100
600
2000

CC1 , L/a = 1.57 , DONNELL

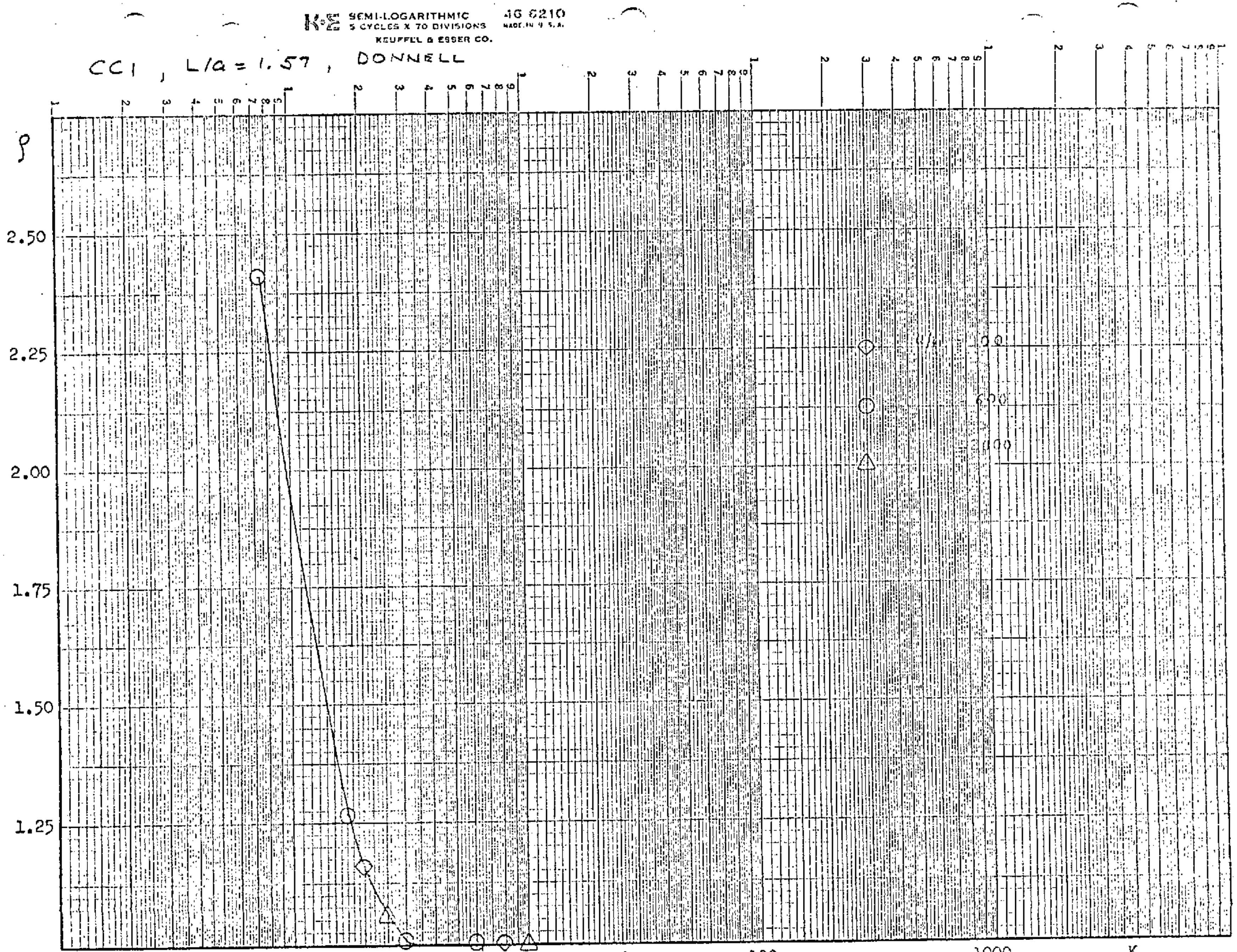

6a

CC2, L/a = 1.57, DONNELL

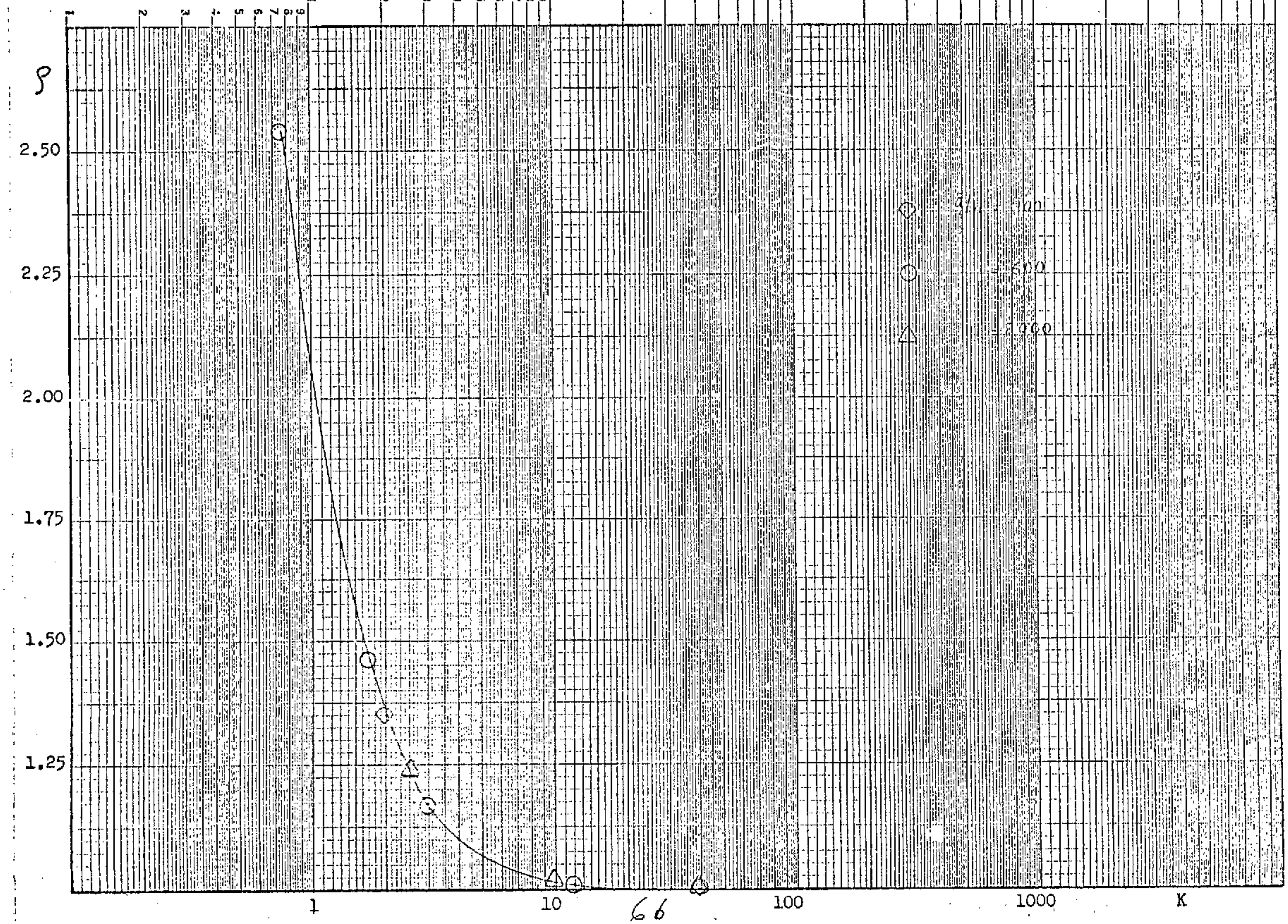

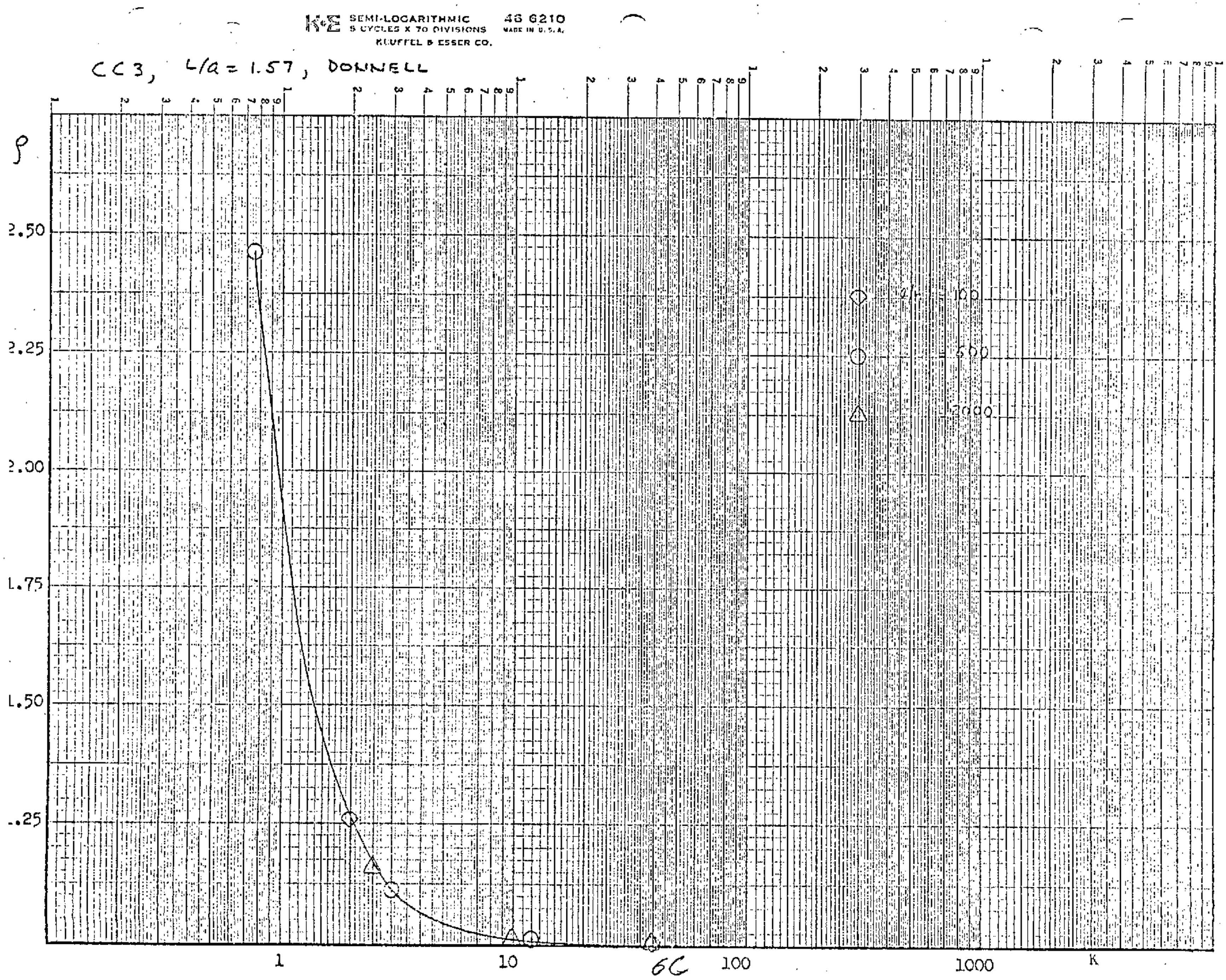
K+E SEMI-LOGARITHMIC 46 6210
5 CYCLES X 70 DIVISIONS MADE IN U.S.A.
KEUFFEL & ESSER CO.
CC3, L/a = 1.57, DONNELL
ρ
2.50
2.25
2.00
1.75
1.50
1.25
1
10
100
1000
K
6C
a/h = 100
500
2000

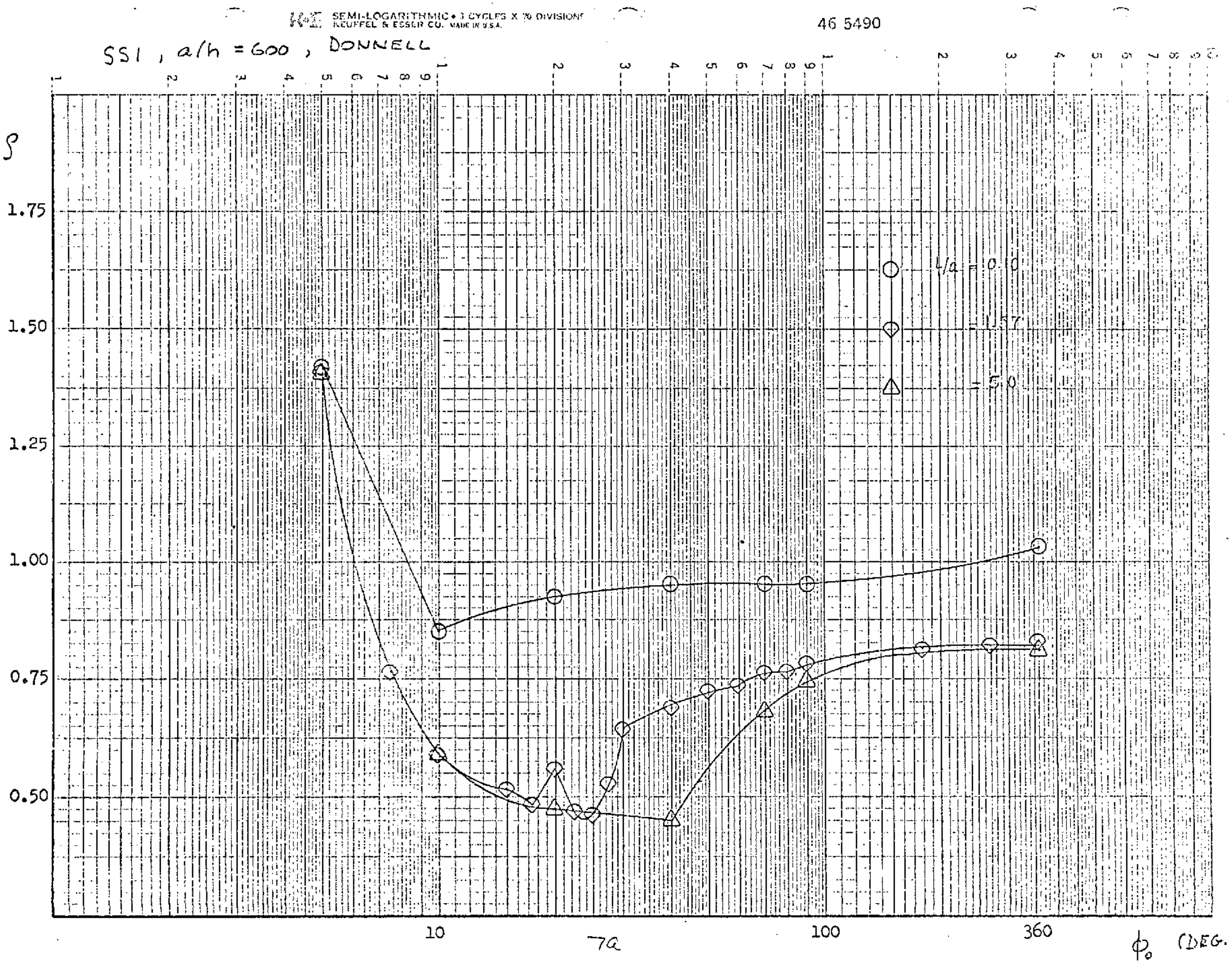
SSI , a/h = 600 , DONNELL
K+E SEMI-LOGARITHMIC 3 CYCLES X 70 DIVISIONS
KEUFFEL & ESSER CO. MADE IN U.S.A.
46 5490
ρ
1.75
1.50
1.25
1.00
0.75
0.50
10
100
360
ϕ_0 (DEG.
l/a = 0.0
= 1.57
= 5.0

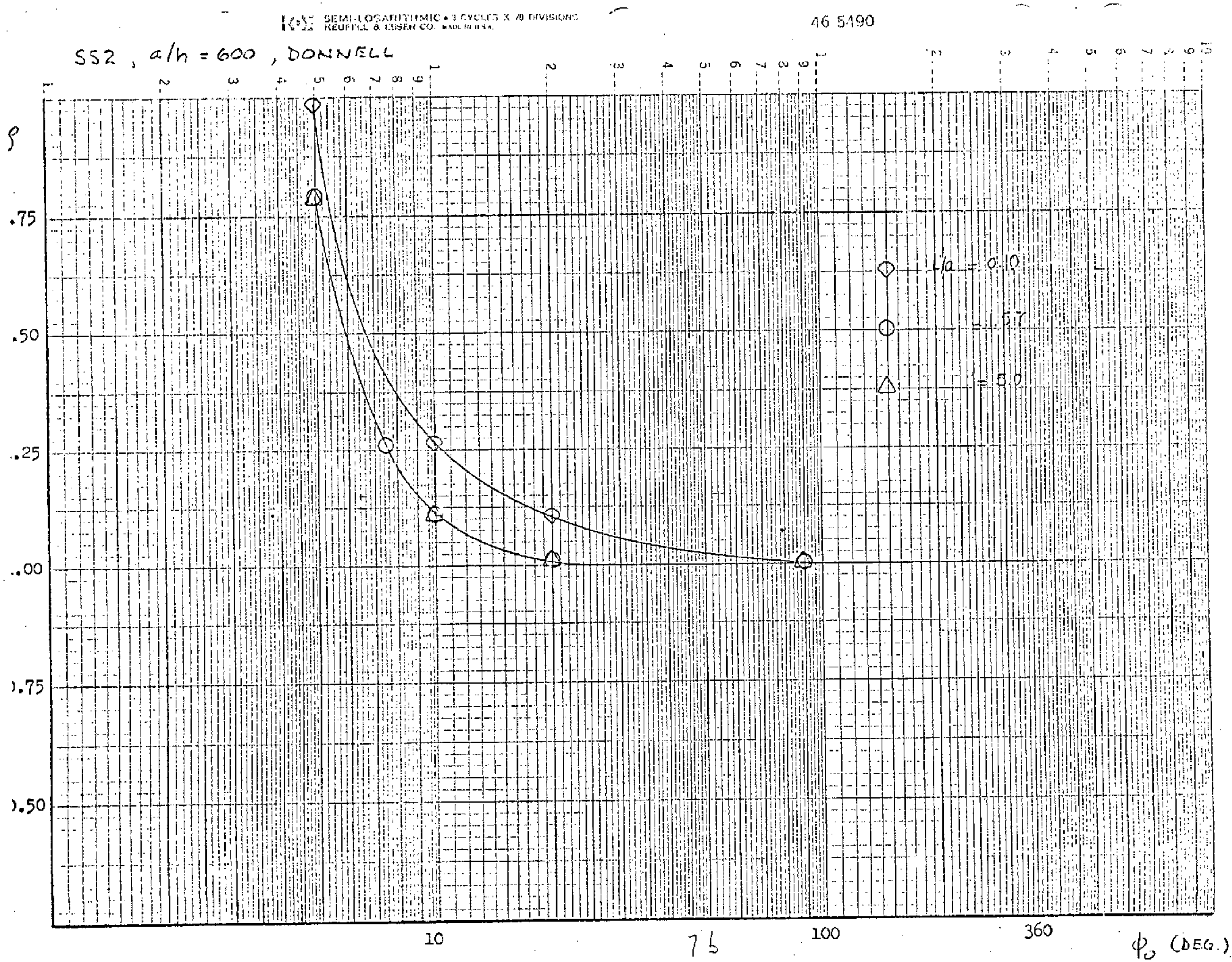
K&E SEMI-LOGARITHMIC • 3 CYCLES X 70 DIVISIONS
KEUFFEL & ESSER CO.
46 5490
SS2 , a/h = 600 , DONNELL
ρ
.75
.50
.25
.00
.75
.50
L/a = 0.10
= .57
= 5.0
10
100
360
ϕ_o (DEG.)

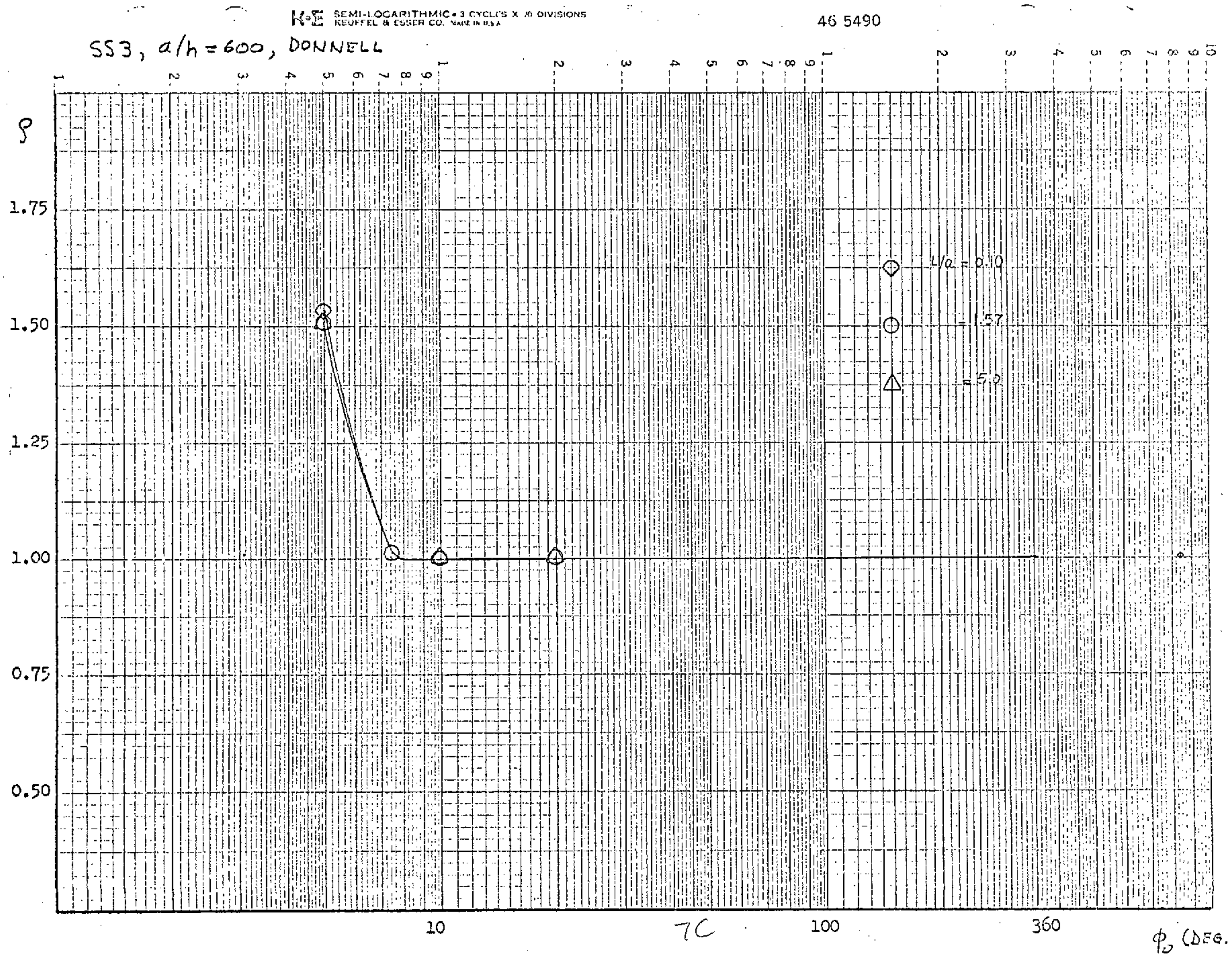
K+E SEMI-LOGARITHMIC 3 CYCLES X 70 DIVISIONS
KEUFFEL & ESSER CO. MADE IN U.S.A.
46 5490
SS3, a/h = 600, DONNELL
ρ
1.75
1.50
1.25
1.00
0.75
0.50
10
100
360
ϕ_0 (DEG.)
L/a = 0.10
= 1.57
= 5.0

7C

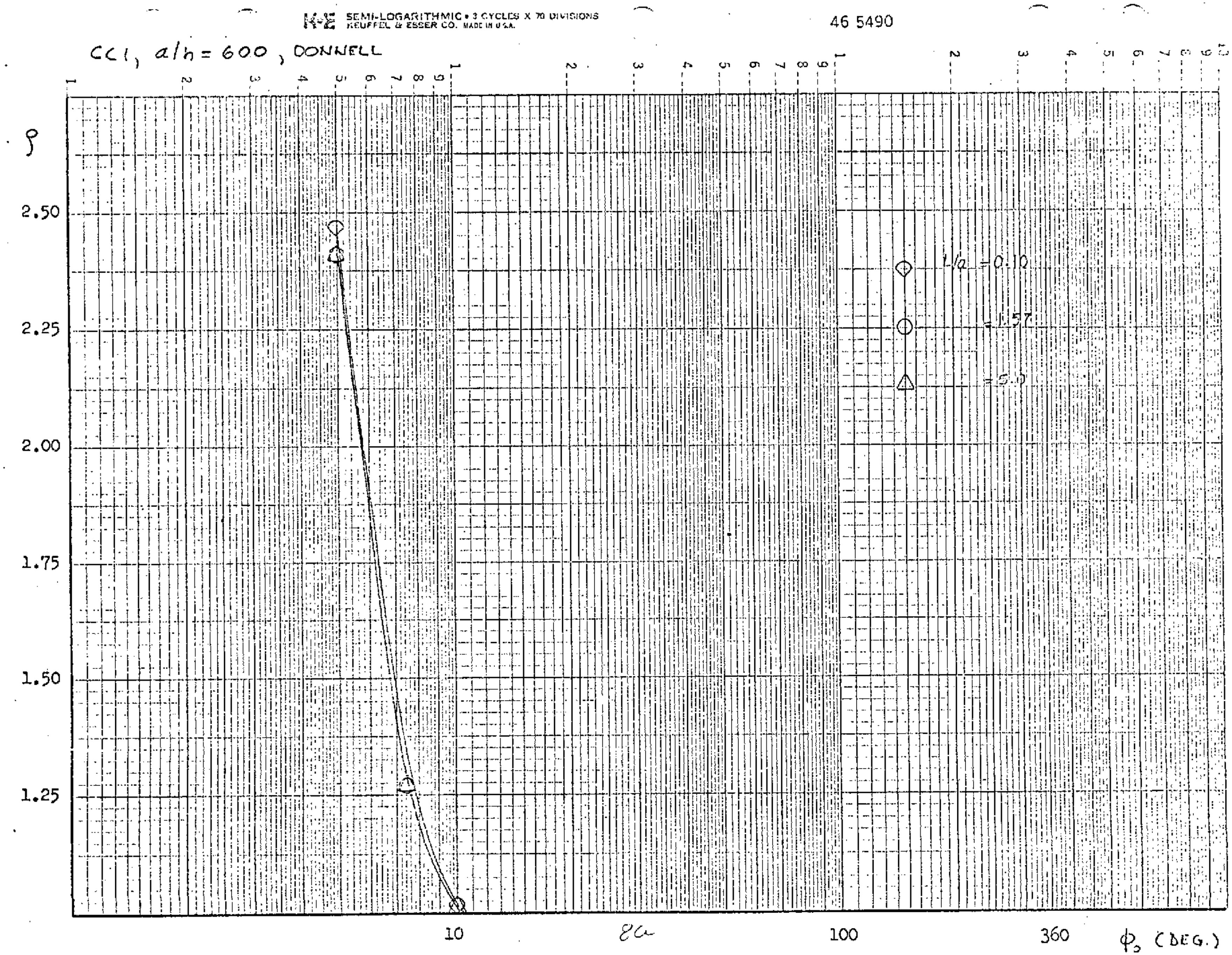
K+E SEMI-LOGARITHMIC • 3 CYCLES X 70 DIVISIONS
KEUFFEL & ESSER CO. MADE IN U.S.A.
46 5490
CCl, a/h = 600, DONNELL
ρ
2.50
2.25
2.00
1.75
1.50
1.25
l/a = 0.10
= 1.57
= 5.0
10
80
100
360
φ₀ (DEG.)

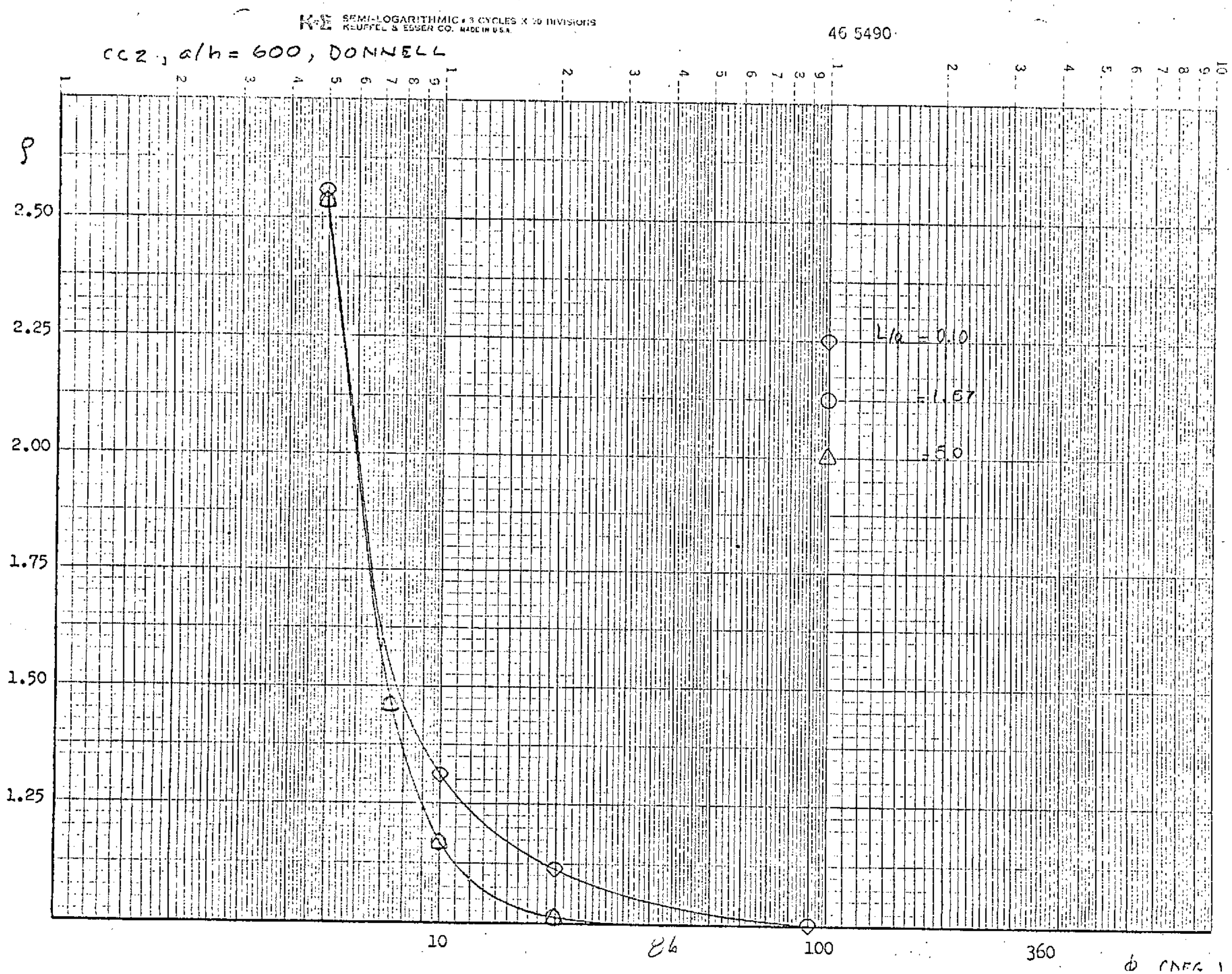
K&E SEMI-LOGARITHMIC 3 CYCLES X 70 DIVISIONS KEUFFEL & ESSER CO. MADE IN U.S.A.
46 5490
CCZ, a/h = 600, DONNELL
ρ
2.50
2.25
2.00
1.75
1.50
1.25
L/a = 0.0
= 1.67
= 5.0
10
100
360
φ (DEG.)

86

46 5490

CC3, a/h = 600 DONNELL

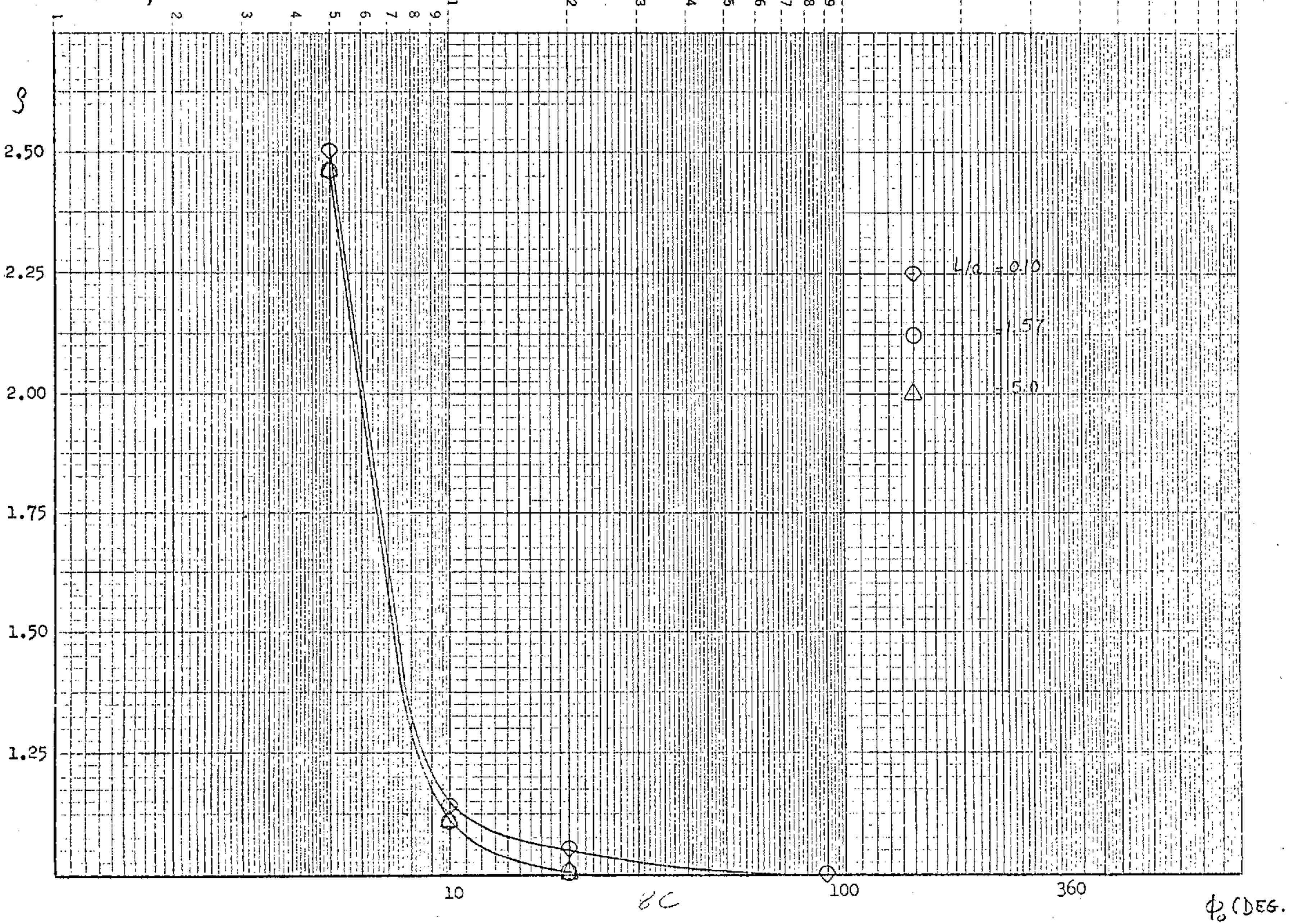

SS1 , L/a = 1.57 DONNELL

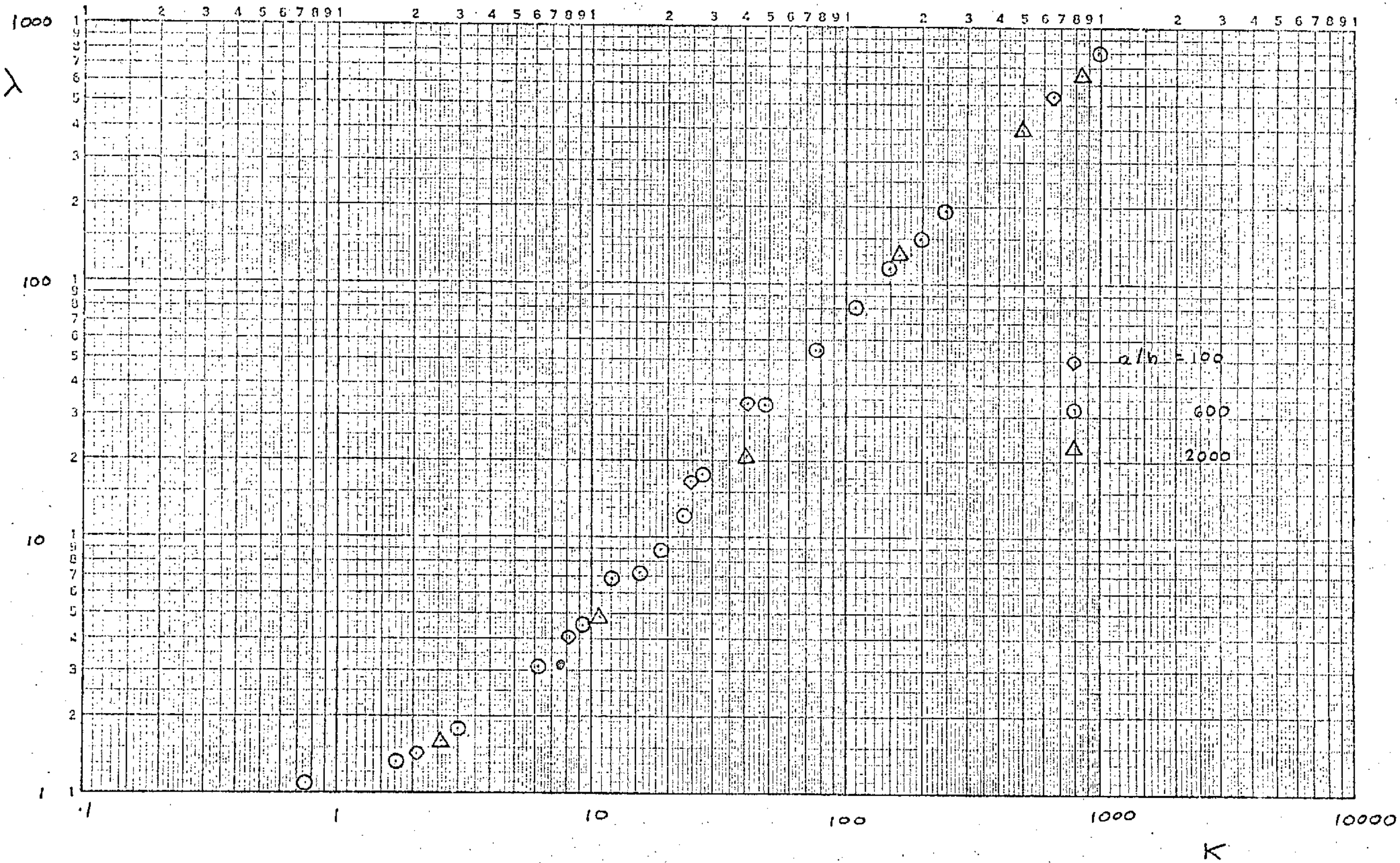

9

A.1 BUCLASP 2

The numerical results presented in this investigation were obtained from the BUCLASP 2 (Buckling of Laminated Stiffened Plates) computer program*. BUCLASP 2 is applicable to stiffened prismatic structures composed of composite flat plate, cylindrical panel, and beam "elements". Classical simple support boundary conditions (Eq. (3)) are assumed for the curved edges, and a linear membrane prebuckling analysis is employed. As a consequence, the axial buckling modes are sinusoidal and a truly one-dimensional analysis is effected through the use of Fourier series representations for the axial variations of the buckling displacement components, u, v, w. Now since the structure is assumed to be prismatic, the equations governing the buckling behavior of each plate, panel, or beam component of the structure possess constant coefficients, and thus "exact" stiffness equations are readily obtained for each element. These elements are then assembled together through the use of the direct stiffness method to yield the "exact" stiffness equation for the entire structure. The elements referred to herein are the structural components that occur naturally in the stiffened structure, such as plates, panels, and beams, and they are not obtained through a spatial discretization as is done in the finite element approach. Buckling loads are then obtained upon specification of the boundary conditions along the straight edges of the structure.

---

* "Elastic Buckling Analysis for Composite Stiffened Panels and other Structures Subjected to Biaxial Inplane Loads", by A. V. Viswanathan, M. Tamekuni, NASA CR-2216, March 1973.

A.2 GOVERNING EQUATIONS

Specialization of the more general equations presented in BUCLASP 2 to the case of the unstiffened, isotropic, cylindrical panel structure considered herein results in the following conventional Donnell shell equations (see Figs. 1 and 2 for sign conventions):

EQUILIBRIUM

$$N_{x,x} + N_{xy,y} = 0$$

$$N_{xy,x} + N_{y,y} = 0$$

$$M_{x,xxx} + 2M_{xy,xy} + M_{y,yy} + \frac{N_y}{a} - N_{xo}w_{,xx}$$

CONSTITUITIVE

$$N_x = \frac{Eh}{1-\nu^2}(\varepsilon_x + \nu\varepsilon_y) \qquad M_x = \frac{Eh^3}{12(1-\nu^2)}(\kappa_x + \nu\kappa_y)$$

$$N_y = \frac{Eh}{1-\nu^2}(\varepsilon_y + \nu\varepsilon_x) \qquad M_y = \frac{Eh^3}{12(1-\nu^2)}(\kappa_y + \nu\kappa_x)$$

$$N_{xy} = Gh\gamma_{xy} \qquad M_{xy} = \frac{Gh^3}{12(1-\nu^2)}\kappa_{xy}$$

KINEMATICS

$$\varepsilon_x = u_{,x} \qquad \kappa_x = -w_{,xx}$$

$$\varepsilon_y = v_{,y} - \frac{w}{a} \qquad \kappa_y = -w_{,yy}$$

$$\gamma_{xy} = u_{,y} + v_{,x} \qquad \kappa_{xy} = -2w_{,xy}$$

Results are also presented herein based on a more complete shell theory that is presented in the BUCLASP 2 documentation.

APPENDIX B

TABLES

$L = 94,\ h = .1,\ a = 60,\ E = 10^7,\ \nu = 1/3$ TABLE I

$\boxed{\frac{a}{h} = 600},\ \boxed{\frac{L}{a} = 1.567},\ Z = 1388,\ (N_x)_{CYL} = 1020.6$

					$(N_x)_{SS3}$		$(N_x)_{CCI}$	
ϕ_a	b	L/b	K	$(N_x)_{\infty PL}$	CLOSED FORM	BUCLASP	CLOSED FORM	BUCLASP
5°	5.2360	17.95	.7560	1350	1543	1542.8	2463.5	2463.4
7.5	7.8540	11.97	1.7010	600	1034	1034.0	1294.7	1294.7
10	10.4719	8.98	3.0241	337	1020.6	1021.1	1029.4	1031.1
15	15.7080	5.98	6.0841	150			912.6	1020.9
17.5	18.3260	5.13	9.2612	110			1018.7	1021.3
20	20.9440	4.49	12.0962	84.4		1021.1	1020.9	1020.6
22.5	23.5619	3.99	15.3093	66.7			1021.1	1020.7
25	26.1799	3.59	18.9004	54.0			1020.6	1020.7
27.5	28.7979	3.26	22.8695	44.6			1020.0	1020.7
30	31.4159	2.99	27.2166	37.5			1020.6	1020.6
40	41.8879	2.24	48.3850	21.1			1020.9	1020.6
50	52.3599	1.80	75.6015	13.5			1020.6	1020.6
60	62.8319	1.50	108.8662	9.38			1021.2	1020.6
70	73.3038	1.28	148.1790	6.89			1020.9	1020.6
80	83.7758	1.12	193.5399	5.27			1020.0	1020.5
90	94.2478	1.00	244.9490	4.17		1020.6	1021.4	1020.6
180	188.4956	.50	979.7959	1.04167		1020.6	1020.6	1020.6
270	282.7433	.33	2204.5408	.46296		1020.6	1020.6	1020.6
350	366.5191	.26	3704.4752	.27551		1020.6	1020.6	1020.6
360	376.9911	.25	3919.1836	.260417	1020.6	1020.6	1020.6	1020.6

NOTE - GOOD CORRELATION BETWEEN CLOSED FORM SOLUTION AND BUCLASP FOR SS3, CCI PANELS FOR ALL VALUES OF a/h & L/a CONSIDERED HEREIN (EXCEPT L/a = .1)

$\boxed{\frac{a}{h} = 600}$ $\boxed{\frac{L}{a} = 1.567}$ TABLE I CONT'D

← BUCLASD (DONNELL) RESULTS →

Φ_o	δ_{SS1} (m)	δ_{SS2} (m)	δ_{SS3} (m)	δ_{SS4} (m)	δ_{CC1} (m)	δ_{CC2} (m)	δ_{CC3} (m)	δ_{CC4} (m)
5°	1.41 (17)	1.79 (23)	1.51 (15)	1.81 (24)	2.41 (27)	2.54 (29)	2.46 (28)	2.55 (29)
7.5	.764 (10)	1.26 (21)	1.013 (12)	1.278 (22)	1.27 (18)	1.46 (23)		1.47 (23)
10	.591 (6)	1.11 (21)	1.00 (5)	1.124 (21)	1.01 (13)	1.17 (21)	1.11 (19)	1.186 (22)
15	.514 (3)	—	—	—	1.00 (20)			
17.5	.483 (2)	—	—	—	1.00 (3)			
20	.561 (2)	1.01 (21)	1.00 (17)	1.01 (21)	1.00 (21)	1.01 (21)	1.01 (21)	1.014 (21)
22.5	.470 (1)				1.00 (21)			
25	.465 (1)				1.00 (19)			
27.5	.527 (1)				1.00 (10)			
30	.645 (1)				1.00 (20)			
40	.682 (1)				1.00 (21)			
50	.727 (1)				1.00 (17)			
60	.735 (1)				1.00 (10)			
70	.765 (1)				1.00 (14)			
80	.765 (1)				1.00 (22)			
90	.786 (1)	1.00 (22)	1.00 (10)	1.00 (22)	1.00 (22)	1.00 (22)	1.00 (22)	1.00 (22)
180	.813 (1)	1.00 (22)	1.00 (10)	1.00 (22)	1.00 (14)	1.00 (22)	1.00 (22)	1.00 (22)
270	.819 (1)	1.00 (22)	1.00 (14)	1.00 (21)	1.00 (19)	1.00 (21)	1.00 (21)	1.00 (21)
350	.819 (1)	1.00 (22)	1.00 (11)	1.00 (21)	1.00 (8)	1.00 (21)	1.00 (21)	1.00 (21)
360	.819 (1)	1.00 (22)	1.00 (11)	1.00 (21)	1.00 (11)	1.00 (21)	1.00 (21)	1.00 (21)

THESE VALUES USED IN ρ-K CURVES

Table 1. contd.

$(N_x)_{cyl} = 999.821$ OBSERVER

BUCLASP - FLÜGGE RESULTS

ϕ_o	$(N_x)_{sss}$ Flügge	$S_{ss1}(m)$	$S_{ss2}(m)$	$S_{ss3}(m)$	$S_{ss4}(m)$		$S_{cc1}(m)$	$S_{cc2}(m)$	$S_{cc3}(m)$	$S_{cc4}(m)$
5	1540.8	1.435(7	1.522(23	1.541(10	1.545(24)		2.421(27	2.588(29	2.510(25	2.601(29)
7.5										
10	1017.6	.593(6	1.133(21	1.019(5	1.147(21		1.028(13	1.197(21	1.130(19	1.210(22)
15										
17.5										
20	999.8	.563(2	1.031(21	1.000(1)	1.033(21		1.008(7	1.033(21	1.023(21	1.035(21
22.5										
25										
27.5										
30										
40		.676(1)					1.002(3)			
50										
60										
70		.755(1)					.990(1)			
80										
90	1016.6	.780(1	1.021(22	1.017(6)	1.021(22		.992(1)	1.021(22)	1.021(22	1.021(22)
180										
270										
350										
360	999.8	.[illegible]	1.016(1)	1.000(1	1.017(1)		.994(1)	1.015(2)	1.014(1)	1.015(2)

$L = 44,\ h = .6,\ a = 60,\ E = 10^7,\ \nu = 1/3$

TABLE 2

$\boxed{\frac{a}{h} = 100},\ \frac{L}{a} = 1.57,\ Z = 231,\ (N_x)_{CYL} = 36,742$

ϕ_0	b	L/b	K	$(N_x)_{\infty\,PL}$	$(N_x)_{SS3}$ CLOSED FORM	$(N_x)_{SS3}$ BUCLASP	$(N_x)_{CC1}$ CLOSED FORM	$(N_x)_{CC1}$ BUCLASP
5°		17.95	.1260	291600	292760	292747	508864	503849
7.5		11.97	.2835	129600	132204		227361	
10		8.98	.5040	72900	77530	77527	129706	129843
15		5.98	1.1340	32400	42817		62443	
17.5		5.13	1.5435	23804	37982		49620	
20		4.49	2.0160	18225	36742	36741	42387	42410
22.5		3.99	2.5516	14400			38545	
25		3.59	3.1501	11664			36931	
27.5		—	—	—			—	
30		2.99	4.5361	8100			36742	
40		2.24	8.0642	4556			36741	36778
50		1.80	12.6002	2916			36742	
60		1.50	18.1444	2025			36742	
70		1.28	24.6965	1488			36748	36745
80		1.12	32.2567	1139			36740	
90		1.00	40.8248	900		36750	36742	36741
180		.50	163.2993	225			36742	
270		.33	367.4235	100			36742	
350		.26	617.4125	59.5			36736	
360		.25	653.1972	56.3	36742	36741	36771	36742

NOTE THAT ONLY 2 FIGURES WERE CARRIED FOR $(N_x)_{\infty\,PL}$ FOR THE HIGHER ϕ_0 VALUES AND THIS IS WHY THERE IS SOME DISCREPANCIES BETWEEN CLOSED FORM SOLUTIONS & BUCLASP RESULTS FOR LARGE ϕ_0

$\bar{h} = 100$ $\bar{a} = 1.51$ TABLE 2 CONT'D

BUCLASP (DONNELL) RESULTS

ϕ_o	S_{SS1} (m)	S_{SS2} (m)	S_{SS3} (m)	S_{SS4} (m)	S_{CC1} (m)	S_{CC2} (m)	S_{CC3} (m)	S_{CC4} (m)
5°	7.951 (18)	8.039 (18)	7.962 (18)	8.047 (18)	13.85 (27)	13.87 (27)	13.86 (27)	13.87 (27)
10	.408 (9)	2.340 (10)	2.110 (9)	2.361 (11)	3.534 (14)	3.617 (14)	3.564 (14)	3.625 (14)
20	.705 (4)	1.204 (9)	1.000 (5)	1.222 (9)	1.154 (7)	1.348 (9)	1.255 (8)	1.364 (9)
40	.499 (1)				1.001 (8)			
70	.672 (1)				1.000 (8)			
90	.822 (1)	1.000 (9)	1.000 (9)	1.001 (9)	1.000 (6)	1.001 (9)	1.001 (9)	1.002 (9)
360	.832 (1)	1.000 (9)	1.000 (5)	1.000 (9)	1.000 (9)	1.000 (9)	1.000 (9)	1.000 (9)

$(N_x)_{q_L} = 35181.0$ (i) OBSERVER

← BUCLASP – FLÜGGE RESULTS →

ϕ_o	$(N_x)_{SS3}$ Flügge	$\rho_{SS1}(m)$	$\rho_{SS2}(m)$	$\rho_{SS3}(m)$	$\rho_{SS4}(m)$		$\rho_{cc1}(m)$	$\rho_{cc2}(m)$	$\rho_{cc3}(m)$	$\rho_{cc4}(m)$
5	292309	.433(1)	8.393(15)	8.309(15)	8.401(15)		1.058(1)	14.484(27)	14.458(27)	14.487(27)
7.5	~~75700~~									
10	77100	1.624(1)	2.442(10)	2.192(9)	2.464(11)		1.829(1)	3.775(14)	3.710(14)	3.783(14)
15										
17.5										
20	36079	.719(4)	1.256(9)	1.026(4)	1.273(9)		1.188(7)	1.404(9)	1.032(8)	1.421(9)
22.5										
25										
27.5										
30										
40		.476(1)					1.042(8)			
50										
60										
70		.646(1)					1.013(3)			
80										
90	35181	.796(1)	1.045(9)	1.000(1)	1.045(9)		1.017(3)	1.045(9)	1.045(9)	1.046(9)
180										
270										
350										
360	34653	.803(1)	1.022(1)	.985(1)	1.026(1)		.971(1)	1.030(1)	1.017(1)	1.030(2)

THINNER MARSHALL PANEL TABLE 3

$L = 94$, $h = .03$, $a = 60$, $E = 10^7$, $\nu = 1/3$

$\boxed{\frac{a}{h} = 2000}$, $\frac{L}{a} = 1.57$, $Z = 4628$, $(N_x)_{CYL} = 91.86$

ϕ_o°	b	L/b	K	$(N_x)_{\infty\ PL}$	$(N_x)_{SS3}$ CLOSED FORM	$(N_x)_{SS3}$ BUCLASP	$(N_x)_{CC1}$ CLOSED FORM	$(N_x)_{CC1}$ BUCLASP
5		17.95	2.5201	36.45	91.86	91.85	96.73	96.73
7.5		11.97	5.6701	16.20			91.86	
10		8.98	10.0802	9.11		91.85	91.83	91.93
15		5.98	22.6804	4.05			91.86	
17.5		5.13	30.8706	2.98			91.99	
20		4.49	40.3208	2.28		91.85	91.93	91.85
22.5		3.99	51.0310	1.80			91.85	
25		3.59	63.0013	1.46			91.98	
27.5		3.26	76.2315	1.20			91.48	
30		2.99	90.7218	1.01			91.63	
40		2.24	161.2833	.57			91.93	91.85
50		1.80	252.0051	.36			90.72	
60		1.50	362.8874	.25			90.72	
70		1.28	493.9300	.19			93.85	91.85
80		1.12	645.1331	.14			90.32	
90		1.00	816.4966	.11		91.85	89.81	91.85
180		.50	3265.9863	.03			97.98	
270		.33	7348.4692	.01			73.48	
350		.26	12348.25	.01			123.48	
360		.25	13063.95	.01	91.86	91.85	130.64	91.85

TABLE 3 CONT'D

$\frac{a}{h} = 2000$ $\qquad$ $\frac{L}{a} = 1.57$

BUCLASP (DONNELL) RESULTS

ϕ_0	ρ_{SS1} (m)	ρ_{SS2} (m)	ρ_{SS3} (m)	ρ_{SS4} (m)	ρ_{CC1} (m)	ρ_{CC2} (m)	ρ_{CC3} (m)	ρ_{CC4} (m)
5°	.632 (13)	1.145 (39)	1.000 (11)	1.160 (37)	1.053 (27)	1.238 (39)	1.159 (35)	1.252 (40)
10	.476 (3)	1.014 (39)	1.000 (11)	1.017 (39)	1.000 (5)	1.018 (39)	1.010 (38)	1.020 (39)
20	.507 (1)	1.001 (40)	1.000 (11)	1.001 (40)	1.000 (25)	1.001 (40)	1.000 (40)	1.001 (40)
40	.798 (2)				1.000 (13)			
70	.804 (1)				1.000 (16)			
90	.790 (1)	1.000 (40)	1.000 (23)	1.000 (40)	1.000 (26)	1.000 (40)	1.000 (40)	1.000 (40)
360	.977 (1)	1.000 (39)	1.000 (23)	1.000 (39)	1.000 (18)	1.000 (39)	1.000 (39)	1.000 (39)

$(N_x)_{cyl} = 91.464(1)$ OBSERVER Table 3. contd.

← BUCLASP – FLÜGGE RESULTS →

ϕ_o	$(N_x)_{sss}$ Flügge	$S_{ss1}(m)$	$S_{ss2}(m)$	$S_{ss3}(m)$	$S_{ss4}(m)$		$S_{cc1}(m)$	$S_{cc2}(m)$	$S_{cc3}(m)$	$S_{cc4}(m)$		
5	91.717	.623(13)	1.150(34)	1.003(11)	1.166(37)		1.057(27)	1.244(32)	1.164(35)	1.257(40)		
7.5	[illegible]											
10	91.667	.475(3)	1.019(34)	1.002(2)	1.021(33)		.999(5)	1.022(34)	1.017(38)	1.024(39)		
15												
17.5												
20	91.667	.500(1)	1.005(40)	1.002(2)	1.005(40)		1.002(7)	1.005(40)	1.005(40)	1.006(40)		
22.5												
25												
27.5												
30												
40		.795(2)					1.002(6)					
50												
60												
70		.794(1)					1.000(4)					
80												
90	91.553	.781(1)	1.004(40)	1.001(4)	1.004(40)		.996(1)	1.004(40)	1.004(40)	1.004(40)		
180												
270												
350												
360	90.707	.805(1)	1.003(1)	.992(1)	1.003(1)		.992(1)	1.003(3)	.991(1)	1.003(3)		

$L = 300$; $h = .1$, $a = 60$, $E = 10^7$, $\nu = 1/3$ TABLE 4

$\frac{a}{h} = 600$, $\boxed{\frac{L}{a} = 5.0}$, $Z = 14142$, $(N_x)_{CYL.} = 1020.6$

					$(N_x)_{SSS}$		$(N_x)_{CC1}$	
ϕ_0	b	L/b	K	$(N_x)_{\infty\ PL.}$	CLOSED FORM	BUCLASP	CLOSED FORM	BUCLASP
5°		57.30	.7560	1350	1543	1543	2463.5	2463.3
7.5		38.20	1.7010	600	1034		1294.7	
10		28.65	3.0241	337	1020.6	1020.6	1029.4	1030.9
15		19.10	6.0841	150			912.6	
17.5		16.37	9.2612	110			1018.7	
20		14.32	12.0962	84.4		1020.6	1020.9	1020.6
22.5		12.73	15.3093	66.7			1021.1	
25		11.46	18.9004	54.0			1020.6	
27.5		10.42	22.8695	44.6			1020.0	
30		9.55	27.2166	37.5			1020.6	
40		7.16	48.3850	21.1			1020.9	1020.8
50		5.73	75.6015	13.5			1020.6	
60		4.77	108.8862	9.38			1021.2	
70		4.09	148.1790	6.89			1020.9	1020.6
80		3.58	193.5399	5.27			1020.0	
90		3.18	244.9490	4.17		1020.6	1021.4	1020.6
180		1.59	979.7959	1.04167			1020.6	
270		1.06	2204.5403	.46296			1020.5	
350		.82	3704.4752	.27551			1020.6	
360		.80	3919.1836	.260417	1020.6	1020.6	1020.6	1020.6

$\frac{a}{h} = 600$ $\boxed{\frac{L}{a} = 5}$

BUCLASP (DONNELL) RESULTS

Φ_o	S_{SS1} (m)	S_{SS2} (m)	S_{SS3} (m)	S_{SS4} (m)	S_{CC1} (m)	S_{CC2} (m)	S_{CC3} (m)	S_{CC4} (m)
5°	1.407 (55)	1.785 (74)	1.517 (57)	1.807 (75)	2.414 (87)	2.535 (93)	2.461 (90)	2.548 (93)
10	.591 (19)	1.110 (57)	1.000 (56)	1.123 (68)	1.010 (43)	1.173 (58)	1.107 (61)	1.185 (59)
20	.476 (5)	1.010 (68)	1.000 (56)	1.012 (68)	1.000 (7)	1.012 (58)	1.007 (67)	1.014 (58)
40	.452 (1)				1.000 (20)			
70	.679 (1)				1.000 (27)			
90	.746 (1)	1.000 (70)	1.000 (39)	1.000 (70)	1.000 (25)	1.000 (70)	1.000 (70)	1.000 (73)
360	.809 (1)	1.000 (69)	1.000 (39)	1.000 (69)	1.000 (25)	1.000 (69)	1.000 (70)	1.000 (69)

$(N_x)_{cyl} = 1019.2(1)$ OBSERVER Table 4. contd.

← BUCLAS9 – FLÜGGE RESULTS →

ϕ_o	$(N_x)_{sss}$ Flügge	$\rho_{ss1}(m)$	$\rho_{ss2}(m)$	$\rho_{ss3}(m)$	$\rho_{ss4}(m)$		$\rho_{cc1}(m)$	$\rho_{cc2}(m)$	$\rho_{cc3}(m)$	$\rho_{cc4}(m)$
										2.568(2)
5	1562.1	1.421(1)	1.984(2)	1.533(1)	1.999(2)		2.473(2)	2.559(2)	2.507(2)	~~[illegible]~~(2)
7.5										1.377(1)
10	1026.4	.858(1)	1.268(1)	1.007(1)	1.306(1)		1.013(1)	1.340(1)	1.144(1)	~~[illegible]~~(1)
15								*		
17.5										
20	1026.4	.926(1)	1.109(1)	1.007(1)	1.122(1)		1.000(1)	1.116(1)	1.056(1)	1.128(1)
22.5										
25										
27.5										
30										
40		.948(1)					1.001(1)			
50										
60										
70		.948(1)					1.001(1)			
80										
90	1019.2	.948(1)	1.006(1)	1.000(1)	1.006(1)		1.000(1)	1.006(1)	1.005(1)	1.006(1)
180										
270										
350										
360	1019.2	1.034(1)	1.000(1)	1.000(1)	1.000(1)		1.000(1)	1.000(1)	1.000(1)	1.000(1)

$L = 6$, $h = .1$, $a = 60$, $E = 10^7$, $\nu = \frac{1}{3}$

TABLE 5 9/10

$\frac{a}{h} = 600$, $\boxed{\frac{L}{a} = .1}$, $Z = 5.66$, $(N_x)_{CYL} = 1020.6$

ϕ_0	b	L/b	K	$(N_x)_{\infty PL.}$	$(N_x)_{SS3}$ CLOSED FORM	$(N_x)_{SS3}$ BUCLASP	$(N_x)_{CC1}$ CLOSED FORM	$(N_x)_{CC1}$ BUCLASP
5°		1.1459	.7560	1350	1543	1564.5	2463.5	2522.8
7.5		.7639	1.7010	600	1034		1294.7	
10		.5730	3.0241	337	1020.6	1027.7	1029.4	1035.1
15		.3820	6.0841	150			912.6	
17.5		.3274	9.2612	110			1018.7	
20		.2865	12.0962	84.4		1027.7	1020.9	1020.6
22.5		.2546	15.3093	66.7			1021.1	
25		.2292	18.9004	54.0			1020.6	
27.5		.2083	22.8695	44.6			1020.0	
30		.1910	27.2166	37.5			1020.6	
40		.1432	48.3350	21.1			1020.9	1022.3
50		.1146	75.6015	13.5			1020.6	
60		.0955	108.8662	9.38			1021.2	
70		.0819	148.1790	6.89			1020.9	1022.9
80		.0716	193.5399	5.27			1020.0	
90		.0637	244.9490	4.17		1020.6	1021.4	1020.9
180		.0318	979.7959	1.04167			1020.6	
270		.0212	2204.5408	.46296			1020.6	
350		.0164	3704.4752	.27551			1020.6	
360		.0159	3919.1836	.260417	1020.6	1020.6	1020.6	1020.6

h   a

TABLE 5 CONT.

BUCLASP (DONNELL) RESULTS

ϕ_o	δ_{SS1} (m)	δ_{SS2} (m)	δ_{SS3} (m)	δ_{SS4} (m)	δ_{CC1} (m)	δ_{CC2} (m)	δ_{CC3} (m)	δ_{CC4} (m)
5°	1.421 (1)	1.986 (2)	1.532 (1)	1.996 (2)	2.471 (2)	2.55 (2)	2.504 (2)	2.565 (2)
10	.850 (1)	1.265 (1)	1.006 (1)	1.304 (1)	1.014 (1)	1.309 (1)	1.144 (1)	1.376 (1)
20	.925 (1)	1.108 (1)	1.006 (1)	1.121 (1)	1.000 (1)	1.115 (1)	1.055 (1)	1.127 (1)
40	.948 (1)				1.001 (1)			
70	.948 (1)				1.001 (1)			
90	.948 (1)	1.006 (1)	1.000 (1)	1.006 (1)	1.000 (1)	1.006 (1)	1.005 (1)	1.006 (1)
360	1.033 (1)	1.000 (1)	1.000 (1)	1.000 (1)	1.000 (1)	1.000 (1)	1.000 (1)	1.000 (1)

Table 5. contd.

$(N_x)_{cyl} = 964.7(1)$

OBSERVER

← BUCLASP – FLÜGGE RESULTS →

ϕ_o	$(N_x)_{SS3}$ Flügge	$S_{SS1}(m)$	$S_{SS2}(m)$	$S_{SS3}(m)$	$S_{SS4}(m)$		$S_{CC1}(m)$	$S_{CC2}(m)$	$S_{CC3}(m)$	$S_{CC4}(m)$		
5	1540.8	.260(1)	1.888(74)	1.547(5)	1.910(75)		2.551(87)	2.685(93)	2602(90)	2.695(93)		
7.5												
10	1014.6	.622(19)	1.174(67)	1.052(15)	1.188(68)		1.065(43)	1.241(68)	1.171(61)	1.253([illegible])		
15												
17.5												
20	995.1	.492(5)	1.069(68)	1.032(3)	1.071(68)		1.032(7)	1.071(68)	1.069(67)	1.072(68)		
22.5												
25												
27.5												
30												
40		.429(1)					1.032(5)					
50												
60												
70		.653(1)					1.019(3)					
80												
90	1004.8	.713(1)	1.053(70)	1.042(4)	1.058(70)		.944(1)	1.058(70)	1.058(70)	1.058(70)		
180												
270												
359												
360	964.7	.781(1)	1.044(1)	1.000(1)	1.054(1)		.969(1)	1.054(2)	1.034(1)	1.055(6)		

SECTION C

LOAD INTRODUCTION TECHNIQUES FOR BORON INFILTRATED ALUMINUM PANELS

Jerry G. Williams

NASA Langley Research Center
Hampton, Virginia

and

Banarsi L. Agarwal

University of Cincinnati
Cincinnati, Ohio

Presented at the
Second Air Force Conference on Fibrous Composites in Flight Vehicle Design

Dayton, Ohio
May 22-24, 1974

LOAD INTRODUCTION TECHNIQUES FOR BORON INFILTRATED ALUMINUM PANELS

Jerry G. Williams
NASA Langley Research Center
Hampton, Virginia

and

Banarsi L. Agarwal
University of Cincinnati
Cincinnati, Ohio

ABSTRACT

Boron infiltration of extruded aluminum stiffeners is a selective reinforcement concept being studied at the Langley Research Center for specialized aerospace applications including an intertank skirt and a wing box panel. One critical design problem associated with this concept is the transfer of loads from end attachments, joints, or splices into the boron reinforced stiffener. The abrupt increase in stiffness in end regions causes high shear stresses to develop: (1) in the metallic web member connecting the end attachment and the boron reinforcement, and (2) in the adhesive bond between the infiltrated boron and aluminum stiffener. High shear stresses in the end region, for example, contributed to premature failure of one previously tested boron infiltrated panel.

To reduce critically high web shear stresses, tapering is proposed so that the axial stiffness of the boron reinforced rod is gradually increased from zero stiffness at the free end. This is physically accomplished in a post-infiltration machining or grinding operation. Critically high epoxy bond shear stresses can be reduced by a grooving operation which removes boron material but retains most of the bond surface area. A linear taper used to reduce web shear stresses, unfortunately, increases the amplitude of bond shear stresses, and a combination of tapering plus grooving may be necessary to satisfy both web and bond allowable shear stress constraints.

This paper presents results of analytical and experimental studies conducted to evaluate the effectiveness of end tapering, grooving, and end fixture sculpturing to reduce critical shear stresses in boron infiltrated extruded structures. The two configurations studied were a bi-element tension specimen and a wing box compression panel.

LOAD INTRODUCTION TECHNIQUES FOR BORON INFILTRATED ALUMINUM PANELS

Jerry G. Williams
NASA Langley Research Center
Hampton, Virginia

and

Banarsi L. Agarwal
University of Cincinnati
Cincinnati, Ohio

INTRODUCTION

NASA has studied, through contract (Ref. 1) and in-house efforts, the selective reinforcement concept in which collimated boron and epoxy resin are infiltrated into cylindrical voids in extruded aluminum alloy stiffeners (see typical stiffener cross sections in Fig. 1). The primary advantage of infiltration compared with bonding high modulus plies directly onto the surface of a metallic stiffener is the protection provided the boron/epoxy by the aluminum annulus. To evaluate the infiltrated stiffener concept numerous strength and crippling specimens have been tested (Ref. 1) and several large components are in various stages of being built and tested. Aluminum stiffeners have been successfully extruded in 6005 and 7075 series alloys. Cross-sectional configutations have included hats, channels, and "T" and "Y" sections.

It is necessary for most practical structural applications of the boron/epoxy infiltrated stiffener concept to incorporate a metallic load introduction end fixture. Loads are carried totally by metal at the end of the stiffener and are transferred into the boron through shear in the metallic web of the fixture and stiffener. The maximum length which boron/epoxy may be infiltrated into the annulus of a stiffener has not been established; however, some applications may employ splice joints which also require loads to be transferred into the boron from an all-metal section. Since the boron typically carries 50 percent or more of the total load, attention must be given the design of the load introduction fixture to prevent premature failure and to minimize the fixture weight.

The present paper summarizes a study of the load transfer problem. The study was prompted by evidence in early test specimens of premature failure in the load introduction region. Recent analytical studies reveal unacceptably high shear strsses in the load introduction region of a proposed wing box panel application. One way found to reduce high shear stresses is to reduce the axial stiffness of the boron/epoxy infiltrated aluminum annulus near the stiffener free end. Boron/epoxy and aluminum material are removed from the stiffener either in a tapered grinding or a grooving operation.

This paper reviews the performance of infiltrated components, presents the philosophy for tapering and grooving to reduce end region shear stresses, describes an analytical and experimental investigation of a double annulus tension specimen to assess the merits of tapering, and finally describes how tapering reduces the shear stresses to acceptable magnitudes in the wing box panel design.

SYMBOLS

L	Length
N_x	Axial load per unit width
x	Axial dimension
σ_x	Axial stress in boron
$\sigma_{x_{max}}$	Maximum axial stress in boron
σ_{xy}	Aluminum web shear stress
$\sigma_{xy_{max}}$	Maximum aluminum web shear stress
τ_{xy}	Epoxy bond shear stress
$\tau_{xy_{max}}$	Maximum epoxy bond shear stress

PERFORMANCE OF INFILTRATED COMPONENTS

Photographs of several boron infiltrated stiffened structural components are presented in Figure 1. The cylindrical interstage tank specimen shown in Figure 1(a) is 1.96 m (77 in.) long and has a diameter of 3.91 m (154 in.). External longitudinal stiffeners are hat sections with boron infiltrated into all four corners. Internal ring stiffeners have "H" shaped cross sections with boron located only in the top half of the stiffener. See inserts in Figure 1(a). The structure is moderately loaded with an axial compressive load equal to 823 kN/m (4700 lbf/in.). This shell structural specimen has been recently tested successfully in the 3.39-MmN (30-million in.-lb) bending test fixture in the Structures Laboratory at Langley Research Center. The DC-10 floor strut (Fig. 9(b)) is being evaluated under a joint AVCO Corporation/McDonnell-Douglas Corporation program and is reported upon in another paper in these proceedings.

The two compression panels shown in Figures 1(c) and 1(d) are constructed with boron infiltrated "Y" stiffeners. These panels weigh 1.18 kg/m^2 (2.6 lbm/ft^2) and are designed to carry an axial load of 1.261 MN/m (7200 lbf/in.). The panels are 1.22 m (48 in.) long and 0.86 m (34 in.) wide and differ only in the end fixture design. The compression panel shown in Figure 1(c) has massive steel end fixtures bolted to the skin of the panel and to the web of the "Y" stiffners. Loads are transferred into the boron/epoxy through shear flow in the metallic stiffener web. A knife-edge end support simulates a simple support end boundary condition. The specimen was tested at Langley Research Center and failed at approximately 65 percent of the design ultimate load. Premature failure was caused in part by high shear stresses in the load introduction region of the stiffeners.

A closeup view of the shear failure in the end region is shown in the photograph in Figure 2. Two characteristic types of shear failures can be seen in the photograph. First, the aluminum web of one stiffener has failed in shear as evidenced by the physical separation of the top of the stiffner from the web (a coin has been slipped between the two separated parts). Second, the epoxy bond between the boron and the aluminum has failed on another stiffener allowing the boron rod to displace relative to the end of the aluminum extrusion.

The end fixture for the second compression panel is designed to permit loads to be transferred directly into the boron/epoxy (Fig. 1(d)). This flat-end test condition permits assessment of the load-carrying capability of the panel without the complications imposed by the load transfer problem in the stiffeners. This specimen was also tested at Langley and failed in an Euler mode at 91 percent of the design ultimate load. No shear type failures in stiffeners were observed.

The latest effort in boron infiltrated structures is a wing box cover panel which is currently in the late stages of design. The structure is designed to be heavily loaded (axial loading equal 4.90 MN/m (28,000 lbf/in.)) and has a sculptured load introduction fixture representative of that required for a joint in the wing box application. The assembly process for this structure involves Tungsten Inert Gas (TIG) welding a "T" stiffener to the web of an integrally machined aluminum plank. Shear stresses in the web weld region are especially important because the weld process reduces the allowable strength of the 2219 aluminum alloy. Initial analytical studies of the wing box load introduction region indicated shear stress magnitudes in the web did exceed the ultimate shear strength. The end tapering approach for reducing web shear stresses was applied to this configuration and results are reported in subsequent sections.

END TAPER CONCEPT DESCRIPTION

The shear stress problem associated with the transfer of loads into the concentrated mass of boron/epoxy in an infiltrated stiffener is basically a twofold problem. First, the abrupt increase in stiffness in the end region causes high shear stresses to develop in the metallic web member connecting the end fixture and the infiltrated boron reinforcement. Second, high shear stresses can develop in the epoxy bond interface between the aluminum and the boron/epoxy materials.

Drawings in Figure 3 show schematically (with distortions greatly exaggerated) how boron stiffener end tapering reduces the shear stress magnitude in the connecting metallic web member. When the encapsulated boron is terminated by a square cut, loads carried by the skin are transferred into the boron over a very short length near the end region, thereby causing high shear stresses to develop in the aluminum web. Straight lines drawn on the web of the deformed structure represent the displaced position of lines which on the undeformed structure would originally be parallel and uniformly spaced. Large rotations of these lines between undeformed and loaded conditions represent high shear stress regions. The shear stresses are largest near the free end and decrease to zero at a point along the stiffener axis where the load redistribution is complete.

In the tapered approach, illustrated at the bottom of Figure 3, the stiffness of the encapsulated boron/epoxy rod is gradually increased from zero at the free end to the nominal value at the termination of the taper. This arrangement results in nearly uniform shear stresses in the web end region (represented by rotated nearly parallel lines in the deformed structure), and the magnitude of stress for the tapered structure is less than the maximum shear stress in the web of the square-cut terminated stiffener. This gradual buildup of stiffness is physically implemented by machining or grinding a taper in the boron infiltrated rod to remove material for a few centimeters near the end. In the present effort a linear taper is employed. A typical example of a linear taper is shown on the top of the specimen shown in the photograph in Figure 4. The tapering approach presented here for the infiltrated boron concept is basically analogous to the approach proposed by deBruyne (Ref. 2) in 1944 for bonded or glued lap joints. deBruyne found that tapering the two ends of a lap joint doubles the failure load compared to nontapered joints.

As previously mentioned, the shear stress in the epoxy bond interface may also be critical. Critically high bond shear stresses can be reduced by a grooving operation such as that shown on the bottom of the specimen in the photograph in Figure 4. Grooving reduces the rate at which load is transferred into the boron while retaining most of the bond surface area.

A linear taper which is effective in reducing web shear stresses also (unfortunately) increases the bond shear stress. This increase occurs since stress is defined as force per unit area and the bond area lost through tapering is reduced by a greater factor than the corresponding rate at which load is transferred through the bond into the boron. For structural applications in which both web and bond shear stresses are critically high, one possible solution is to machine a linear taper followed by a grooving operation which removes boron but leaves the bond surface area intact.

TENSION SPECIMEN

Specimen and Experiment Description

A tension specimen used to study the load transfer problem is shown in the photographs of Figure 5. The specimen consisted of a 6005-T5 aluminum bi-element extrusion which had an overall length of 48.3 cm (19 in.). The web was removed for 10.2 cm (4 in.) in the center of the specimen resulting in a load introduction length of 19.1 cm (7.5 in.) at either end. This cutout permits loads introduced at the end tabs to be fully transferred into the boron reinforced stiffener in the specimen center. Each aluminum annulus was filled with 857, 0.14 mm (5.6 mil) diameter boron filaments and subsequently infiltrated with a room-temperature curing epoxy resin. Steel load introduction straps 2.54 mm (0.1 in.) thick were bonded and bolted to the web of the test specimen in a symmetrical double lap configuration. The cross section of the two boron infiltrated stiffeners was reduced at one end of the specimen by grinding a linear taper 9.54 cm (3.75 in.) long. The boron at the other end of the specimen was terminated by a transverse square cut. This configuration permitted comparison on the same specimen of the load transfer response for a tapered and nontapered end.

Geometric constraints make it impractical to measure experimentally the shear strains in the aluminum web and epoxy bond. Instead, axial strains were measured on the surface of the boron stiffened aluminum annulus using 38 strain gages positioned along the specimen length. Comparison was made between experimental and analytical results and the analysis was then used to determine shear stresses in the aluminum web and epoxy bond. Bond shear stresses were determined by calculating the rate at which loads are transferred into the boron and dividing by the circumferential bond dimension. It was assumed that the bond shear stress is uniform around the circumference. Tests were performed using a 445-kN (100,000-lb) capacity hydraulic testing machine and strains were recorded using an automatic data acquisition system.

NASTRAN Model

The finite-element computer program NASTRAN (NAsa STRuctural ANalysis) was used to analyze the shear stress load introduction problem. Loads which stress the boron to its ultimate strength may result in stress concentrations which produce plasticity effects in the aluminum. In the current study, only a linear analysis was conducted; however, plasticity effects usually reduce peak stresses so that an elastic analysis is conservative. The study was restricted to mechanical loads; stresses due to potential thermal expansion differences between the aluminum and boron (due to curing or temperature effects) were not considered.

A schematic of the finite-element model used to represent the boron reinforced bi-element specimen is shown in Figure 6. Rectangular constant strain elastic membrane plate elements were used to represent the aluminum, boron, and steel components. Although the full model is shown in Figure 6, symmetry about three axes was used to reduce the computational model size. A total of 264 plate elements and 191 grid points were used in the computational model. No attempt was made to represent details of the aluminum annular cross-section geometry. The aluminum and boron materials were assumed to have moduli of elasticity of 68.9 GPa (10 million psi) and 206.8 GPa (30 million psi), respectively. A uniform tension load was imposed on the steel straps at the specimen ends.

Analytical and Experimental Results

Comparison of analytical and experimental results for the axial stress in the boron rod of the bi-element tension specimen is presented in Figure 7. Results are presented for both tapered and nontapered cases. Experimental results shown were calculated using strain-gage data by assuming the boron and aluminum strains are identical. The stress magnitude has been normalized by the maximum stress amplitude ($\sigma_{x_{max}}$ = 800 MPa (116,000 psi)) which occurs at the center of the specimen where the load is completely carried by the infiltrated boron circular stiffener. Results are presented for the complete specimen to establish correlation between experiment and theory. Shear stress studies, however, are focused on the end region (i.e., $x/L < 0.5$) since this region is representative of the load introduction problem.

Correlation between experimental and analytical results is reasonably good. The effect of tapering in the end region is to increase the stress in the boron over the nontapered result (Fig. 7). This increase, as explained earlier, occurs since the bond area lost through tapering is reduced by a greater factor than the corresponding rate at which load is transferred through the bond into the boron. The total force in the boron and the rate at which load is transferred into the boron, however, is reduced for the tapered case. This situation results in a reduction in the maximum shear stress in the aluminum web for the tapered end of approximately 60 percent as can be seen in the NASTRAN results presented in Figure 8. When the boron rod at the center of the test specimen is stressed to σ_x = 1.38 GPa (200,000 psi), the maximum web shear stress for the nontapered case is $\sigma_{xy_{max}}$ = 128 MPa (18,500 psi). The ultimate shear stress of 6005 aluminum is 138 MPa (20,000 psi) (Ref. 3) and the web shear stress, therefore, is not critical at this load even for the nontapered case.

The preceding example demonstrates the effectiveness of boron stiffener tapering to reduce high web shear stress in the end region of boron infiltrated structures. A comparison of the epoxy bond shear stress in the end region for the tapered and nontapered tension specimen is presented in Figure 9. As indicated previously, the net effect of tapering is to increase the maximum bond shear stress. In this example with the boron stressed at σ_x = 1.38 GPa (200,000 psi) in the center test section, the tapered end maximum bond shear stress is $\tau_{xy_{max}}$ = 19.3 MPa (2800 psi). This value is approximately 100 percent higher than the maximum bond shear stress for the nontapered end. The recommended allowable shear stress for the epoxy bond used in these specimens is approximately 15.2 MPa (2200 psi). Tests conducted by the AVCO Corporation, however, indicate shear stress concentrations as high as 41.4 MPa (6000 psi) can be carried by the bond.

The analytical assumption of constant shear stress in the bond is nonconservative. The maximum bond shear stress near the intersection of the stiffener with the web is greater than the average bond shear stress and is reduced in magnitude from that point around the bond circumference. If a more refined analysis were conducted which included local bond shear stress gradients, the maximum bond shear stress would increase by a greater amount for the nontapered than the tapered case and, in effect, would decrease the relative disadvantage shown for a linear taper.

WING BOX PANEL

Structure Description

The wing box panel structure consists of boron reinforced extruded stiffeners which are TIG welded to an integrally machined aluminum plank. The end fixture is also machined integrally with the wing plank and is sculptured to permit the gradual transfer of loads into the boron reinforced stiffener. The concept and weld location is shown schematically in Figure 10. The weld is made by joining two extrusion elements to the web of the integrally machined plank to form a "T" stiffener. The compression panel of the wing box is designed to carry an ultimate axial compression load of 4.90 MN/m (28,000 lbf/in.). Constraints imposed by welding, heavy loading, and a requirement to show a weight savings over an all-metal design combine to make the load introduction an important design problem. The weld area is critical since TIG welding reduces the allowable shear stress for the 2219 aluminum material used in the wing plank from 262 MPa (38,000 psi) to about 138 MPa (20,000 psi).

Analyses of the wing box panel preliminary design showed the shear stress in the vertical web weld region to be substantially greater than 138 MPa (20,000 psi) for a boron reinforced stiffener terminated by a square cut. End region tapering was studied to determine the capability of this approach to solve the problem.

NASTRAN Model

Drawings of the NASTRAN model used to represent the load introduction region of a typical wing box stiffener are presented in Figure 11. Selected cross sections show the sculpturing of the load introduction fixture. Symmetry about the midplane of the "T" stiffener was utilized to reduce the computational model size. Three-dimensional constant strain solid elements were used to model the thick end fixture and skin components. A total of 727 constant strain plate and solid elements were used in the computational model to represent the vertical and horizontal webs and 36 bar elements having axial stiffness only were used to represent the boron infiltrated circular stiffener.

The wing box compression test panel is 2.44 m (96 in.) long, 0.91 m (36 in.) wide and has rib supports every 0.61 m (24 in.). Although the load introduction model studied was only 0.49 m (19.4 in.) long, analyses indicate that most of the load transfer takes place within this length. In the analysis, loads were assumed to be applied by imposing a uniform displacement to the end of the load introduction fixture and restraining the axial displacements at the other end of the model. The aluminum and boron were assumed to have moduli of elasticity of 68.9 GPa (10 million psi) and 241 GPa (35 million psi), respectively.

NASTRAN Results

The effectiveness of end tapering to reduce the shear stress in the vertical web weld region for the wing box compression panel loaded with an axial load of 4.90 MN/m (28,000 lb/in.) is presented in Figure 12. The maximum shear stress $\sigma_{xy_{max}}$ for the nontapered case of 207 MPa (30,000 psi) was used to normalize the ordinate and the analytical model length L of 49.3 cm (19.4 in.) was used to normalize the abscissa. The shear stress for the nontapered case exceeds the 138 MPa (20,000 psi) allowable shear stress by 50 percent. Linear tapers of 0.171 L ((8.41 cm (3.31 in.)) and 0.325 L (16.0 cm (6.31 in.)) reduce the maximum shear stress in the weld region to 0.9 $\sigma_{xy_{max}}$ (186 MPa (27,000 psi)) and 0.67 $\sigma_{xy_{max}}$ (138 MPa (20,000 psi)), respectively. The 0.325 L taper permits loads to be transferred into the boron without exceeding the linear elastic shear stress allowable. The peak shear stress near the end for the nontapered case has been replaced for the 0.325 L taper by a nearly uniform stress for the first 0.21 L (10.2 cm (4 in.)) of the stiffener.

The epoxy bond shear stress for the 0.325 L taper and nontapered cases for the wing box panel loaded with an axial compressive load of 4.90 MN/m (28,000 lb/in.) is presented in Figure 13. The maximum shear stress for the 0.325 L linearly tapered case is 29.6 MPa (4300 psi) and this value has been used as $\tau_{xy_{max}}$. The recommended allowable bond shear stress value of 15.2 MPa (2200 psi) (0.51 $\tau_{xy_{max}}$) is not exceeded for the nontapered case. The 0.325 L taper increased the bond shear stress compared to the nontapered result by approximately 53 percent and the value exceeds the recommended allowable by approximately 50 percent.

The effectivensss of a combination taper and groove to reduce the bond shear stress was studied analytically by adding a groove to the 0.325 L taper case. The groove was assumed to be rectangular in cross section and 3.8 mm (0.15 in.) wide. The groove was begun at a distance 0.077 L (3.81 cm (1.5 in.)) from the stiffener end and continued parallel to the stiffener over a distance of 0.103 L (5.1 cm (2 in.)). The groove slope from that point was such that the bottom of the groove intersected the termination point of the taper. The reduction in bond shear stress which results is presented in Figure 13. A substantial reduction occurs in the region of the taper. The groove cross section was insufficient, however, to reduce the bond shear stress to the 15.2 MPa (2200 psi) recommended allowable. To be fully effective, the taper should be initiated around 0.036 L (1.8 cm (0.7 in.)) from the stiffener end near the point where the tapered boron begins and additional boron should be removed.

The small change in stiffness provided by the groove modifies only slightly the shear stress distribution in the aluminum web weld region. This result can be seen in the comparison of tapered and tapered plus grooved web shear stress distributions plotted in Figure 12.

DESIGN IMPLICATIONS

Most practical structural applications of boron infiltrated stiffener selective reinforcement concepts require an end fitting in which loads are transferred through shear from an all-metal joint into a cross section containing boron reinforcement. High web shear stresses can be reduced by tapering the boron infiltrated stiffener cross section and high bond shear stresses can be reduced by grooving operation which removes boron but retains most of the bond surface area. A load introduction fixture design which meets both web and bond allowable shear stress requirements may require both tapering and grooving. Each structural application has unique design constraints and determination of a satisfactory load introduction fixture design may require several iterations. Note, however, that load introduction shear stress problems can be solved by removing rather than adding material.

The web which connects the skin to the boron reinforced annulus must be sufficiently thick (1) to carry the shear loads imposed in the load introduction region, and (2) to carry axial loads without crippling locally. For the wing box panel, the thickness required to meet shear stress requirements exceeded the crippling requirement. Constraints imposed by TIG welding restricted thickening the web in the end region and additionally reduced the allowable shear stress in this critical section. Alternate assembly techniques such as riveting also present design problems, especially for heavily loaded structural applications. This illustration emphasizes that the combined effect must be considered when making design decisions.

The feasibility of both the taper and groove machining operations has been successfully demonstrated in the machine shop. Grinding a linear taper is a simple operation. Cutting a groove in a tapered stiffener requires greater precision since it is necessary to center the cut in order to retain the desired quantity of boron and leave the bond interface surface undamaged. Accessibility to the boron stiffener free end must be provided when "tight fit" geometric constraints are imposed such as in the wing box panel load introduction fixture.

Shear stress problems can also develop in the end region from thermal expansion incompatibility between the boron and aluminum. Typically, the contributions of mechanical and thermal loads superpose to amplify the problem. The removal of web material in the vicinity of the free end is suggested in Reference 4 as a technique for separating the maximum bond shear stress amplitudes for these two types of loading. Web removal transfers the maximum bond shear stresses caused by mechanical loading away from the free end.

Based on bond shear stress calculations (Ref. 4), the maximum diameter which can be used for a boron infiltrated stiffener subjected to a 222 K (400° F) temperature differential has been determined to be 0.71 cm (0.28 in.).

For a room-temperature cured epoxy such as used in the current investigation, typical thermal excursions would be less than 222 K (400° F). Only limited work has been done on thermal cycling for the boron infiltrated stiffener concept, and more study is needed.

CONCLUSIONS

An analytical and experimental study has been made of the load transfer mechanics of structures stiffened by boron infiltrated extrusions where loads must be transferred through shear in an aluminum web from a load introduction fixture into a boron infiltrated stiffener. It was found that critically high shear stresses in the aluminum web can develop in the load introduction region, especially for heavily loaded structures. Removing material to reduce the axial stiffness of the boron infiltrated aluminum annulus for several inches near the stiffener end using a linear taper was found effective in reducing the aluminum web shear stress. Reductions in the web maximum shear stress of 60 and 30 percent, respectively, were demonstrated for a tension test specimen and projected for a wing box panel. Analytical and experimental results for the axial stress in the boron for the tension specimen showed reasonably good agreement. A 16.0-cm (6.31-in.) long linear taper was sufficient to allow critically high shear stresses in the aluminum web weld region of the wing box panel to be reduced to an acceptable value.

Critically high shear stress in the bond between the boron/epoxy and the aluminum can be reduced by grooving a cut in the circular stiffener. Grooving reduces the shear stress in the bond by reducing the magnitude of force which must be transferred across the bond while maintaining a high percent of effective bond area. Although a linear taper reduces shear stress concentrations in the aluminum web, it increases the shear stress magnitude in the epoxy bond joining the boron to the aluminum annulus. The simultaneous reduction of web and bond shear stress magnitudes can be accomplished by a combination of tapering and grooving.

REFERENCES

1. Roy, Paul A., McElman, John A., and Henshaw, Jim: Development of Lightweight Aluminum Compression Panels Reinforced by Boron-Epoxy Infiltrated Extrusions. NASA CR-2145, 1973.

2. deBruyne, N. A.: The Strength of Glued Joints. Aircraft Engineering, 16, 115-118, 140, 1944.

3. Anon.: Military Standards Handbook Metallic Materials and Elements for Aerospace Vehicle Structures. Military Handbook-5B. September 1971.

4. Hart-Smith, L. J.: Non-Classical Adhesive-Bonded Joints in Practical Aerospace Construction. NASA CR-112238, 1973.

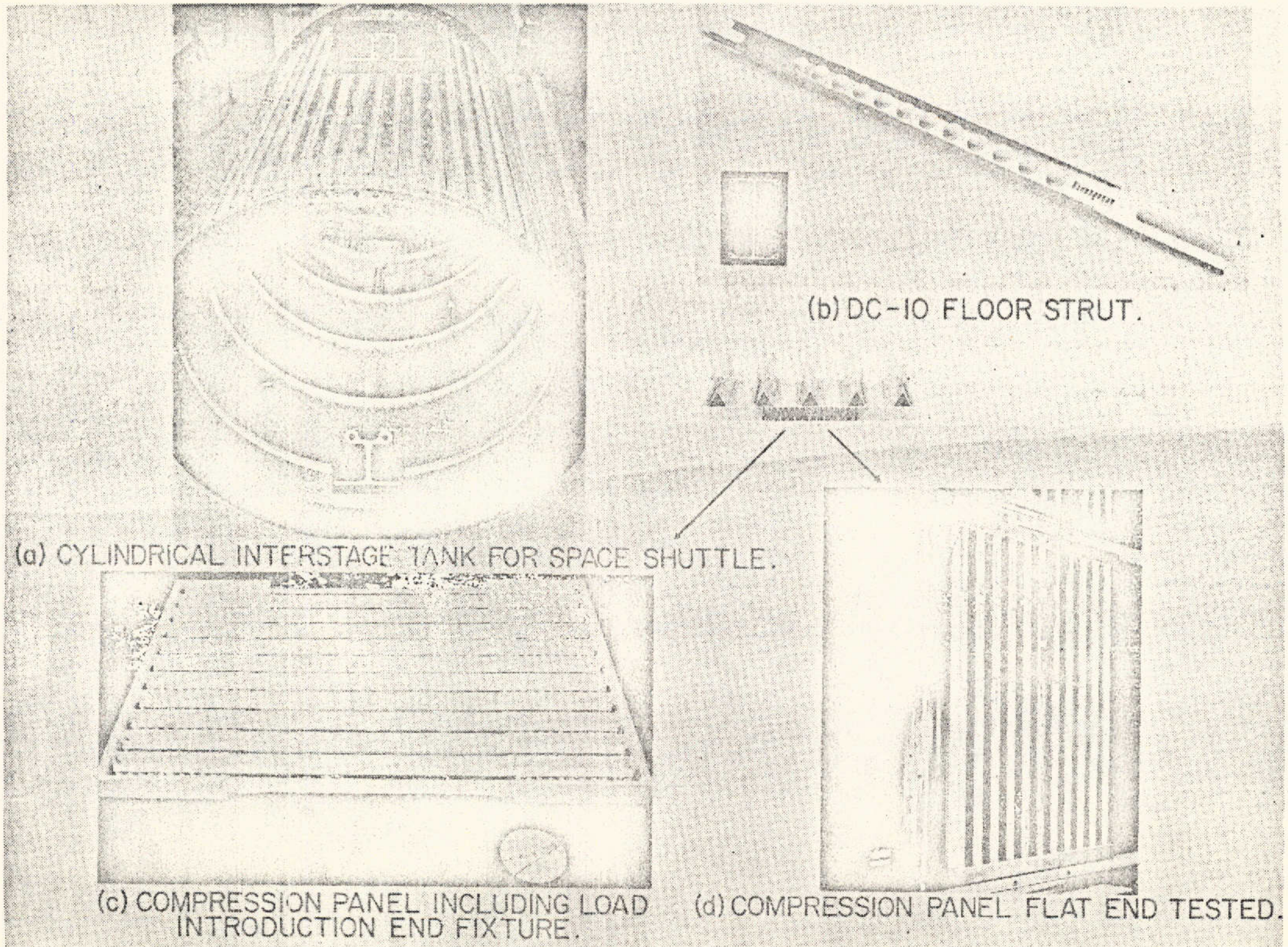

Figure 1. Boron infiltrated stiffener structural applications.

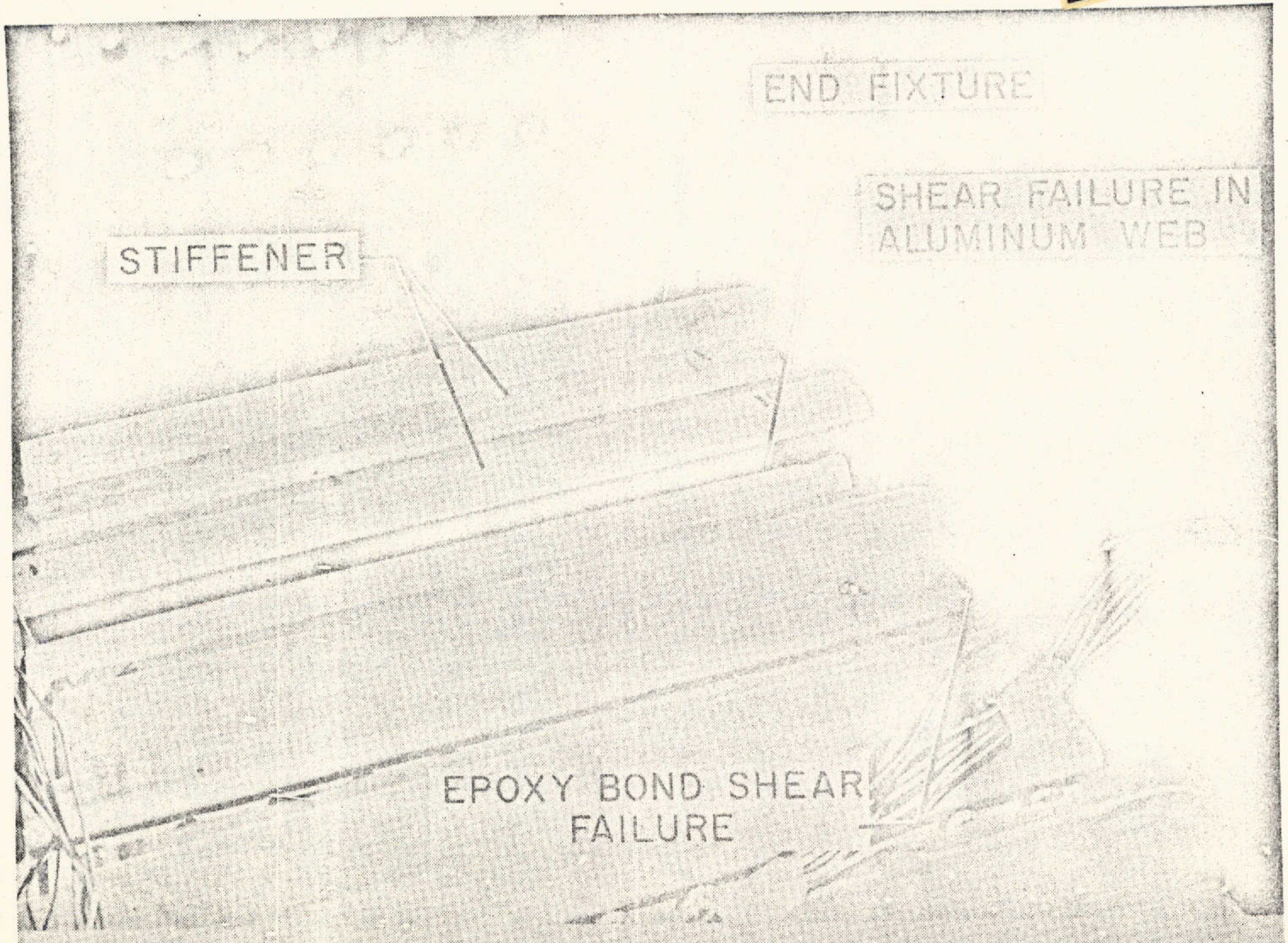

Figure 2. Photograph showing web and bond shear failure.

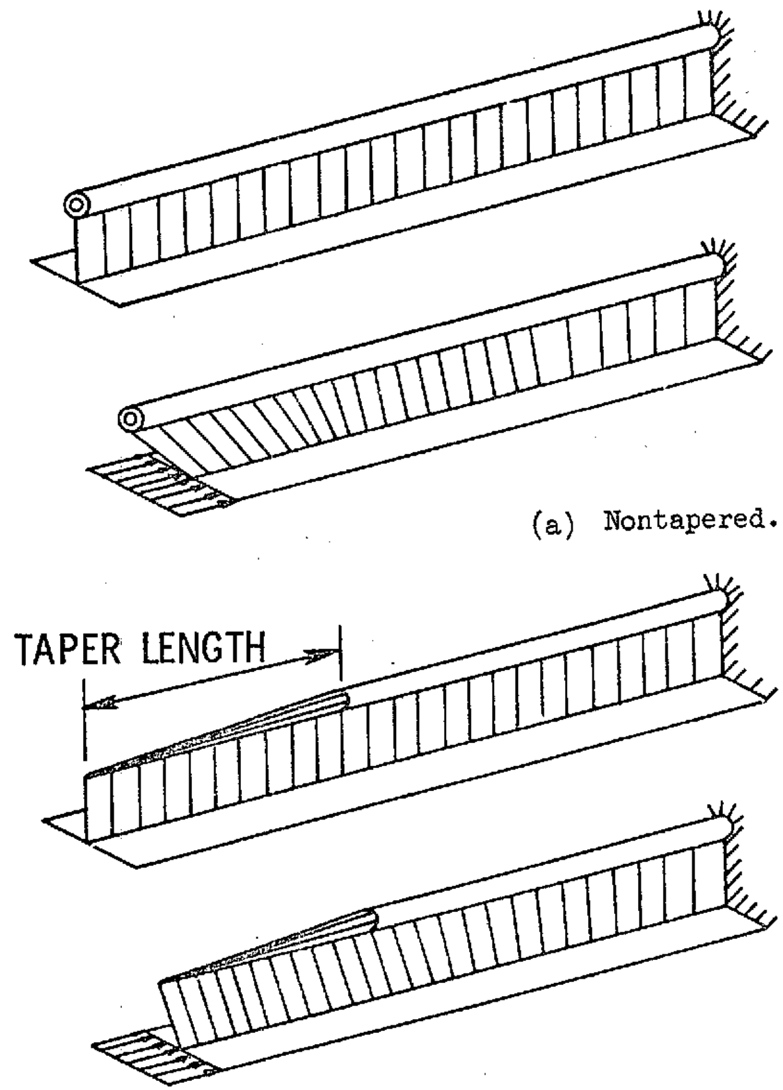

(a) Nontapered.

(b) Linear taper.

Figure 3. Tapering of boron infiltrated stiffener to reduce critical web shear stresses.

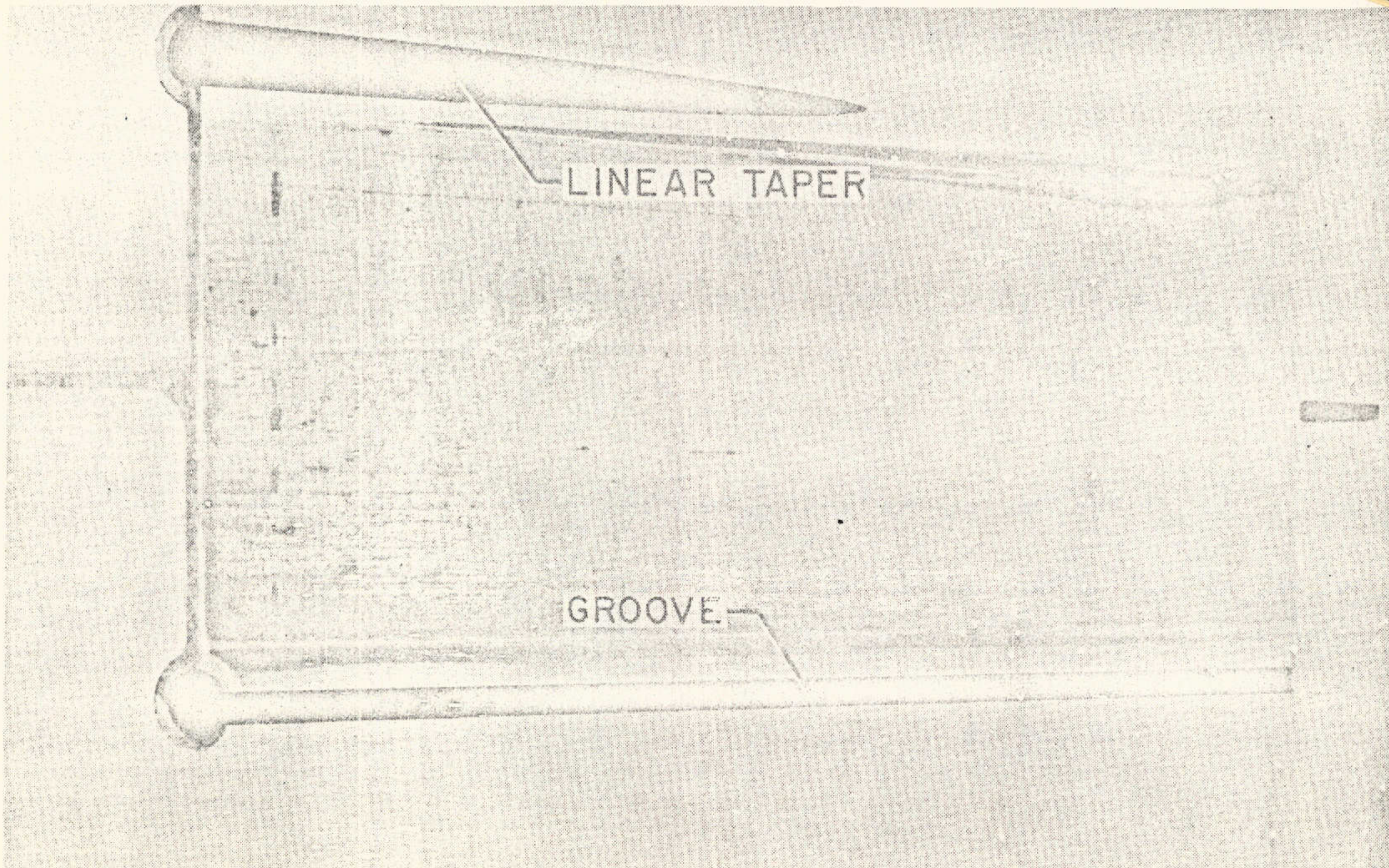

Figure 4. Photograph of specimen with machined linear taper and groove.

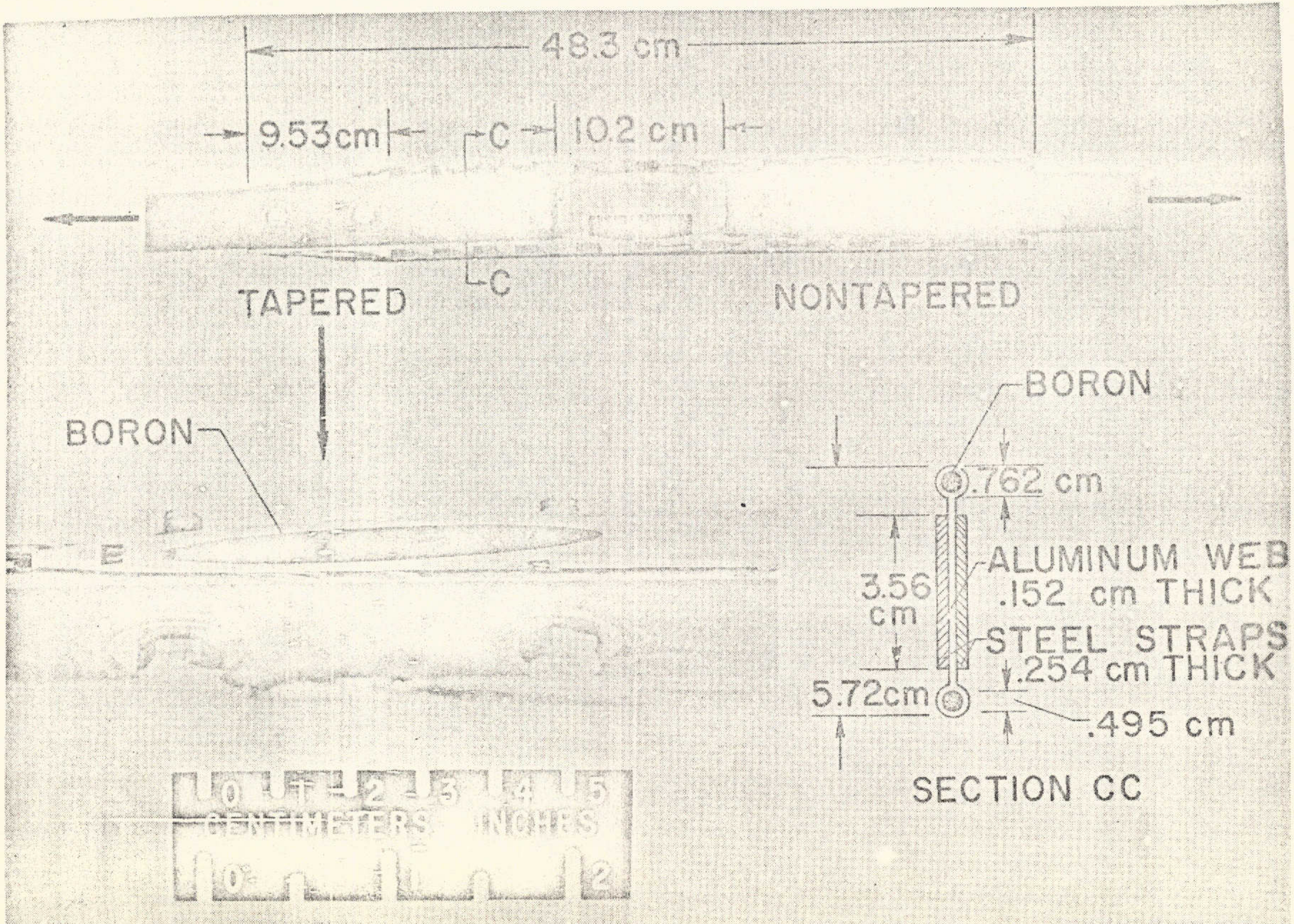

Figure 5. Boron infiltrated bi-element tension specimen.

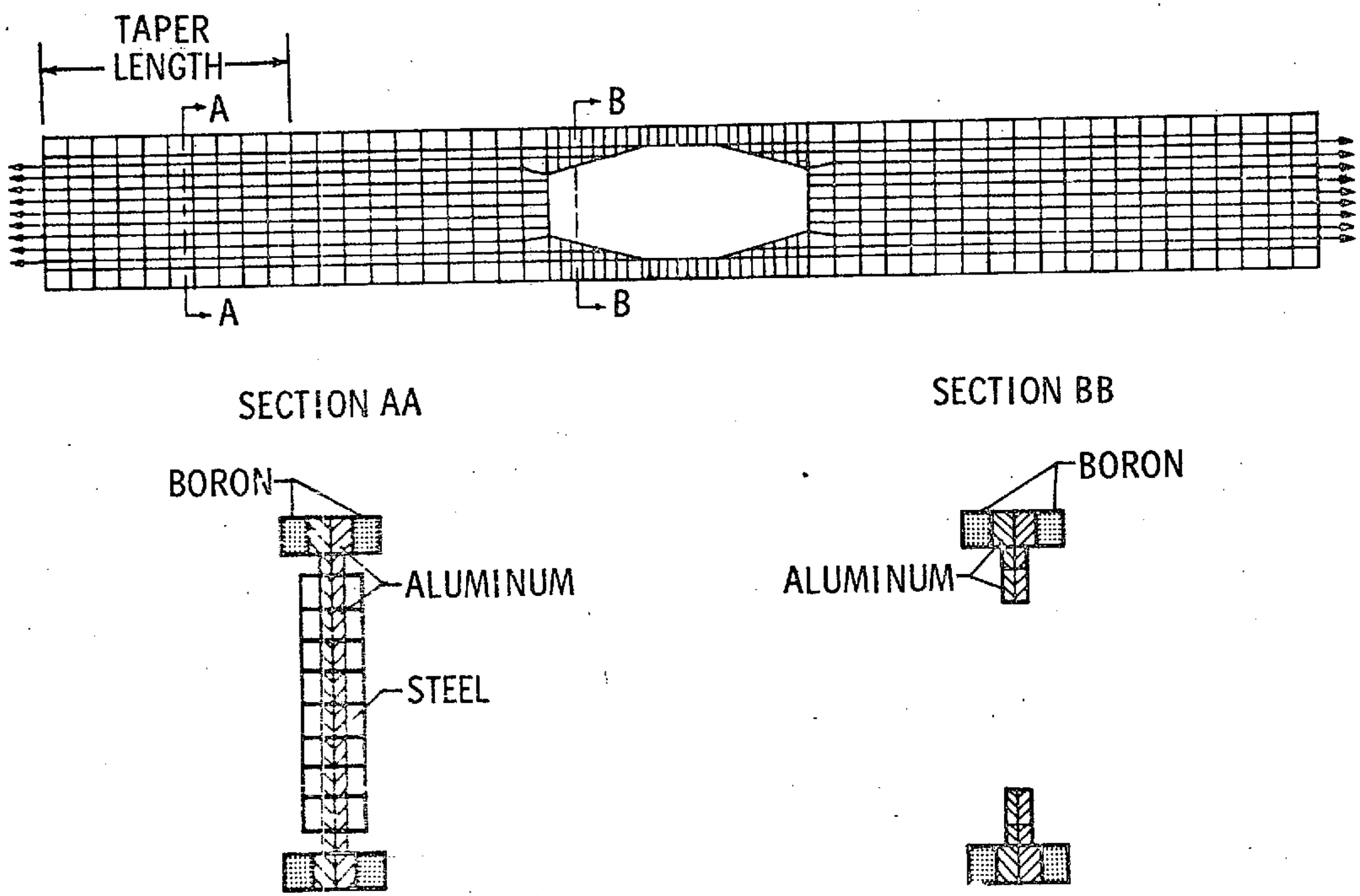

Figure 6. NASTRAN model of bi-element tension specimen.

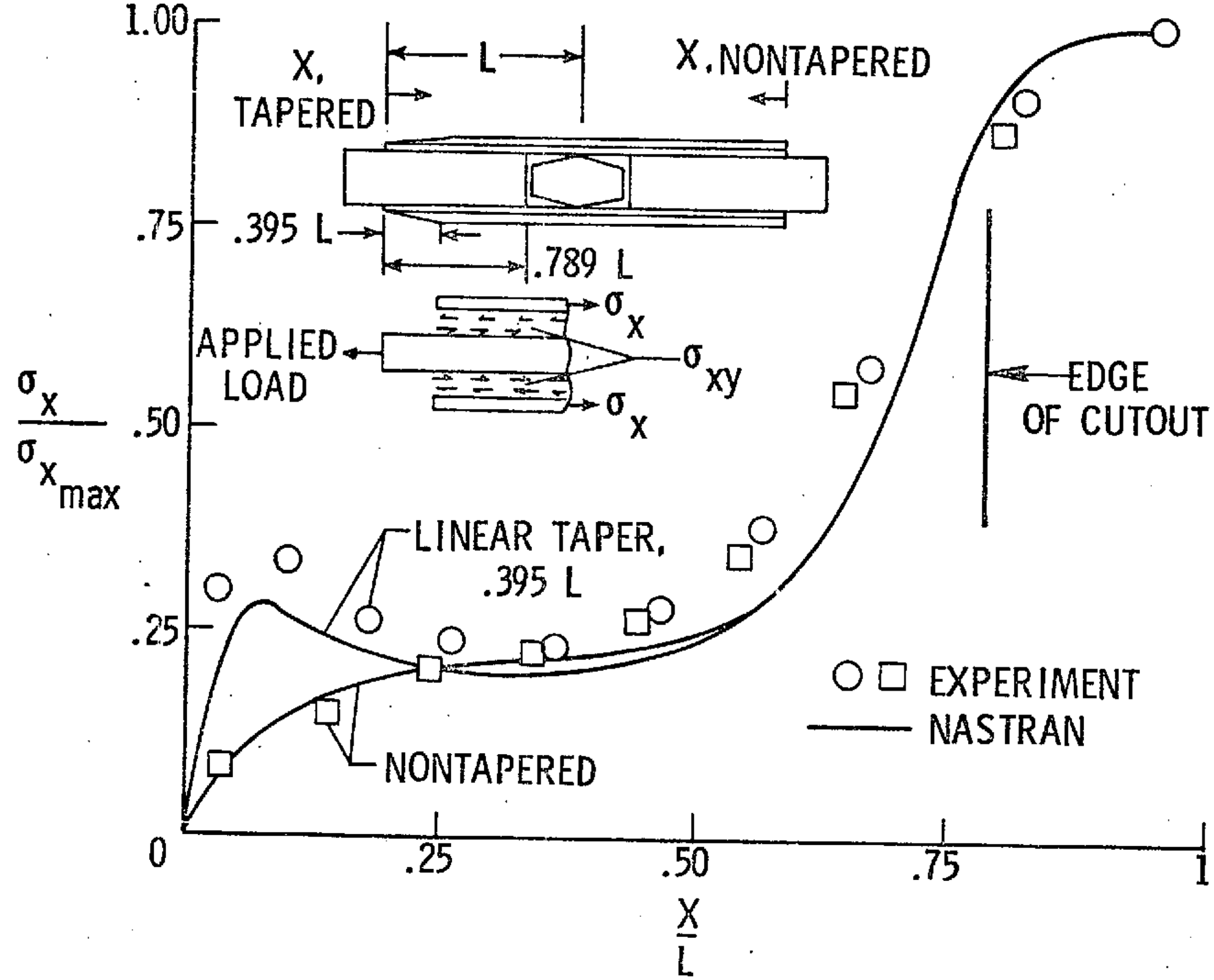

Figure 7. Comparison of axial stress in boron of bi-element tension specimen for nontapered and linearly tapered end regions. L = 24.13 cm (9.5 in.). $\sigma_{x_{max}}$ = 800 MPa (116,000 psi).

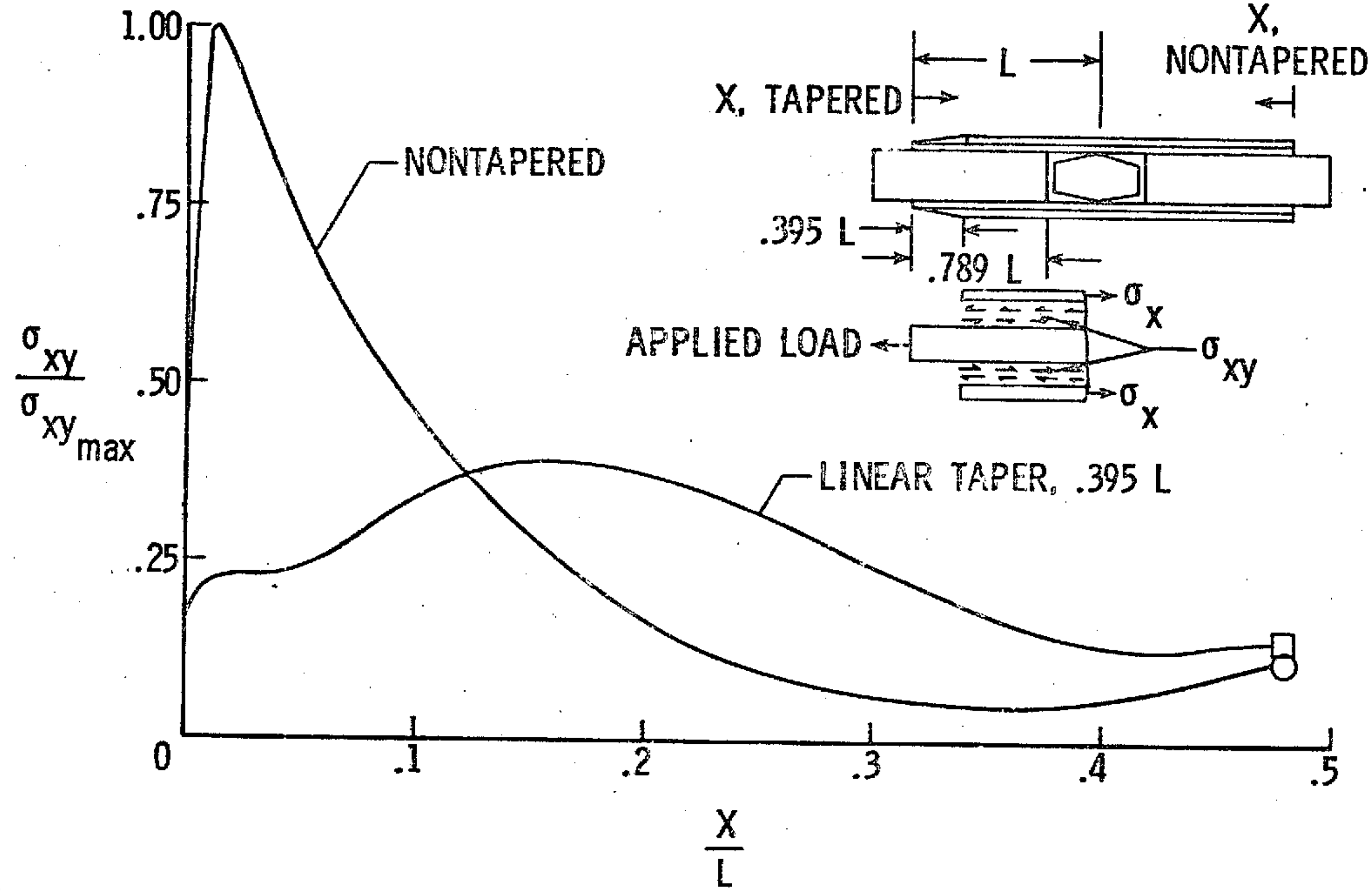

Figure 8. Comparison of calculated shear stress in aluminum web adjacent to stiffener of bi-element tension specimen for tapered and nontapered end regions. L = 24.13 cm (9.5 in.). $\sigma_{xy_{max}}$ = 128 MPa (18,500 psi) when σ_x in boron at specimen center equal 1.38 GPa (200,000 psi).

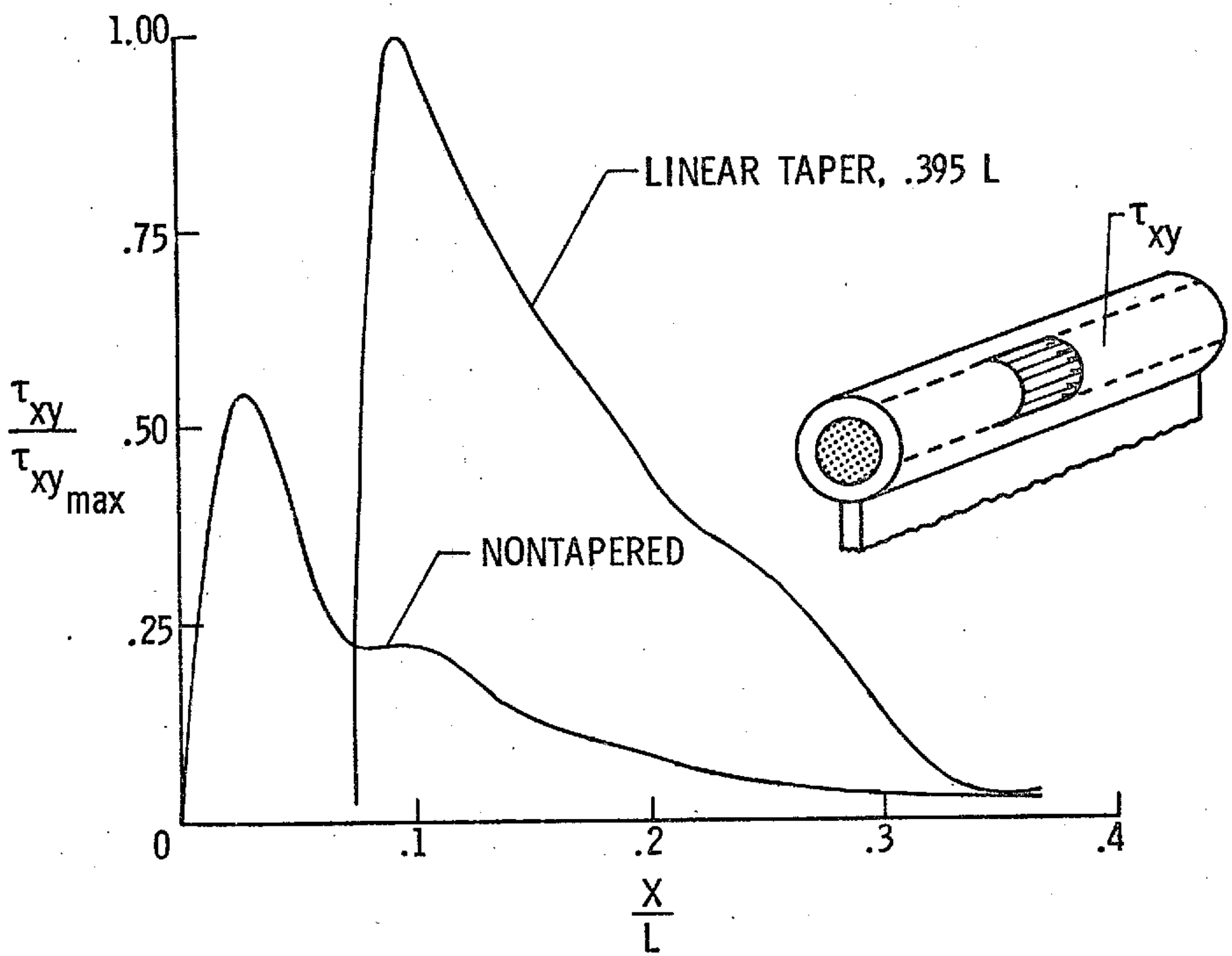

Figure 9. Comparison of calculated shear stress in epoxy bond of bi-element tension specimen for tapered and nontapered end regions. L = 24.13 cm (9.5 in.). $\tau_{xy_{max}}$ = 19.3 MPa (2800 psi) when σ_x in boron at specimen center equal 1.38 GPa (200,000 psi).

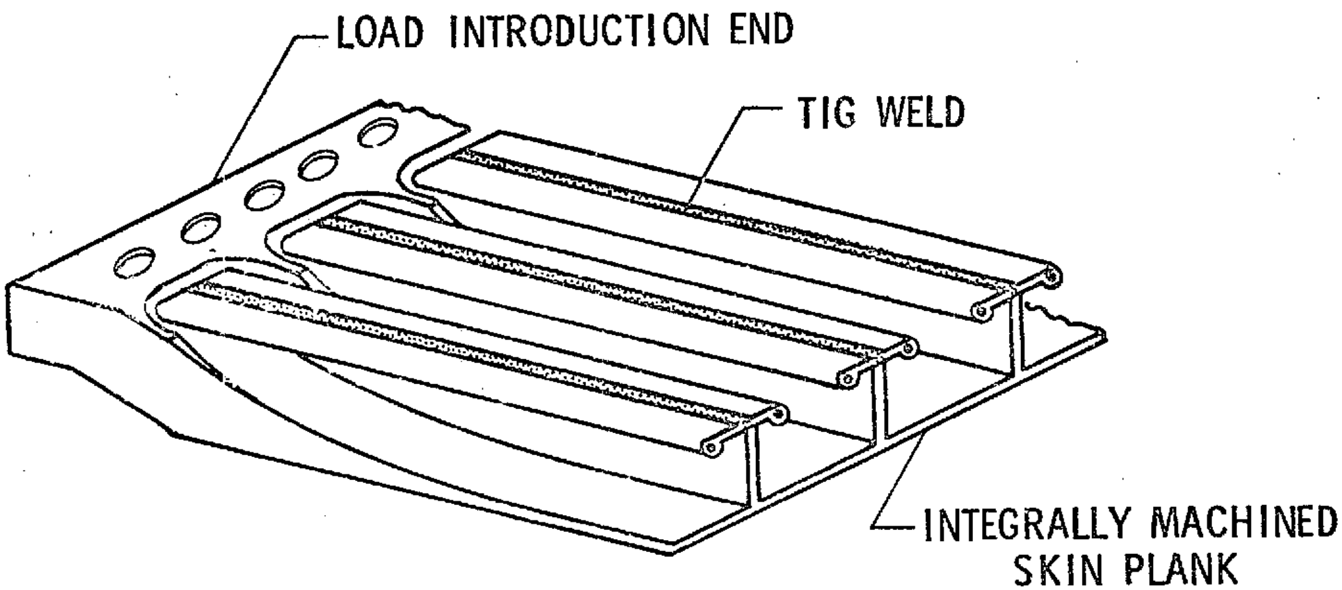

(a) Wing box compression panel.

Figure 10. Wing box integrally machined compression panel with TIG welded "T" boron infiltrated stiffeners.

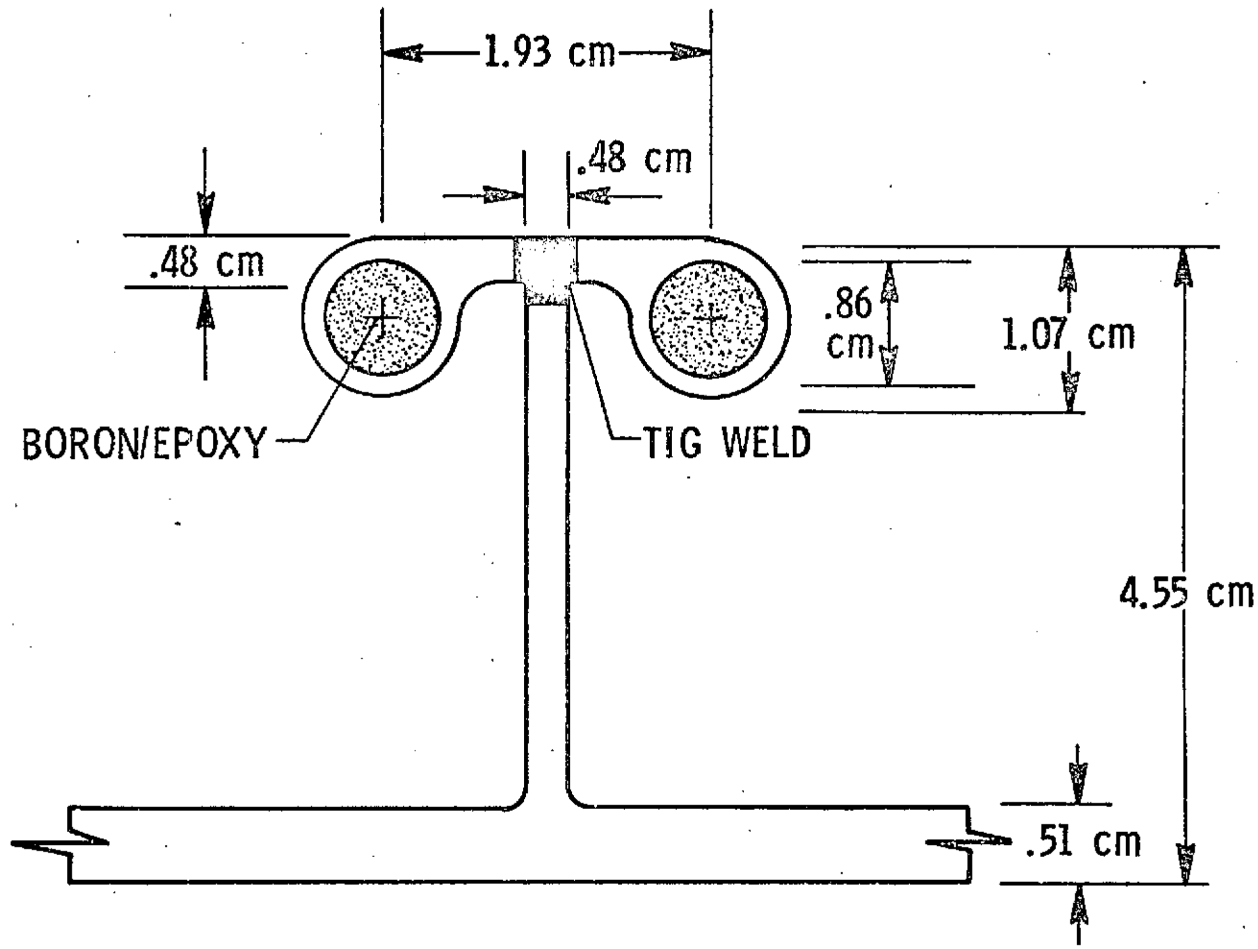

(b) Typical stiffener.

Figure 10. Concluded.

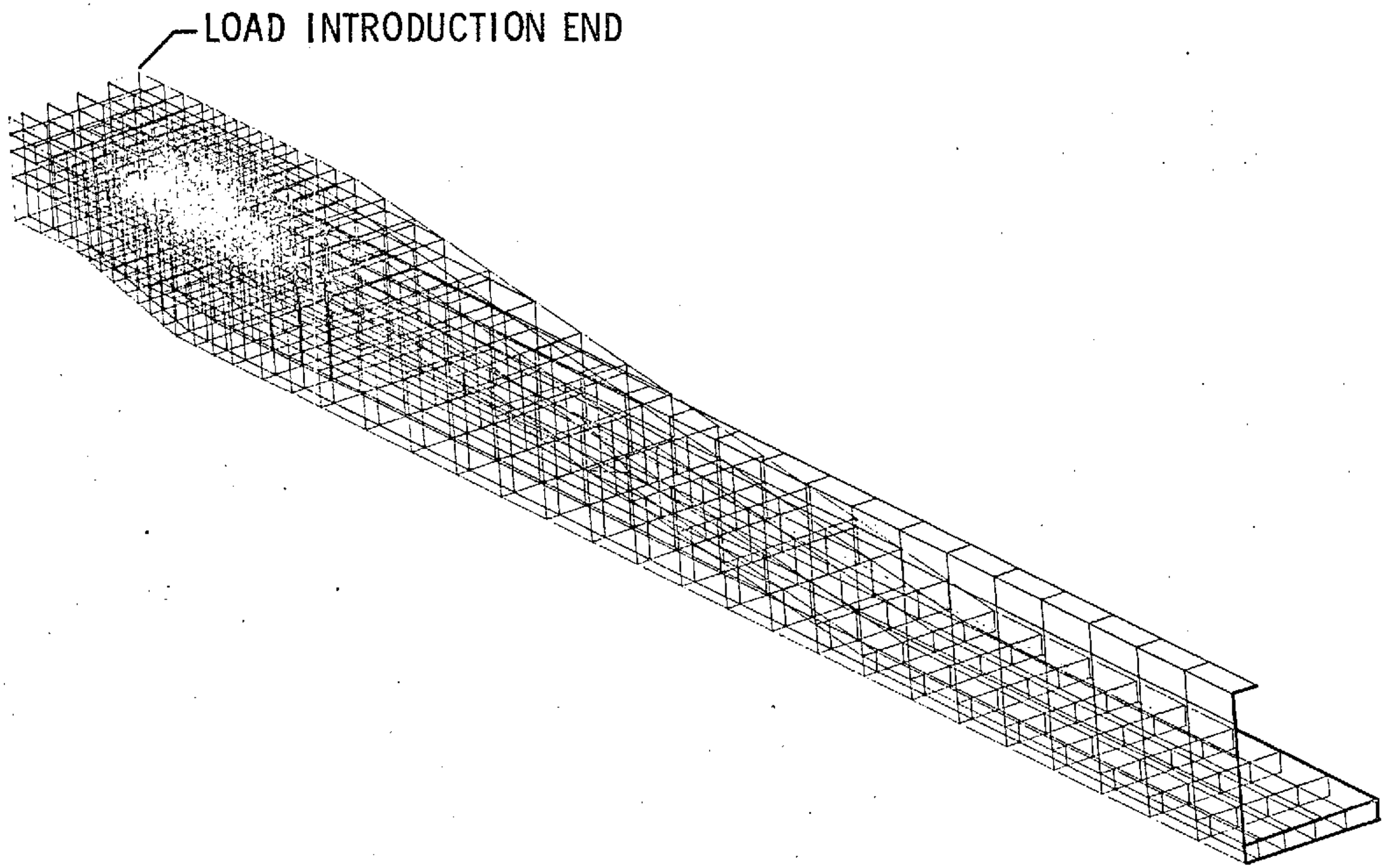

(a) Assembled half model.

Figure 11. NASTRAN model of sculptured load introduction region of wing box compression panel typical stiffener.

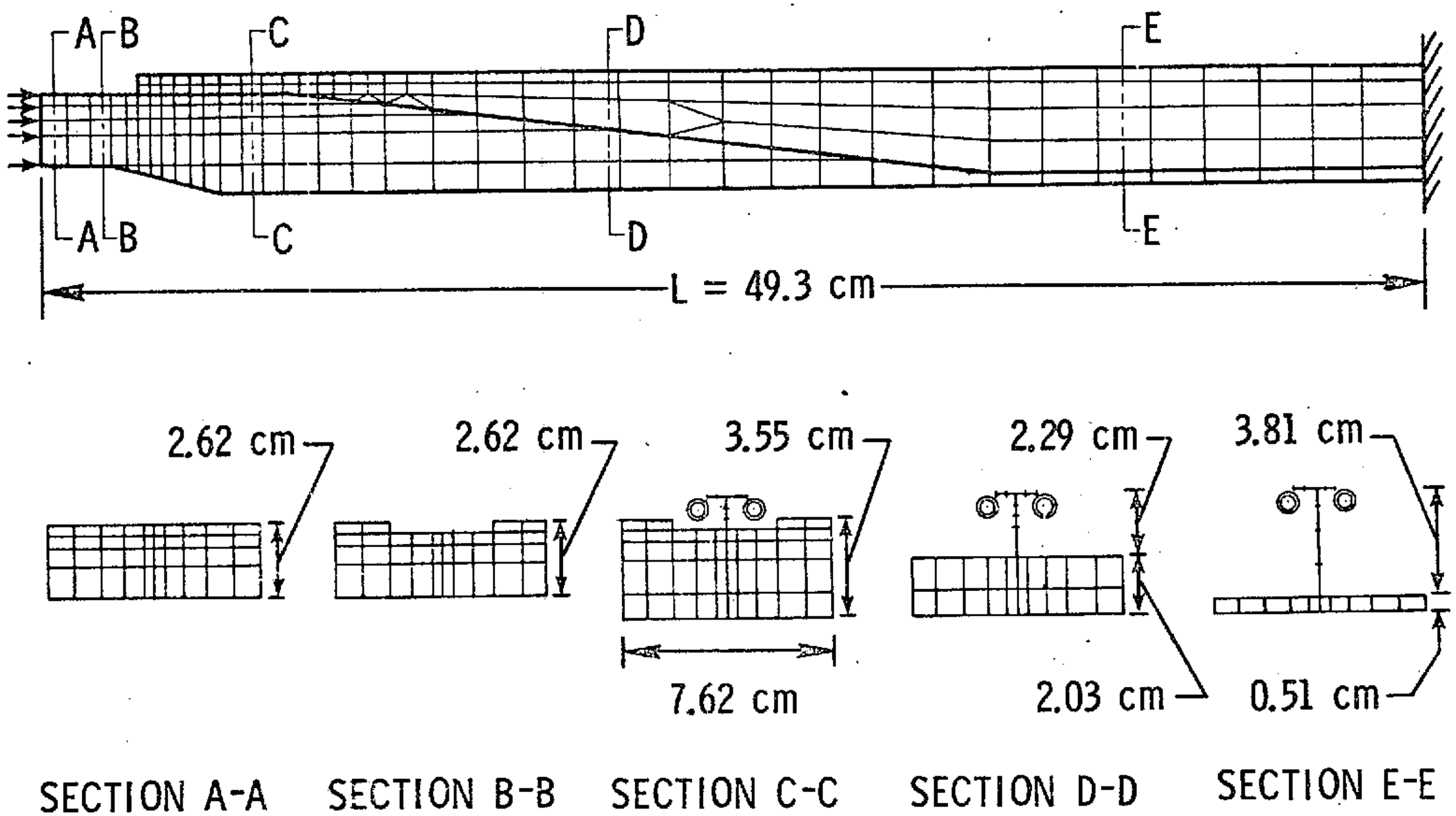

(b) Cross-section detail.

Figure 11. Concluded.

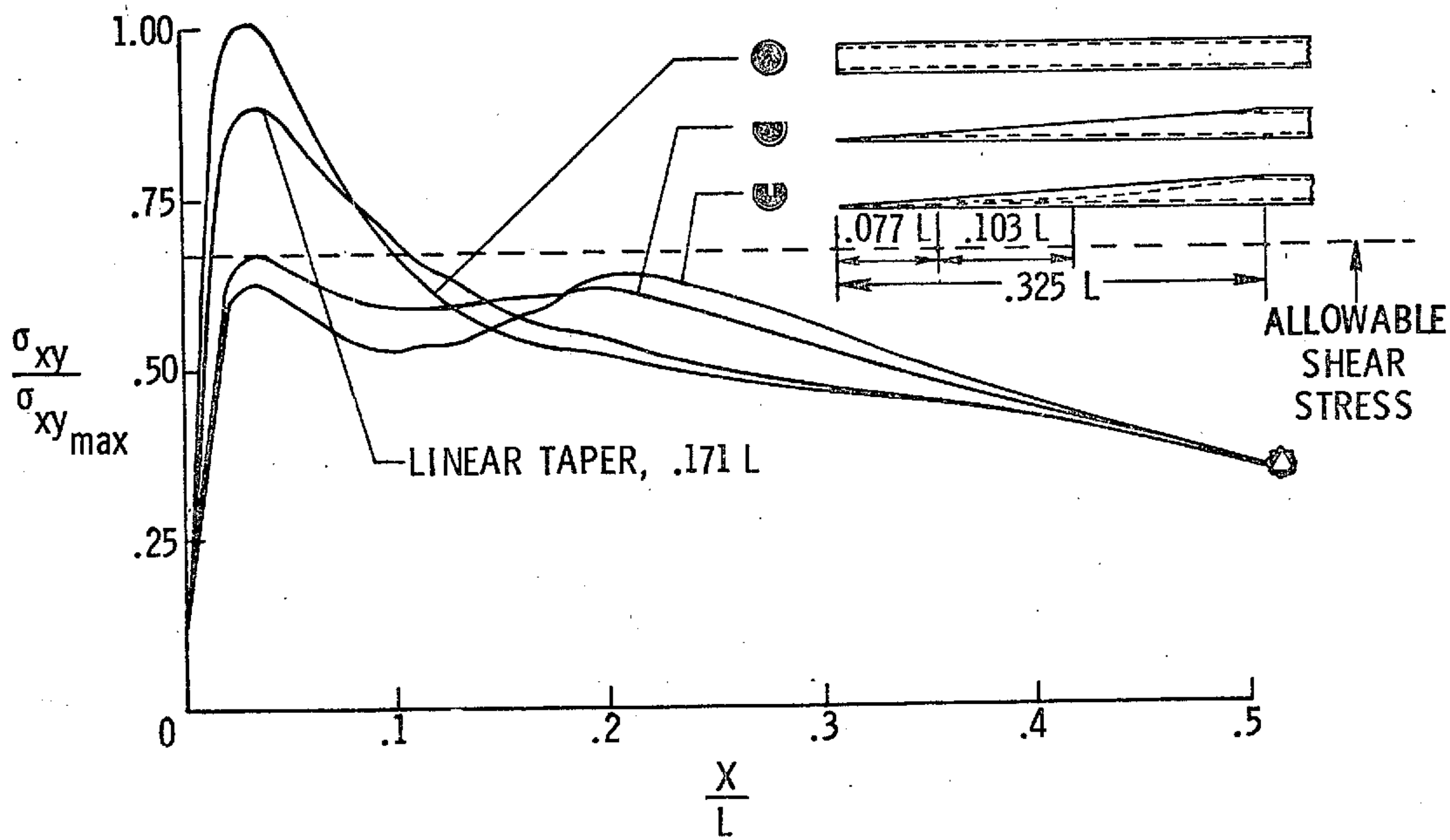

Figure 12. Comparison of calculated shear stress in wing box web weld region for tapered and nontapered stiffener end regions. L = 49.3 cm (19.4 in.). $\sigma_{xy_{max}}$ = 207 MPa (30,000 psi) when specimen loaded with axial load of 4.90 MN/m (28,000 lbf/in.).

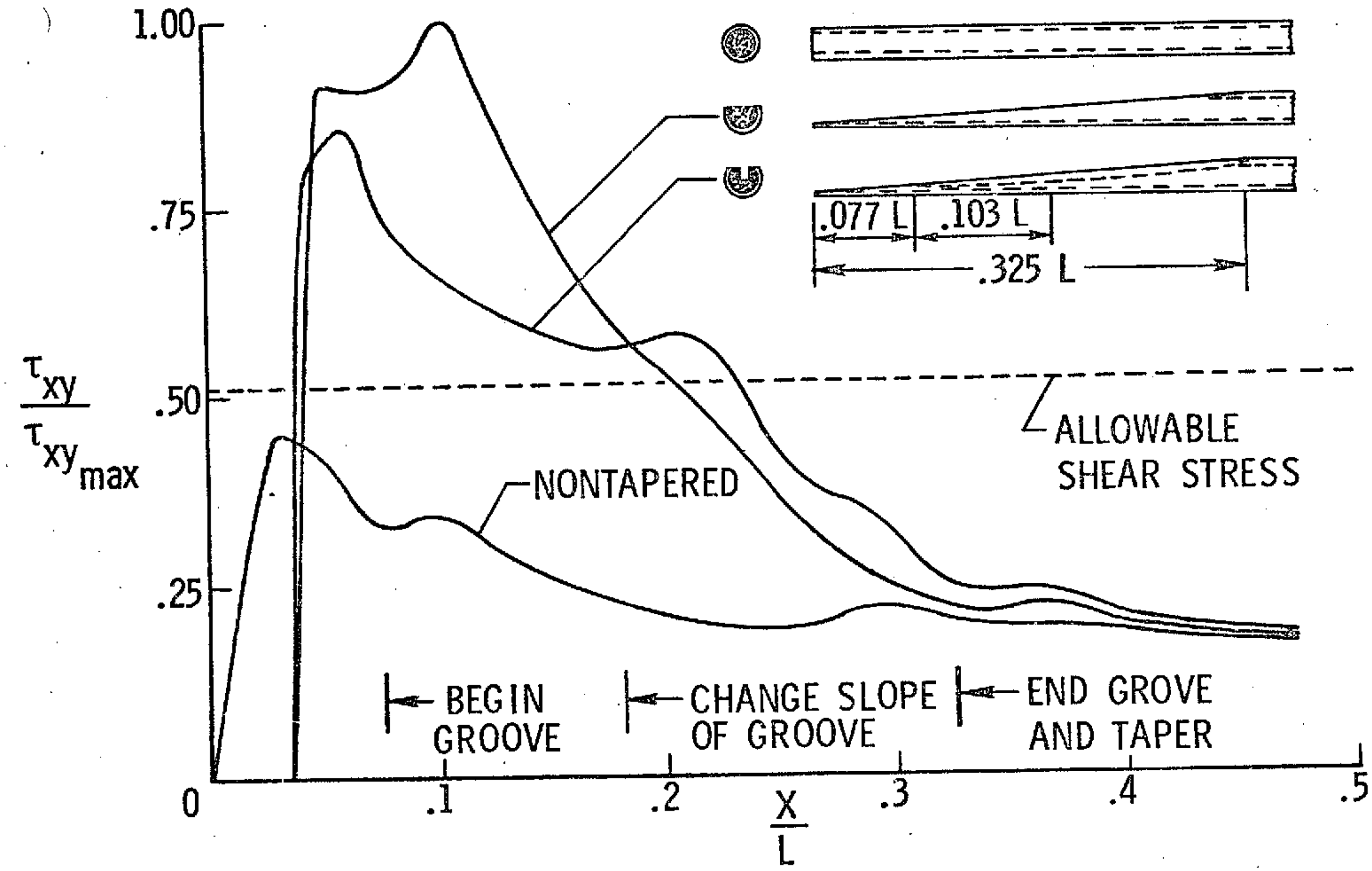

Figure 13. Comparison of shear stress in epoxy bond of wing box for tapered and nontapered stiffener end regions. L = 49.3 cm (19.4 in.). $\tau_{xy_{max}}$ = 29.6 MPa (4300 psi) when specimen loaded with axial load of 4.90 MN/m (28,000 lbf/in.).